Effect of the Insulin-like Growth Factor (IGF) Axis on the Transport Properties of Endothelial and Epithelial Cells *In Vitro*

Julie Melissa Davis Paye

Dissertation submitted to the Faculty of the
Virginia Polytechnic Institute and State University
in partial fulfillment of degree requirements for the degree of

Doctor of Philosophy
in
Chemical Engineering

Kimberly F. Williams, Chair
R. Michael Akers
Aaron S. Goldstein
Kevin Van Cott
Brian J. Love

10 September, 2003
Blacksburg, Virginia

Keywords: insulin-like growth factor-I (IGF-I), insulin-like growth factor binding proteins (IGFBPs), endothelial, epithelial, computational model, transport

Effect of the Insulin-like Growth Factor (IGF) Axis on the Transport Properties of Endothelial and Epithelial Cells *In Vitro*

Julie M. D. Paye

(Abstract)

The overall objective of this research consists of two main parts: (1) provide evidence that autocrine production of IGF-I modulates tight junction permeability and (2) demonstrate the ability of IGFBPs to regulate IGF-I delivery across cell layers. To meet the first objective, parental and IGF-I secreting bovine mammary epithelial cells were tested for cell layer permeability, tight and adherens junction proteins, IGF-IR, and a downstream signaling components of IGF-IR. In comparison with parental cells, IGF-I secreting cells had high levels of IGF-IRs, but low levels of the junction components E-cadherin, β-catenin, and occludin. The differences in parental and IGF-I secreting cells was not due to extracellular stimuli since inclusion of IGF-I, IGFBP-3, or co-culture with SV40-IGF-I cells did not alter the barrier properties of parental cells, suggesting that intracrine signaling may alter cell connectivity. The second objective focused on exogenous rather than endogenous IGF-I and the role of IGFBPs and IGF-IRs in ligand transcytosis. Bovine aortic endothelial cells (BAECs) cultured on surfaces optimized to minimize paracellular transport were utilized to investigate the kinetics involved in the transport of insulin-like growth factor-I from the apical side of confluent monolayers to the basolateral side. Binding competitors were used to determine the role of the cell surface insulin-like growth factor-I receptor (IGF-IR) and cell surface insulin-like growth factor binding proteins (IGFBPs) in this transport process. Although IGFBPs initially retard delivery of IGF-I, using a computation model, this report shows that pulse durations of less than 6 hrs resulted in enhanced delivery of IGF-I in the presence of IGFBPs, above that for delivery in the absence of IGFBPs. In addition, the model was utilized to identify key parameters to target when developing engineered growth factors for the treatment of diseases. It is shown that the sorting factions and internalization rates

are reasonable targets for the design of engineered growth factors. Since the sorting fractions are dictated by binding affinities in the acidic environment of the endosomes, it may be beneficial to design and analog of IGF-I that is more resistant to changes in pH, similar to those develop from epidermal growth factor.

Acknowledgements

I would like that thank my advisor, Dr. Kimberly Forsten Williams, for all the support, guidance, and knowledge she has provided, which has allowed me to become the researcher I am now. I would also like to show my appreciation to my entire dissertation committee, composed of Dr. R. Michael Akers, Dr. Aaron S. Goldstein, Dr. Kevin Van Cott, and Dr. Brian J. Love.

Many thanks to Dr. Akers and his lab, especially Pat Boyle, for everything they have done to help me, from iodinating IGF-I to training me in conducting ligand blots. In addition, I would like to that Dr. Goldstein and his lab for training me on the use of their microscope and imaging system.

I would also like to acknowledge everyone in Dr. William's lab, past and present, for helping me with my techniques and for always being there for a good laugh. In particular, I want to thank Laura for all the assistance she has provided to help me with my research and I will certainly miss her company and help. I would also like to thank Rose for the much needed coffee breaks and consultations.

Many thanks to my friends, both in lab and out, family, and fuzzies who have always been there through thick and thin. Thanks especially to Mom and Dad for everything they have ever done for me. They have done whatever they could at whatever cost to encourage, promote and facilitate the success of both of the children. Words, alone can not express everything they have done for Jay and me.

Finally, I would like to dedicate this to my husband, Corey, who has been a tremendous resource for support and encouragement. He constantly encouraged me to do what I needed to do in lab, even though it involved long hours of work for both of us and little time together. I could not have done this without his help at home and he made sure I stayed focused and grounded.

Table of Contents

List of Figures

List of Tables

Chapter 1: Introduction and Overview

1.1 Transport properties

1.1.1 Background

One of the primary functions of epithelial cells, the cells that cover all surfaces of the body (69), is to maintain a protective barrier that regulates the transport of proteins and other substances to underlying tissues. Endothelial cells, a specialized form of epithelial cells that line blood vessels (69), serve a similar function in the vasculature. Transport properties of these cell layers, once characterized, may be utilized to design methods of delivering drugs, such as growth factors. To aid in drug delivery, receptors on the surface of these cells can be utilized to deliver compounds that would not normally cross these barriers, a process known as receptor-mediated transport (3, 51, 178). Alternatively, compounds may be added to enhance barrier permeability and increase transport of drugs through the pathway mediated by cell-cell junction pathway, known as paracellular transport (133). Since increased paracellular transport is associated with various diseases, such as Gaucher disease (81) and diabetes (150), disrupted barrier properties may be utilized to delivery therapeutics specifically to the affected area via the paracellular pathway. However, use of this pathway is limited and does not always result in optimal delivery. This dissertation characterizes the transport properties of endothelial and epithelial cells and develops a mathematical model to aid in the development of effective delivery strategies.

1.1.2 Paracellular transport

There are two modes of transport by which molecules cross endothelial and epithelial barriers: paracellular and transcellular. Paracellular transport is a passive transport process where compounds pass between adjacent cells. Transport of molecules via the paracellular pathway, including growth factors, depends on physico-chemical properties of the molecule (e.g. size and charge), properties of the cells, and hemodynamic force (64). This transport pathway can be characterized through several means, such as measuring transmonolayer electrical resistance (TER) (Figure 1.1A) or by measuring the

transport of compounds that do not interact with the cell, such as phenol red (Figure 1.1B) or inulin.

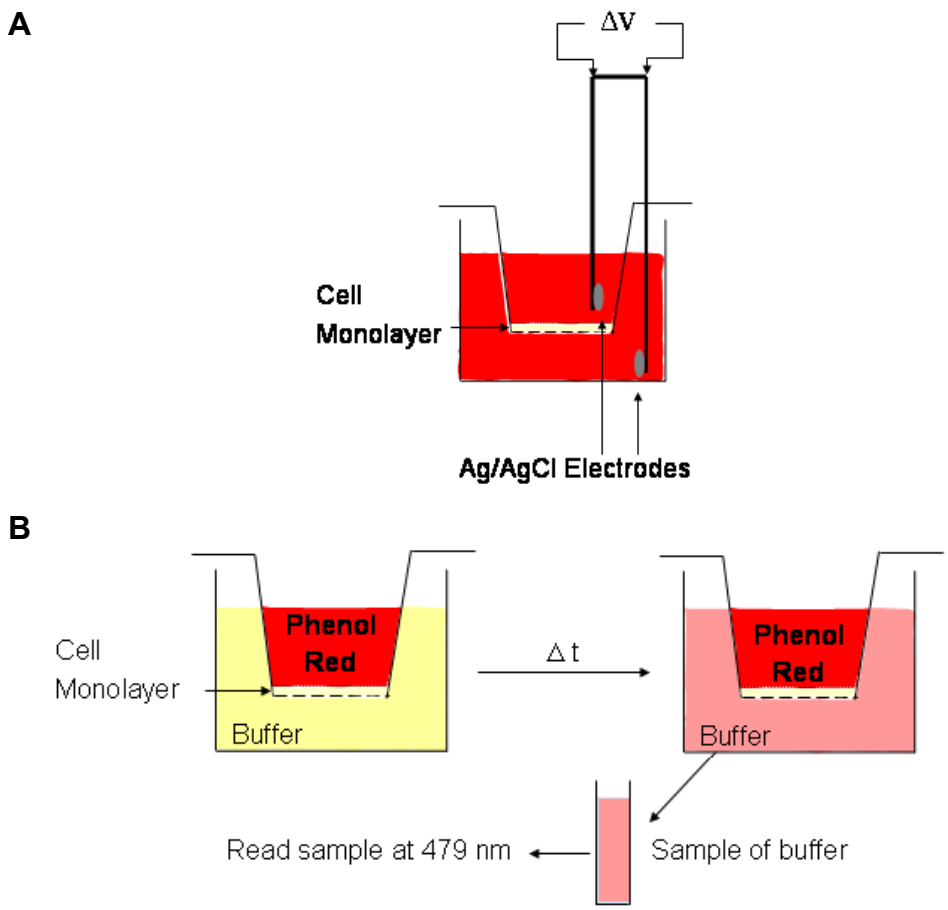

Figure 1.1: Transmonolayer electric resistance and phenol red transport.

(A) Transmonolayer electric resistance (TER) quantifies the ability of ions and electrolytes to permeate cell layers. (B) Phenol red transport quantifies the ability of small molecules to cross cell layers.

Paracellular transport is regulated by a series of dynamic junction components that connect neighboring cells (Figure 1.2). These cell-cell connections are altered during various states, such as development (189), wound healing (180), and tumor cell metastasis (17). The upper-most cell-cell junctions are known as tight junctions since they are the most restrictive and are largely responsible for the regulation of paracellular transport. Tight junctions are composed of the transmembrane protein occludin from

neighboring cells that bind one another. In addition, the intracellular portion of occludin associates with the actin binding proteins known as zonula occludens (Z0-1, 2, and 3). However, West et al. recently showed that E-cadherin, a component of adherens junctions, localized with occludin in bronchial epithelial cells and contributed to barrier integrity (195). The actions of E-cadherin are modulated by catenins that function either as junction-associated proteins or as regulators of intracellular signaling (68, 78, 116), depending on the needs of the cell. Hence, the functionality of these junctions and thus the exclusivity of the paracellular pathway, not only relies upon protein expression, but also on cellular location and the organization of the proteins.

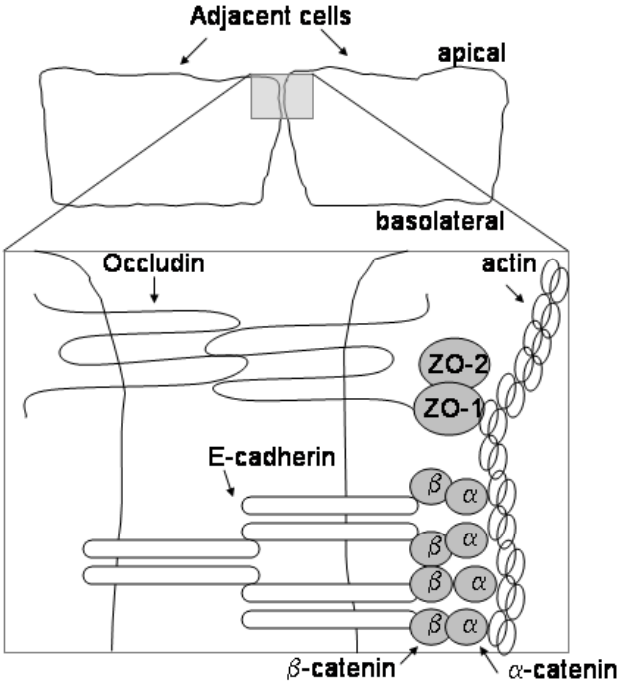

Figure 1.2: Proteins that regulate cell-cell junctions

Extracellular occludin associates with zonula occludens 1 and 2 which in turn connect to the actin cytoskeleton. Similarly, extracellular epithelial cadherin (E-cadherin) and/or vascular endothelial cadherin (VE-cadherin) interact with intracellular β- and α- catenins, which connect to the actin cytoskeleton.

1.1.3 Transcellular transport

Transcellular transport (Figure 1.3) is an active transport pathway relying upon cell-mediated uptake, sorting, and delivery. Substantial research has been conducted with

transferrin and immunoglobulin-A (IgA) to characterize the internal mechanisms involved in transcellular transport. Within 2 minutes after receptor binding (65, 107, 166), transferrin and IgA are detected in early endosomes proximal to the surface of origin (apical or basolateral) and almost completely co-localize with soluble markers such as low density lipoprotein (LDL) and horseradish peroxidase (HRP), suggesting that at this point, soluble and receptor-bound ligands have similar intracellular pathways (65, 107). These early endosomes, which appear as relatively large vesicles (107) with a pH of 5.8 (192), progress to form sorting endosomes. The half-life of transferrin in sorting endosomes is 2 -3 minutes and, within the cell in general, is 5 – 8 minutes (65). These sorting endosomes have long extensions, whose contents are destined for recycling endosomes. The remaining contents of the sorting endosomes mature into late endosomes, which are then delivered to lysosomes. Membrane bound transferrin and IgA are sorted to recycling endosomes while soluble markers such as LDL and HRP are sorted to lysosomes (65, 107, 166), suggesting that receptors and ligand/receptor complexes are destined for recycling, while dissociated ligands are destined for degradation. Gibson et al. report that when added to the basolateral side of Madin-Darby canine kidney cells, approximately 80% of transferrin and 40% of IgA were recycled and approximately 20% and 60%, respectively, were transcytosed to the apical side (66). In contrast, when epidermal growth factor (EGF) was added, nearly 80% was degraded, suggesting that intracellular trafficking varies from one ligand to another.

The sorting of growth factors, such as EGF, depends on their ability to bind their receptors in the acidic environment of the endosomes. The receptor for EGF can also bind with high affinity to similar molecules, such as transforming growth factor-α (TGF-α . At normal physiological pH, mouse EGF (mEGF), human EGF (hEGF), and TGF-α have very similar binding kinetics (56). However, at acidic pH, such as that found in endosomes, the ratio of binding affinities of TGF-α at pH 6 and pH 7.4 is 9 times that of mEGF. These differences in binding lead to a difference in sorting kinetics for each EGF receptor ligand (56, 120). Similarly, Bevan et al. report that analogues of insulin with enhanced receptor binding at acidic pH undergo less degradation (39% for X10 analog

and 25% for H2 analog) *in vivo* than insulin (55%) (19). They also report that insulin undergoes maximum degradation at pH 6, the conditions found in endosomes.

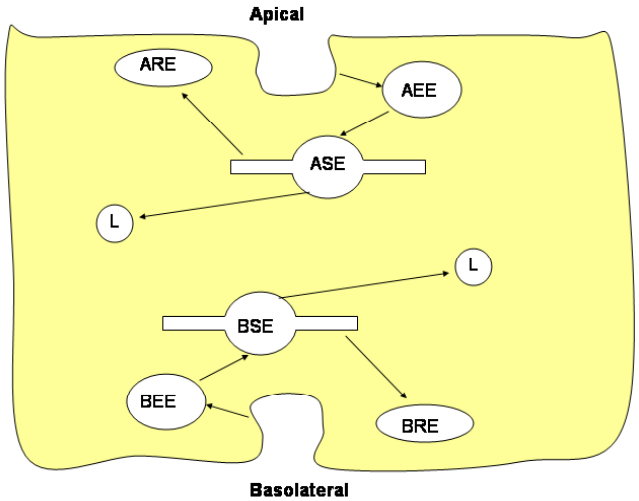

Figure 1.3: Theoretical intracellular sorting pathways

Cells internalize ligands and receptors through both apical and basolateral membranes. Once internalized, early endosome (EE) are formed (either apical, AEE, or basolateral, BEE) which mature into sorting endosomes (apical, ASE, or basolateral, BSE). From the sorting endosomes, recycling endosomes separate (ARE or BRE) and sorting endosomes mature into late endosomes or lysosomes (L).

1.2 Insulin-like growth factor-I (IGF-I)

Growth factors, such as insulin-like growth factor-I (IGF-I), are important regulators of cell division and tissue proliferation and, consequently, play a vital role in embryonic development (4, 43), wound healing (144), as well as in the development and treatment of various pathological conditions (6, 42, 73, 76, 96, 98, 99, 108, 136, 137, 149, 152-154, 179, 183). IGF-I is a 7.6 kDa polypeptide member of the insulin superfamily, which also includes insulin, insulin-like growth factor-II, relaxin, insulin like-3 and insulin like-4. The actions of IGF-I are mediated by high affinity interactions with its cell surface receptor (IGF-IR) and with IGF binding proteins (IGFBPs). Due to structural similarities (Figure 1.4), IGF-I also participates in lower affinity interactions with the insulin receptor. Insulin can also bind to IGF-IRs, but not to IGFBPs.

Similar to other growth factor receptors, IGF-IR is a transmembrane tyrosine kinase that is autophosphorylated after ligand binding and can, in many cells, activate signaling cascades, such as phosphatidylinositol-3 kinase (PI3K) and mitogen activated protein kinase (MAPK) (1, 193). IGF-IR is composed of a disulfide-linked dimer, thereby eliminating the need for the ligand-induced dimerization that is characteristic of many growth factor receptors.

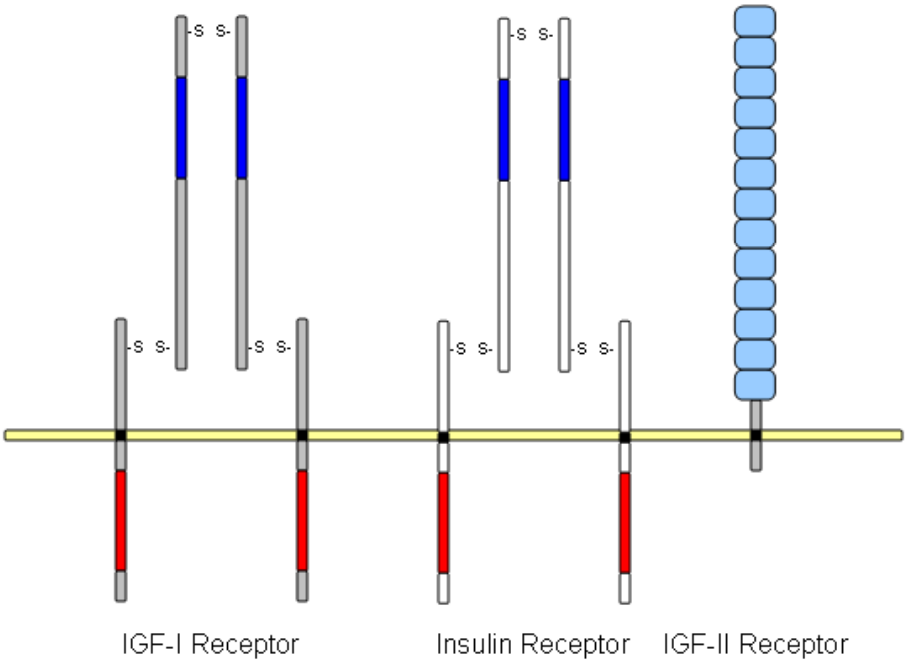

Figure 1.4: Receptors for the insulin superfamily

The insulin-like growth factor-I (IGF-I) receptor has high sequence homology with the insulin receptor, particularly in the tyrosine (red) signaling domains and the cysteine rich (blue) domains. Even though IGF-I and IGF-II are homologous, the IGF-II receptor is a member of the mannose-6-phosphate, not insulin, family of receptors.

There are six known IGFBPs and they have been shown to participate, to varying degrees, in IGF-inhibiting, IGF-enhancing, and IGF-independent actions (22, 30, 32, 44, 46, 50, 70, 127-129) (Figure 1.5). Since over 90% of circulating IGF-I is found in a complex with IGFBP-3 and an acid labile subunit (ALS), it has long been thought that the main function of IGFBPs was as carrier proteins for IGF-I. However, recent research suggests IGFBPs serve a larger function than just carrier proteins (104, 105, 143, 194).

While several IGFBPs bind to cell surfaces with high affinity, IGFBP receptors have not yet been identified. However, it has been suggested that the type V transforming growth factor β receptor (104, 105) and membrane-bound matrix metalloprotease-9 may also function as a receptors for IGFBP-3 (132) and the α5β1 integrin receptor may function as a receptor for IGFBP-1 (88). Due to the large size of the IGF-I/IGFBP-3/ALS complex, it does not cross intact endothelium. However, smaller IGFBPs (e.g. IGFBP-1 and 2) have been shown to cross the endothelium. Several researchers (106, 110, 165) have reported nuclear localization of IGFBP-3 and Lee et al. report cooperativity between nuclear IGFBP-3 and retinoids (106).

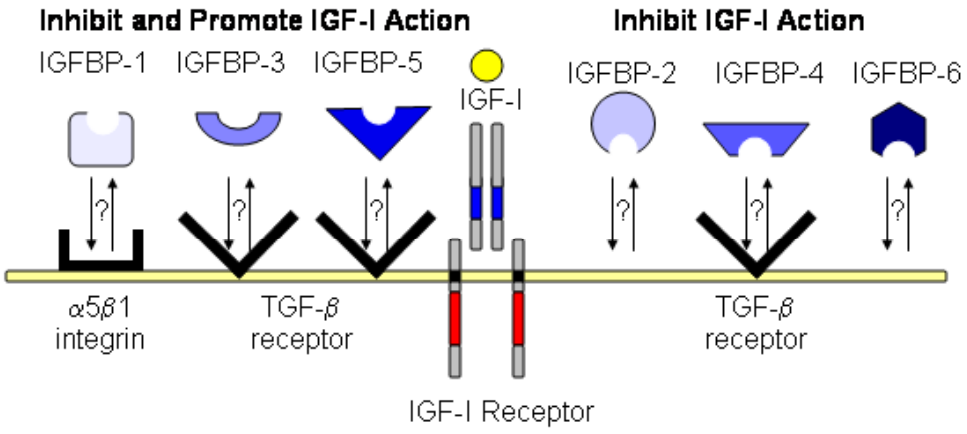

Figure 1.5: Actions of insulin-like growth factor binding proteins (IGFBPs)

The actions of IGF-I are mediated by interactions with its receptor and with solution and cell surface insulin-like growth factor binding proteins (IGFBPs). IGFBPs have the ability to inhibit and promote the actions of IGF-I.

1.3 Biological Applications involving the IGF-I axis

1.3.1 Tight junction permeability in metastasis

When cellular proliferation becomes unregulated, i.e. through autocrine production of growth factors, benign or malignant tumors may form. Malignant cells proliferate and invade their local environment by degrading extracellular matrix proteins to create a migration pathway (182). As these malignant cells migrate, there is a disruption in the

cell-cell contacts that mediate paracellular transport. The malignant cells then enter the bloodstream and are transported to a new locale, a process known as metastasis, where they again proliferate and invade the local environment.

Most cancer cells are of epithelial origin and loss of cell-cell contacts, such as those mediated by occludin and E-cadherin, is a necessary step towards tumor cell metastasis. Many tumors overexpress either IGF-I, IGF-II, or IGF-IR (73, 76, 136, 149, 179, 183) and high serum levels of IGF-I have been associated with an increased risk of developing cancer (60, 170). Increased activation of IGF-IR has been associated with altered expression of cell-cell junction proteins, such as decreased membrane expression of E-cadherin in human colonic adenocarcinoma cells reported by Andre et al (5). Changes in junction protein expression have been connected to increased tumor cell invasion and metastasis, as reviewed by Mauro et al (125). For example, human breast cancer cells transfected with antisense IGF-IR had increased mobility and decreased aggregation and adhesion (146). It is clear that activation of IGF-IR can disrupt cellular junctions and promote migration and metastasis, however studies investigating the role of autocrine production of IGF-I in the modulation of cell-cell junctions have not been undertaken until now.

Growth factor action can occur through several different mechanisms, including autocrine and intracrine activation (173). In autocrine signaling, endogenous growth factors produced by cells bind to cell surface receptors and initiate signaling cascades. However, intracrine signaling occurs following binding of endogenous growth factors to receptors inside the cells. Autocrine signaling through the epithelial growth factor receptor (EGFR) has been found in 72% of lung squamous cell carcinomas that rarely develop ras mutations (83) and inhibition of autocrine signaling through the transforming growth factor-β receptor in mammary epithelial and mouse colon carcinoma cells reduced tumor cell invasive growth (142). The insulin-like growth factor-I (IGF-I) autocrine system also affects tumor growth, such as the growth of esophageal carcinoma cells (115) and mammary epithelial cells (163). Lahm et al. reported that blockage of the IGF-I receptor with a neutralizing monoclonal antibody prevented autocrine signaling by

IGF-II, decreased proliferation, cell number, and increased the double time in colon carcinoma cells (100). Autocrine production of IGF-I also substantially increased the growth of a human thyroid cancer line (145).

1.3.2 Delivery of therapeutics

IGF-I has the potential to treat a variety of disorders, such as severe insulin resistance (99, 153), leprechaunism (6), renal failure (98), neurological disorders (108), Laron Syndrome (154), and diabetes (42, 96, 137, 152). Current strategies to treat these diseases involve intravenous infusions of supraphysiological doses of IGF-I (42, 96, 137). Since these high doses cause unwanted side effects, such as hair loss, upper respiratory infections, increased production of IGF-I antibodies, and increased heart rate (71, 135), an understanding of the mechanisms involved in the transport of IGF-I from the bloodstream to underlying tissues may foster the development of better treatment strategies that minimize these side effects.

Endothelial cells line the inside of blood vessels and constitute the primary barrier against transport from the bloodstream and thus play a key role in regulating the delivery of IGF-I to tissues (Figure 1.6). IGF-I has been reported to bind a variety of endothelial cells, including bovine brain microvessels (55), rat fat pad capillary endothelial cells (8), bovine aortic endothelial cells (BAEC) (8), bovine periaortic endothelial cells (11), and bovine pulmonary arterial endothelial cells (11). Once bound, IGF-I is processed predominantly through non-degradation pathways (8, 11). Non-degradation pathways have also been reported in human osteosarcoma cells (59), opossum kidney cells (46) and rat chondrocytes (164). Schalch et al. report that degradation of ^{125}I-IGF-I in rat chondrocytes was inhibited by chloroquine and ammonium chloride by raising the intralysosomal pH (164), suggesting that pH dependent intracellular binding kinetics dictate the overall fate of IGF-I.

It remains unclear how IGF-I is transported across the endothelium. IGF-I has been shown to bind to endothelial cells both *in vitro* (94) and *in vivo* (10, 23). *In vitro* studies with human umbilical vein endothelial cells (HUVECs) indicated that IGF-I was

transported across the cell layer (14). However, this transport was not affected by blocking antibodies against IGF-IR or by excess IGF-I, indicating the transport was, in their system, mediated by the paracellular pathway. *In vivo*, the actions of IGF-I are further complicated by the presence of IGFBPs. In perfused rat hearts, approximately 3 – 5% of the IGF-I was delivered to subendothelial tissues (12). Shoubridge and Read report a 2 fold preferential transport of the longR3-IGF-I, which does not bind IGFBPs, over IGF-I in the intestines of rats (167).

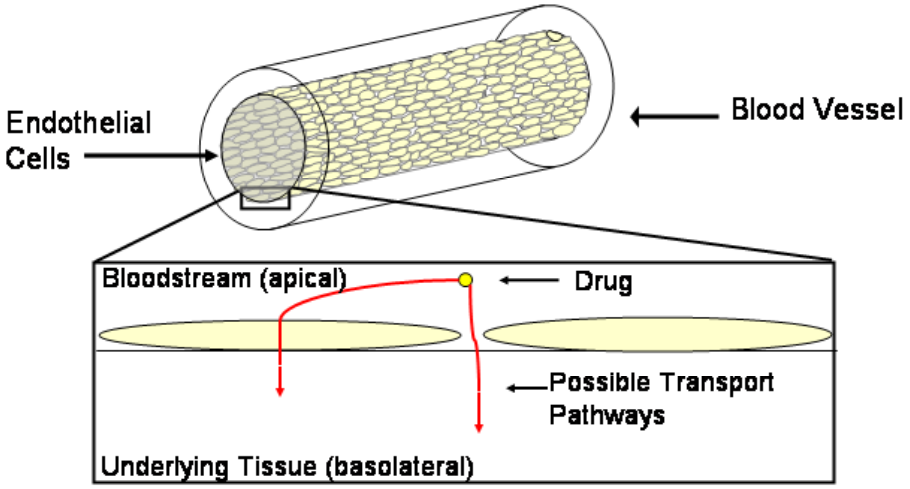

Figure 1.6: Drug delivery across endothelial cells

Drugs may be transported across the endothelial barrier by either paracellular or transcellular transport.

Recently, Grulich-Henn et al. reported substantial binding of ^{125}I-IGF-I to the extracellular matrix produced by HUVECs, which contains IGFBP-2, suggesting IGFBP-2 prevented ^{125}I-IGF-I from binding to cell surface IGF-IR. Further, IGFBPs, most likely IGBFP-6, mired the transport of ^{125}I-IGF-I across bovine articular cartilage (62). Bastian et al. demonstrated that the clearance rate of ^{125}I-IGF-I in wound chambers implanted in rats was slower than that of ^{125}I-LongR3-IGF-I, presumably due to binding to IGFBPs (15). Previous reports have shown that IGFBPs can cross endothelial boundaries (9, 12) and transport IGF-I (23), but this has only been reported for endothelial cells in the rat heart or in cells with compromised barrier function (174).

Due to the pathological conditions requiring IGF-I treatment, endothelial cells of these patients may also be affected. Therefore, it is important to consider how the mechanisms involved in IGF-I delivery may be altered in these conditions. In a mouse model for Laron syndrome (LS), reduced levels of IGFBP-3 and IGF-I have been reported while levels of IGFBP-1, -2, and -4 remained unchanged (33). Since IGFBP-3 functions as a carrier protein for IGF-I that regulates its actions, further consideration needs to be given to the pharmacokinetics involved. It has not been reported that there are changes in IGFBPs or IGF-IR levels in Gaucher disease, however, increased paracellular porosity is associated with this disease (81). Increased paracellular porosity has also been reported in patients with type 1 diabetes mellitus (150). Since these diseases may be treated with IGF-I, it may be feasible to target the paracellular pathway when designing delivery strategies. Patients with diabetes also have increased levels of IGFBPs and IGF-IRs. In insulin dependent diabetes mellitus, patients have increased production of IGFBP-1, and -2 and occasionally increased proteolysis of IGFBP-3 is reported (18, 58). Federici et al. found increased presence of insulin/IGF-I hybrid receptors in muscle and adipose tissue of patients with non-insulin dependent diabetes mellitus (47, 48), which could affect the kinetics of IGF-I binding.

1.4 Computational Modeling

Computational models have been utilized to expand the knowledge base of the mechanisms by which growth factor act, as reviewed recently by Wiley et al (196). Significant contributions have been made in the past decade that aid in an understanding of the mechanisms involved in sorting and signaling of the EGF receptor and its family of ligands, which may facilitate the development of therapeutic strategies involving the EGF family to treat various pathological conditions. Models have been developed that describe sorting of EGF and several EGF analogs (56, 79, 176) and the dependence of acidic binding on sorting outcome (56). Shvartsman et al. have developed a model of EGF signaling (168) and more recently, Resat et al. have developed a model that incorporated sorting as well as signaling events (157). Models of sorting and transport of FGF and transferrin have also been developed (40, 166, 172). Similar to the approach utilized in this dissertation, the model developed by Sperinde and Nugent described the

processing of FGF was based on the Law of Mass Action, which states that the rate of a chemical reaction is directly proportional to the active masses of each of the reactants. The parameters utilized by Spreinde and Nugent were determined from experiments, and the model was solved using numerical analysis. In contrast, the model developed by Sheff et al. to describe transport of transferrin and IgA assumed first order kinetics, negligible dissociation, unidirectional transport, and the entire model was fit to the data using Microsoft Excel.

Until now, modeling of intracellular sorting and transport has focused mainly on epithelial, not endothelial, cells. Since many drugs are delivery systemically, it may prove beneficial to develop a model of drug transport across endothelial cells. Further, few models of IGF-I action have been reported. Boroujerdi et al. developed a compartmental model of *in vivo* IGF-I metabolism (24), however the mechanisms involved in IGF-I delivery were not included in the model.

1.5 Overview of Dissertation

The overall objective of this research consists of two main parts: (1) demonstrate that autocrine production of IGF-I modulates tight junction permeability and (2) demonstrate the ability of IGFBPs to regulate IGF-I delivery across cell layers. The first part of this dissertation focuses on the role of autocrine production of IGF-I in modulating the permeability of epithelial cells (Chapter 2). Changes in cell connectivity occur in various states, such as cell proliferation, wound healing, and tumor cell metastasis. However, the mechanisms behind these changes largely remain unknown. Cell connectivity was determined by measuring phenol red transport across monolayers of parental mammary epithelial cells (MAC-T) compared with transfected MAC-T that constitutively secrete IGF-I (Figure 1.7). Since IGF-I secreting cell lines (TK-IGF-I and SV40-IGF-I) formed poor transport barrier and the parental cell line formed a complete barrier, co-culture studies between parental and IGF-I secreting cells were conducted to attempt to elicit altered barrier properties in parental cells. Expression of the junction components occludin, E-cadherin, and β-catenin were quantified in parental and IGF-I secreting cell lines. In addition, levels of IGF-IRs and one of its downstream signaling components,

Akt, were also quantified to aid in an understanding of the intracellular mechanisms involved in reduced barrier formation in the autocrine cell lines.

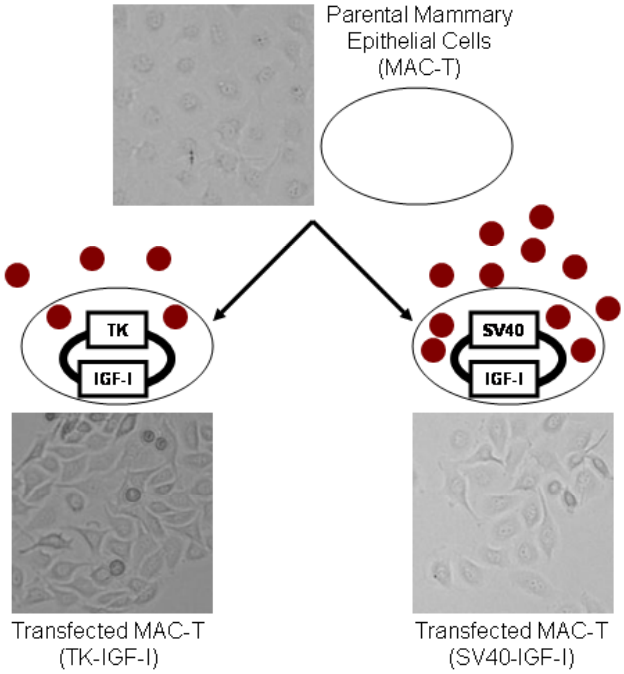

Figure 1.7: Parental and autocrine epithelial cells

Parental (MAC-T) and IGF-I secreting cells (TK-IGF-I and SV40-IGF-I) were utilized to investigate the role of autocrine production of IGF-I in modulating cell layer permeability. TK-IGF-I cells secreted moderate levels of IGF-I and SV40-IGF-I cells secreted high levels.

The second objective focused on exogenous rather than endogenous IGF-I and the role of IGFBPs and IGF-IRs in ligand transcytosis. Since Bastian et al. report predominantly paracellular transport of IGF-I in both epithelial (13) and endothelial (14) cells, culture conditions were optimized to develop an *in vitro* model endothelial system that minimized paracellular transport and was more representative of *in vivo* endothelium (Chapter 3). In culturing endothelial cells *in vitro*, various parameters may affect the properties of the cells. For example, cells have been shown to have altered behavior when cultured on surfaces coated with different compounds (37, 61, 155, 184, 188), plated at different initial cell densities (90, 159), at different periods of culture time (13, 155) and with different cell types (80, 92, 118, 131). All of these parameters need to be optimized in order to develop a reliable and accurate *in vitro* model of the *in vivo*

endothelium. Since there is interest in modeling the human endothelium, it is only natural to investigate the use of human endothelial cells *in vitro*. However, due to cost and ease of culture, bovine endothelial cells also provide an excellent model mammalian cell system. Investigations included human aortic endothelial cells (HAECs), human microvascular endothelial cells derived from the lung (HMVEC-L), and bovine aortic endothelial cells (BAECs), cultured on a varied of surface coatings (gelatin, collagen, and collagen-fibronectin). Cells were plated at a variety of densities ($5 \times 10^4 - 2 \times 10^5$ cells/cm^2) and cultured from 2 – 16 days. Assessment was based on the ability of the cells to form a confluent cell layer in a timely manner that was restrictive to the transport of compounds paracellularly.

After optimizing conditions for a model endothelium that minimized paracellular transport, studies were conducted to characterize the transport of IGF-I across these cell layers (Figure 1.8) and the ability of IGFBPs to regulate this delivery (Chapter 4). Since IGF-I can bind with high affinity to both IGF-IRs and IGFBPs, competitive binding experiments, similar to those used to generate Scatchard plots (103), were conducted to determine the binding affinity of IGF-I for each binding site, as well as the number of IGF-IR and IGFBP binding sites present. Internalization experiments were conducted and Satin plots (119) were created to quantify internalization rates of IGF-I/IGF-IR and IGF-I/IGFBP complexes. Transport experiments were also conducted to measure the apical to basolateral transport of IGF-I. Binding competitors, such as insulin, Y60L-IGF-I, and LongR3-IGF-I, were utilized to determined the contributions of each binding site, IGF-IR or IGFBP, in the delivery of IGF-I. TCA and PTA precipitation experiments were conducted on the transported ligands to determine if any degradation had occurred.

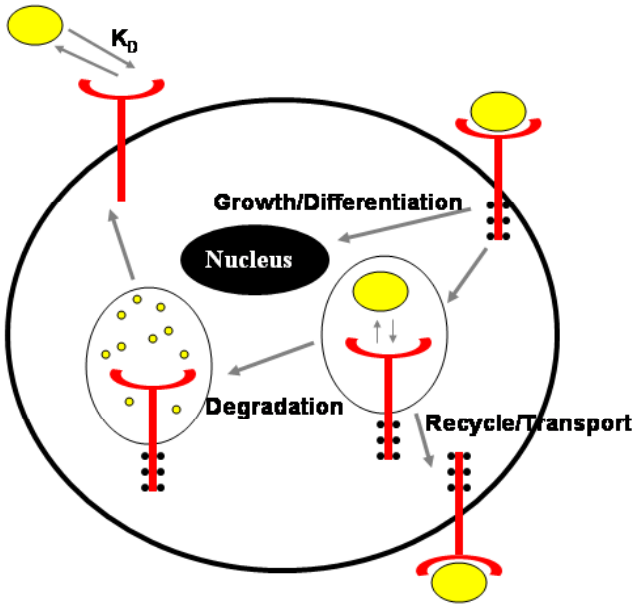

Figure 1.8: Transcellular delivery of growth factors

Transcellular delivery of growth factors depends on binding affinities to extracellular and intracellular receptors. Changes in binding affinity in the acidic environment of the endosome dictate the sorting outcome, either degradation or delivery, of the growth factor.

To aid in future development of therapeutic strategies, a computational model was developed (Chapter 5) based on experimental data collected from the optimized endothelial cell system (Chapter 4). The model displayed similar trends as the experimental results reported in Chapter 4 and allowed further investigation of the system that was not possible through experiments. Parameters, such as paracellular transport, ligand binding kinetics, and sorting parameters were varied to determine possible mechanisms to target for the design of therapies to facilitate IGF-I delivery to tissues.

The final chapter (Chapter 6) reports conclusions and identifies future directions of this research. Additional information is also included in the appendices.

Chapter 2: Autocrine Production of Insulin-like Growth Factor-I (IGF-I) Impacts Cell Connectivity

Julie D. Paye[1], R. Michael Akers[2], Laura J. Delo[1], Kimberly F. Williams[1]*

Departments of [1]Chemical Engineering and [2]Dairy Science, Virginia Polytechnic Institute & State University, Blacksburg, Virginia 24061

*Correspondence to:
Kimberly F. Williams
Department of Chemical Engineering
Virginia Polytechnic Institute & State University
133 Randolph Hall
Blacksburg, VA 24061
(540) 231-4851 (office)
(540) 231-5022 (FAX)
kfw@vt.edu

2.1 Abstract

Changes in cell connectivity occur in various states, such as cell proliferation, wound healing, and tumor cell metastasis. However, the mechanisms behind these changes largely remain unknown. This report describes how autocrine production of insulin-like growth factor-I (IGF-I) alters cell connectivity. Cell connectivity was determined by measuring phenol red transport across monolayers of parental mammary epithelial cells (MAC-T) compared with transfected MAC-T that constitutively secrete IGF-I. Parental cells formed a complete barrier to the transport of phenol red while IGF-I secreting cells provided essentially no barrier. Neither co-culture studies between parental and IGF-I secreting cells nor addition of exogenous IGF-I or IGF binding protein-3 (IGFBP-3) altered parental cell phenol red transport properties. IGF-I secreting cells expressed higher levels and activation of IGF-IR but lower levels of the junction components occludin, E-cadherin, and β-catenin than parental cells. These results suggest that localized activity or intracrine mechanisms are involved in the decreased cell connectivity in the IGF-I secreting cell lines via changes in both the tight and adherens junction protein levels.

2.2 Introduction

Epithelial cells are essential for maintaining functional barriers that restrict the transport of proteins and other substances to underlying tissues. This restricted transport is regulated via a series of cell-cell junction complexes that connect neighboring cells (138). These cell-cell connections are altered during various states, such as development (189), wound healing (180), and tumor cell metastasis (17). Altered expression and function of junction proteins has been linked to the ability of epithelial cells to migrate (5, 109) and metastasize (26, 95), and increased paracellular permeability has been associated with the formation of tumors (171).

Expression of proteins that form cell-cell junctions are altered following activation of signaling cascades involving downstream signaling pathways (25, 31), such as

phosphatidylinositol-3-kinase (PI3K) and mitogen-activated protein kinase (MAPK), similar to those activated by growth factor receptors (89). For example, Grande et al. determined that reduced production of E-cadherin in thyrocytes following addition of epidermal growth factor (EGF) and transforming growth factor-β1 depended on signaling through the MAPK pathway (15). Dependence on MAPK signaling has also been shown for hepatocyte growth factor stimulation of retinal pigment epithelial migration and β-catenin signaling (113). Treatment with insulin-like growth factor-I (IGF-I) caused sequestration of β-catenin away from E-cadherin in both colorectal and melanoma cancer cells (148) following Akt signaling.

IGF-I is a polypeptide member of the insulin superfamly that is composed of 70 amino acids, has a molecular weight of ~7,600 Da, and binds with high affinity to its cell surface receptor (IGF-IR). Similar to other growth factor receptors, IGF-IR is a transmembrane tyrosine kinase that is autophosphorylated after ligand binding and can, in many cells, activate signaling cascades, such as PI3K and MAPK (1, 193). IGF-IR is a dimer composed of two alpha and two beta subunits linked by disulfide bonds, thereby eliminating the need for the ligand-induced dimerization that is characteristic of many growth factor receptors.

Most cancers are of epithelial origin and many overexpress IGF-I, IGF-II or IGF-IR (149, 179, 183). Activation of IGF-IR has been associated with altered expression of cell-cell junction proteins, such as decreased membrane expression of E-cadherin in human colonic adenocarcinoma cells, as reported by Andre et al. (5). Changes in junction protein expression have been connected to increased tumor cell invasion and metastasis, as reviewed by Mauro et al. (125). For example, human breast cancer cells transfected with antisense IGF-IR had increased mobility and decreased aggregation and adhesion (146). It is clear that activation of IGF-IR can disrupt cellular junctions and promote migration and metastasis, however little is known about how autocrine production of IGF-I affects the cell-cell junctions.

The research presented in this chapter focuses on the relationship between autocrine production of IGF-I and loss of cell connectivity. Cell connectivity was determined by measuring phenol red transport across cell layers of mammary epithelial cells (MAC-T) and transfected MAC-T, which constitutively secrete IGF-I. Parental cells formed a complete barrier to the transport of phenol red while IGF-I secreting cells provided essentially no barrier. Neither co-culture studies between parental and IGF-I secreting cells nor addition of exogenous IGF-I altered parental cell phenol red exclusion properties, suggesting that exogenous factors produced by the IGF-I secreting cells are not responsible for the altered barrier properties. The hypothesis is that localized IGF-I, possibly through intracrine mechanisms, accounts for these changes in barrier properties.

Materials and Methods

2.2.1 Epithelial cell lines.

The normal mammary epithelial cell line (MAC-T), and two IGF-I secreting cell lines (SV40-IGF-I and TK-IGF-I) and plasmid control cell lines developed from the MAC-T cell line were used in these studies. The IGF-I secreting cells were transfected to secrete IGF-I under the control of the SV40 and TK promoters respectively (162). The plasmid control cell lines were transfected with a plasmid containing the SV40 promoter without IGF-I cDNA. All cells were grown in DMEM (Gibco, Grand Island NY) with 10% FBS (Hyclone, Logan UT) and 50 units/ml of penicillin/streptomycin (Mediatech, Herndon VA). The plasmid control cell lines were also grown in the presence of 0.1 mg/ml hygromycin B (Calbiochem, San Diego CA).

2.2.2 Cell culture.

To compare the effects of autocrine and paracrine (or exogenous) IGF-I on cell connectivity, cells were cultured in several experimental configurations, either on the upper (Figure 2.1A) or lower (Figure 2.1B) surface of tissue culture inserts. Additionally, co-culture studies were conducted using one cell type cultured on tissue culture inserts and another cell type cultured in the tissue culture well (Figure 2.1C and Figure 2.1D). In all configurations, cells were plated at 5 x 10^4 cells/cm^2 on either

Transwell® inserts (Corning Costar, Cambridge MA) (12 mm, 0.4 μm pore size) or in 12 well plates (Corning Costar) and cultured for 8 days, with media replenished every 2 – 3 days.

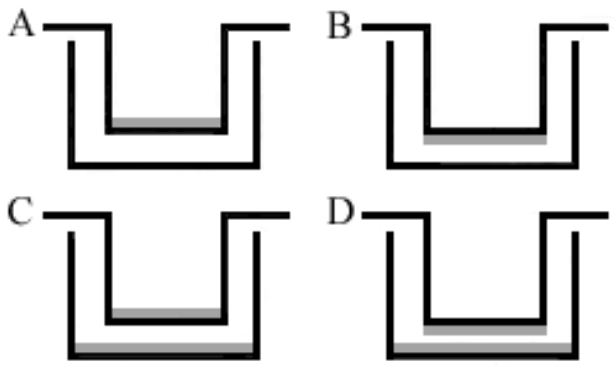

Figure 2.1: Configuration of cell monolayers using tissue culture inserts in well plates

The cells were plated on the upper (A) or lower (B) surface of the tissue culture insert or in co-culture with cells plated on the well surface (C and D).

2.2.3 Phenol red transport.

The transport of phenol red was evaluated based on a protocol described previously (198). Briefly, cells were washed with Dulbecco's phosphate buffered saline (DPBS). The media in the apical chamber was replenished with DMEM+ (DMEM with phenol red, 50 units/ml penicillin/streptomycin, and 10% FBS) and the media in the basolateral chamber was replaced with DMEM- (phenol red free DMEM, 50 units/ml penicillin/streptomycin, and 10% FBS). Cultures were incubated at 37°C for 12 hours. Following incubation, 1 ml samples were taken from the basolateral chamber and analyzed in a spectrophotometer at 479 nm.

2.2.4 Total protein quantification.

Total protein quantification based on protein binding to colloidal gold was conducted using Quantigold (Diversified Biotech, Boston MA) as described by the manufacturer. Briefly, membranes were cut from the insert using a hypodermic needle and incubated in

trypsin and EDTA (Mediatech) overnight. Following incubation, buffer (0.1 M Na_2HPO_4, 4 M NaCl, 0.004 M $Na_2EDTA\text{-}2H_2O$, pH 7.4) was added and samples were sonicated at setting 5 for 10 seconds using Model 60 Sonic Dismembrator (Fisher Scientific). Samples were combined with Quantigold and analyzed in a spectrophotometer at 595 nm.

2.2.5 ECM Isolation.

Extracellular matrix (ECM) was isolated as described previously (140). Briefly, media was aspirated and inserts were washed with DPBS. Cells were then solubilized with DPBS, 0.5% Triton X-100, and 20 mM NH_4OH for 5 minutes at room temperature. Inserts were aspirated and washed 4 times with DPBS. The remaining material has been previously characterized by others as ECM (67, 190).

2.2.6 Western Ligand Blot.

Ligand blot analysis was conducted as described previously (82). Briefly, cells were grown on Transwell® inserts for 8 days with media changed every 2-3 days and conditioned media (CM) was collected on day 8. CM samples were concentrated using a SpeedVac® Model SC110 (Savant, Holbrook NY) and reconstituted in water. Samples were then diluted with 2x loading buffer (0.125 M TRIS, 4% SDS, 20% glycerol, 1% bromophenol blue), loaded into a 12.5% acrylamide gel, and separated at constant current. Samples were then transferred to nitrocellulose membranes and incubated overnight with ^{125}I-IGF-I. Membranes were exposed to film for 3-7 days at -70ºC.

2.2.7 Western Immunoblot.

Cells were grown on Transwell® inserts for 8 days with media changed every 2-3 days and collected in Laemmli buffer for Western blot analysis. Samples were sonicated, boiled, and loaded (20 μg total protein per lane for phospho-Akt and total Akt, and 50 μg for all others) into 5% (for E-cadherin and β-catenin), 7% (for occludin, phospho-Akt, and total Akt) or 10% (for IGF-IR) tris-glycine gels. Samples were separated at constant voltage and transferred to PVDF membranes. Membranes were then probed with rabbit anti-IGF-IRβ (1:10,000) (Santa Cruz Biotechnology, Santa Cruz CA) and anti-rabbit (1:15,000) (Zymed, San Francisco CA), mouse anti-E-cadherin (1:5000) (BD

Biosciences, San Jose CA) and anti-mouse (1:15,000) (Zymed), mouse anti-β-catenin (1:2500) (BD Biosciences) and anti-mouse (1:15,000), rabbit anti-occludin (1:16,000) (Zymed) and goat anti rabbit (1:20,000) (Zymed), or rabbit anti-phospho-Akt (1:1000) (Cell Signaling Technology, Beverly MA) and goat anti-rabbit (1:15,000) (Zymed). The phospho-Akt blots were stripped (2% SDS, 62.5 mM Tris-HCl, 100 mM β-mercaptoethanol, pH 6.7) and reprobed for total Akt using rabbit anti-Akt (1:5000) (Cell Signaling Technology) and goat anti-rabbit (1:15,000) (Zymed) to insure comparable Akt protein levels were found in all lanes. Blots were developed using Pierce Super Signal West Pico Kit (Rockford, IL).

2.2.8 IGF-I Binding Studies.

Cells were plated on Transwell® inserts ($5x10^4$ cells/cm^2) and cultured for either 4 or 8 days, with media exchanged every 2–3 days. Cells were washed with DPBS and binding buffer (0.05% gelatin, 120 mM NaCl, 5 mM KCl, 1.2 mM $MgSO_4$, 15 mM sodium acetate, 25 mM Hepes, 10 mM dextrose, pH 7.4) was added to the apical chamber and cells were incubated at 4°C for 20 minutes. Following incubation, ^{125}I-IGF-I (2 ng/ml) and Y60L-IGF-I (10 μg/ml) were added and cells were then incubated at 4°C for 12 hrs. On ice, binding buffer was aspirated, cells were washed twice with ice cold DPBS, and lysed with 0.3 N NaOH. Samples were collected and analyzed in a COBRA II Auto-Gamma counter (Perkin Elmer Life Sciences, Downers Grove IL).

2.2.9 Statistical Analysis.

All experiments were performed a minimum of three times and number of samples within an individual experiment used to calculate the mean ± standard error of the mean is stated within the figure legend. Blots are representative of at least three blots run from material obtained from three independent experiments. Statistical comparisons were conducted by two-tailed t-tests in Microsoft Excel with significance defined as $p < 0.05$.

2.3 Results

2.3.1 Effect of autocrine IGF-I production.

Epithelial cells both *in vivo* and *in vitro* are known to form junctions that prevent the unregulated movement of proteins across the cell barrier (138). Since MAC-T cells are derived from primary mammary epithelial cells (84), it was not surprising that, when cultured on tissue culture inserts, a nearly complete barrier to paracellular transport was evident using a phenol red transport assay (Figure 2.2). Since the IGF-IR is believed to affect cell-cell junction formation (125), the hypothesis was that autocrine production of IGF-I, which can impact IGF-IR levels, would alter cell barrier properties. To evaluate this, the barrier properties of two MAC-T derived cell lines that were stably transfected to secrete IGF-I under the control of two different constitutive promoters (162), were evaluated. Neither of these cell lines (Figure 2.2) formed a barrier to the transport of phenol red (94 ± 7 % (mean ± SE, n = 4) of control, where control represents inserts without cells). Moreover, prolonged culture of IGF-I secreting cells for up to 16 days failed to elicit substantial barrier activity compared with the non-IGF-I secreting parental cells (Appendix D). In additional, several plasmid control clones of cells (MAC-T cells transfected with a plasmid containing the SV40 promoter but lacking the IGF-I cDNA)

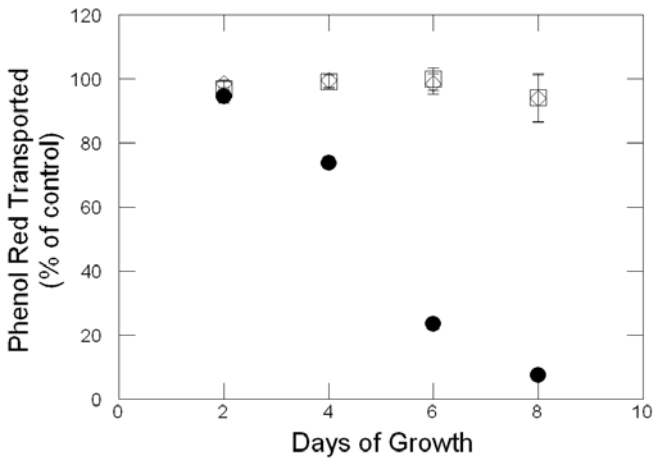

Figure 2.2: Phenol red transport across parental and IGF-I secreting bovine mammary epithelial cells

Phenol red transport across MAC-T (●), SV40-IGF-I (□), and TK-IGF-I (◊) cells plated on tissue culture inserts at an initial density of 5 x 10^4 cells/cm^2. Measurements (mean ± S.E., n=4) are representative of 3 independent experiments.

yielded barrier activity similar to the parental cells (Appendix D). Since TK-IGF-I and SV40-IGF-I cell lines secrete substantial levels of IGF-I (162), this suggested that the difference in transport barrier properties observed between the normal and IGF-I secreting cells was induced by the secretion of IGF-I and not due to the transfection process or promoters.

2.3.2 Cell Density and Barrier Properties.

Differences in transport properties could be related to the density of cells covering the transport area. However, the formation of a transport barrier was not directly related to the cell number present (Figure 2.3). The number of TK-IGF-I cells present after 8 days of growth, as determine by total protein content, was not significantly different from that of MAC-T cells, even though they have significantly different barrier properties (Figure 2.2). Further, SV40-IGF-I and TK-IGF-I cells had identical barrier properties at all time points, but significantly different protein levels. Since similar barrier properties were measured for the two IGF-I secreting cell lines, subsequent studies utilized the SV40-IGF-I cells, which secrete higher levels of IGF-I (162).

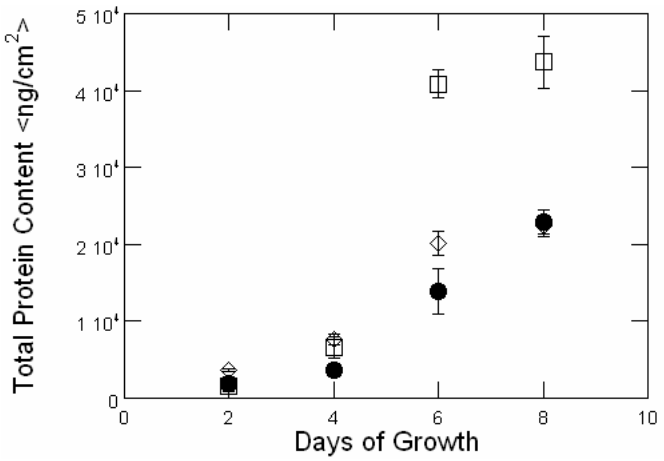

Figure 2.3: Total protein content of parental and IGF-I secreting bovine mammary epithelial cells

Total protein content of MAC-T (●), SV40-IGF-I (□), and TK-IGF-I (◊) cells plated on tissue culture inserts at an initial density of 5 x 10^4 cells/cm^2. Measurements (mean ± S.E., n=2) are representative of 3 independent experiments.

2.3.3 Effect of extracellular matrix (ECM) formation.

Since IGF-I can alter ECM production (151), studies were conducted to determine whether the ECM produced by the parental cells was responsible for differences in barrier properties between the parental and IGF-I secreting cells. Removal of the MAC-T cells nearly eliminated phenol red exclusion (89 ± 1 % of control) and yielded similar results to either the isolated ECM from SV40-IGF-I cells or intact SV40-IGF-I cells (90 ± 1 % and 91 ± 0.1 % of control, respectively).

2.3.4 Exogenous IGF-I or IGFBP-3 does not impact MAC-T barrier properties.

Since secretion of IGF-I is the primary difference between the autocrine and parental cells, studies were conducted to determine if addition of exogenous IGF-I could disrupt the ability of MAC-T cells to form a transport barrier. Addition of IGF-I, at levels comparable and higher to those secreted by SV40-IGF-I cells (162), did not alter the ability of MAC-T cells to form a restrictive barrier (Figure 2.4). However, differences in the IGF binding protein profiles from the MAC-T and SV40-IGF-I cells were also detected (Figure 2.5A). IGFBP-3 was not evident in either the apical or basolateral conditioned media from MAC-T cells but was abundant in the SV40-IGF-I samples (~250% apically and ~30% basolaterally more than complete media). To ascertain if

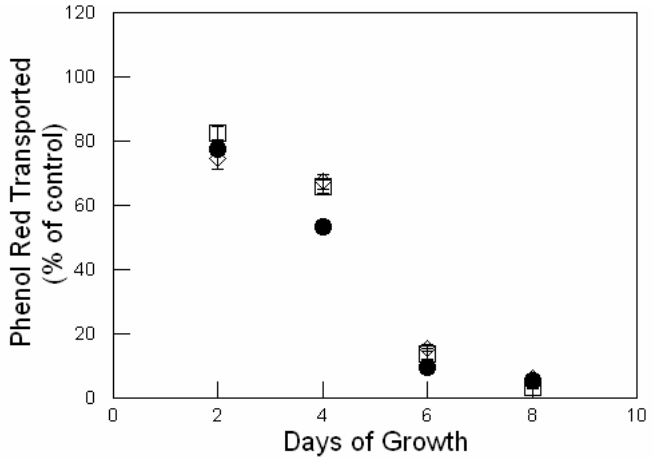

Figure 2.4: Phenol red transport across MAC-T in the presence of IGF-I

Phenol red transport across MAC-T cultured in complete DMEM supplemented every media change with 0 (●), 50 (□), or 100 ng/ml (◊) IGF-I plated on tissue culture inserts at an initial density of 5 x 10^4 cells/cm^2. Measurements (mean ± S.E., n=4) are representative of 3 independent experiments.

exogenous IGFBP-3 might alter the barrier properties of MAC-T cells, MAC-T cells were plated and incubated in complete media supplemented with IGFBP-3. Inclusion of exogenous IGFBP-3 did not impair the ability of MAC-T cells to form a restrictive barrier (Figure 2.5B).

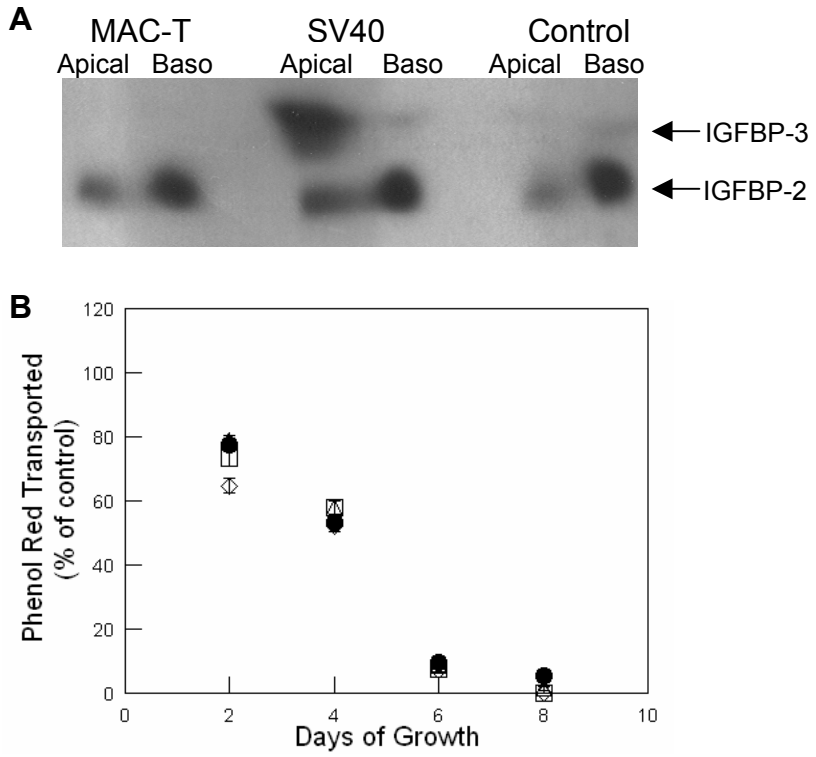

Figure 2.5: Affect of IGFBP-3 on phenol red transport

(A) Western ligand blot of MAC-T and SV40-IGF-I conditioned media and control (complete media). Conditioned media was collected from the apical (0.5 ml) and basolateral (1.5 ml) compartments and treated as described in the Materials and Methods. Blots are representative of 3 independent experiments. (B) Phenol red transport across MAC-T incubated with 0 (●), 10 (□), 100 (◇), and 1000 (△) ng/ml IGFBP-3. Measurements (mean ± S.E., n=4) are representative of 3 independent experiments.

2.3.5 Co-culture does not alter barrier properties.

IGF-I can induce secretion of a number of other effectors, such as vascular endothelial growth factor (27) and estradiol (97). In addition, it is reported ere that SV40-IGF-I cells secreted ~15% more apical and ~40% more basolateral IGFBP-2 than MAC-T cells (Figure 2.5A). Co-culture systems (Figure 2.1) were utilized to address whether these other factors might be responsible for the loss of phenol red exclusion. Inclusion of

SV40-IGF-I cells only slightly impacted phenol red exclusion by MAC-T cells cultured on either the upper or lower surface of the insert (Table 2.1). Similarly, inclusion of MAC-T cells did not alter the poor barrier properties of SV40-IGF-I, suggesting that a "barrier-promoting" factor was not being secreted by the parental cell line. The slight difference in barrier properties that was detected between cells in single culture cells and cells in co-culture is likely due to depletion of nutrients and accumulation of cellular waste products within the culture media since changes in media color that were noticed within the testing period were not seen in the single culture systems. There was no difference in phenol red exclusion between cells cultured on either the basolateral or apical surface of the insert, which suggested that there was no polarity in response to factors secreted by cells on the tissue culture well.

Table 2.1: Phenol red transport across MAC-T in single culture and in co-culture with SV40-IGF-I cells.

Measurements (mean ± S.E., n=4) are representative of 3 independent experiments and are normalized to % of inserts without cells.

Days of	Apical Surface		Basolateral Surface	
Growth	Single Culture	Co-culture	Single Culture	Co-culture
2	68 ± 6 %	74 ± 7 %	93 ± 5 %	98 ± 5 %
4	20 ± 2 %	23 ± 3 %	40 ± 12 %	49 ± 11 %
6	7 ± 1 %	38 ± 13 %	15 ± 2 %	34 ± 11 %
8	4 ± 1 %	13 ± 4 %	16 ± 1 %	29 ± 4 %

2.3.6 Decreased IGF-IR binding for parental cells at day 8.

Previous work indicated that, on tissue culture plastic, SV40-IGF-I cells had reduced IGF-IR binding when compared to the MAC-T cells (162). Since IGF-IRs have been shown to influence cell-cell adhesion (125), binding of IGF-I to IGF-IR was compared after 4 and 8 days in culture (Figure 2.6A). Receptor binding studies were conducted in the presence of Y60L-IGF-I, an analog with normal affinity to IGFBPs but minimal

affinity for IGF-IR (16), to block binding of tracer to IGFBPs. MAC-T cells bound significantly more ^{125}I-IGF-I per cell than either of the IGF-I secreting cell lines at day 4 which is in agreement with the previous studies for cells cultured on plastic. However, significantly less IGF-IR binding to the parental cells than either autocrine cell line on day 8 was measured ($p < 0.05$). Further, this change was not due to an increase in IGF-IR capacity for the IGF-I secreting cell lines but to a downregulation by parental cells, suggesting that the decreased IGF-IR was advantageous for phenol red transport inhibition. Verification that reduced binding correlated with reduced protein levels was performed through western immunoblotting (Figure 2.6B). After 8 days in culture, levels of IGF-IR in the parental cells were below detection while SV40-IGF-I cells expressed

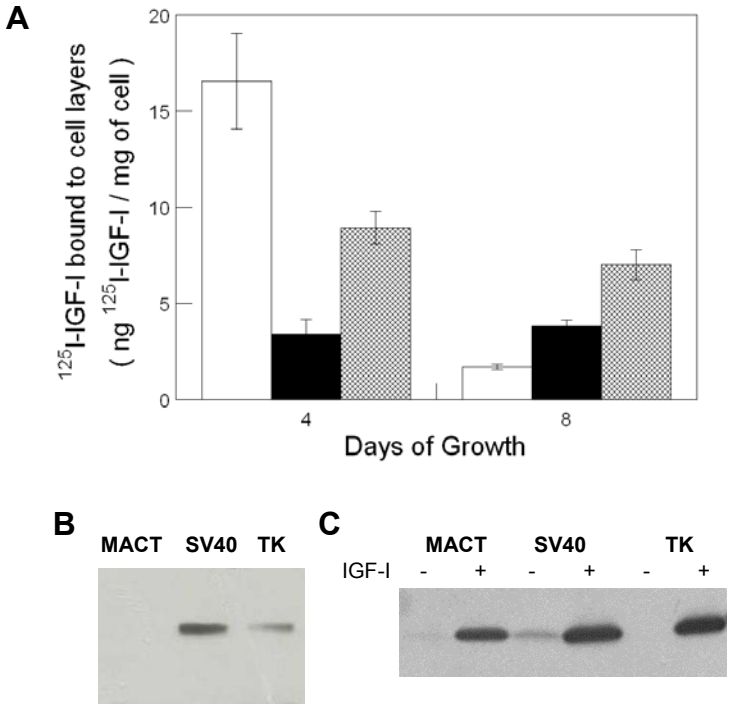

Figure 2.6: MAC-T cells express reduced levels of IGF-IR at Day 8.

A. Binding of ^{125}I-IGF-I to MAC-T (□), SV40-IGF-I (■), and TK-IGF-I (⊗) cells at 4ºC after 4 or 8 days in culture. Measurements (mean ± S.E., n=2) are representative of 3 independent experiments. B. Western immunoblot of MAC-T, SV40-IGF-I, and TK-IGF-I cell lysates probed for IGF-IRβ. Cells were plated on tissue culture inserts at 5 x 10^4 cells/cm^2, lysed after 8 days of culture, and probed. C. Western immunoblot of MAC-T, SV40-IGF-I, and TK-IGF-I cell lysates probed for phospho-Akt on day 8 ± IGF-I (100 ng/ml).

the most IGF-IR, three times that of TK-IGF-I cells (Figure 2.6A). Despite the reduced levels measured, IGF-IRs on the parental as well as the autocrine cells were responsive to IGF-I as evident by phosphorylation of Akt (Figure 2.6C). In addition, there was some endogenous phosphorylation of Akt in the SV40-IGF-I cells that was not evident with either the TK-IGF-I cells or MAC-T cells.

2.3.7 Autocrine cells express reduced levels of adherens and tight junction proteins.

Since cell-cell junctions regulate transport barriers, western immunoblots were conducted to identify the junction proteins associated with the differences in barrier properties between parental and IGF-I secreting cells. A decrease in the tight junction protein occludin was found for the autocrine cells when compared to the parental cell lines (Figure 2.7A). Further, expression of the adherens junction protein E-cadherin and its intracellular binding partner β-catenin were also reduced when compared to the parental cell line (Figure 2.7B and C). Specifically, TK-IGF-I cells had approximately 50% less occludin, 20% less E-cadherin and 20% less β-catenin than MAC-T cells and SV40-IGF-I cells had approximately 50% less occludin, 90% less E-cadherin and 40% less β-catenin than MAC-T cells.

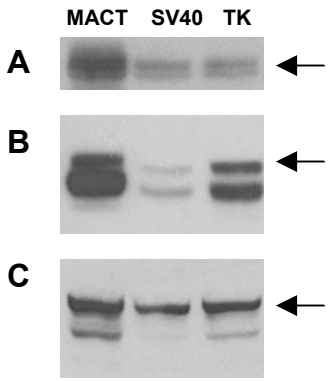

Figure 2.7: Autocrine cells have decreased levels of adherens and tight junction proteins.

Western immunoblots of MAC-T, SV40-IGF-I, and TK-IGF-I cell lysates. Cells were plated on tissue culture inserts at 5 x 10^4 cells/cm^2, lysed after 8 days of culture, and probed for occludin (A), E-cadherin (B), and β-catenin (C). Arrows indicate the expected molecular weights of occludin (65 kDa), E-cadherin (120 kDa), and β-catenin (92 kDa).

2.4 Discussion

Growth factors and their receptors, including IGF-I and IGF-IR, are capable of altering cell barrier formation (76, 146, 183) but that effect can be cell type specific. For example, McRoberts et al. report increased permeability in human colonic epithelial cell after 2 days of basolateral exposure to IGF-I (130). However, Ericson et al. did not detect any significant increase in permeability of pig thyrocytes until after 16 days of treatment and the increase was only a partial loss of barrier properties, not the nearly complete loss reported by McRoberts et al. (130). This report shows that autocrine production, but not exogenous treatment, of IGF-I in mammary epithelial cells increased paracellular permeability (Figure 2.2). Moreover, this was accompanied by reductions in occludin, E-cadherin and β-catenin expression levels (Figure 2.7).

Various growth factors, such as fibroblast growth factor (FGF) (158), transforming growth factor (117), and hepatocyte growth factor (87) have been reported to decrease levels of occludin, resulting in increased paracellular permeability, However, until now, there has been little reported on the effect of IGF-I on occludin expression levels. Recent studies have suggested a relationship between increased paracellular permeability and expression of cadherins (57, 141, 181, 186). Zabner et al. report that treatment of various types of epithelial cells with histamine resulted in increased permeability that was attributed to a reduction in E-cadherin-mediated junctions, not tight junctions (200). Further, blocking peptides to the EC-1 domain of E-cadherin produced a three fold increase in the permeability of Madin-Darby canine kidney epithelial cells (169). E-cadherin co-localizes at tight junctions (195), which have traditionally been thought to regulate paracellular transport (177). This report shows that IGF-I secreting cells expressed less E-cadherin than the non-IGF-I secreting parental cell line and that this expression is inversely correlated with the level of IGF-IR. Further, lost E-cadherin expression was coincident with increased paracellular permeability and seemingly dependent on the amount of IGF-I secreted as the highest IGF-I secreting cell line expressed the least amount of E-cadherin but the most IGF-IR. In contrast, Mauro et al. found that overexpression of IGF-IR in MCF-7 cells did not change E-cadherin or β-catenin expression but altered ZO-1 levels (124). Interestingly, Guvakova et al. report

that overexpression of IGF-IR in MCF-7 cells did not change E-cadherin expression in *most* clones, however, decreased expression was detected in one clone following treatment with IGF-I (72). Further, expression of E-cadherin co-localized with IGF-IR in these MCF-7/IGF-IR cells. Andre et al. report that the expression levels of E-cadherin, α-catenin, and β-catenin in human colonic adenocarcinoma cells were not altered following treatment with des(1-3)IGF-I, however, there was increased tyrosine phosphorylation of these junction components, which has been shown to decrease cell-cell adhesion (5). This suggested that the pattern of expression and phosphorylation as well as the total expression of junction components should be considered.

Increased cell layer permeability and decreased expression of E-cadherin have been detected in a variety of metastatic cells, suggesting a relationship between loss of cell-cell contact and tumor progression. Normal cells, upon reaching confluence, undergo contact growth inhibition whereby signaling cascades are initiated when E-cadherin molecules on adjacent cells adhere to each other and β-catenin is sequestered away from the nucleus into the plasma membrane (68). Dietrich et al. measured a 9 fold increase in E-cadherin and a 4 fold increase in β-catenin expression in confluent cultures of human keratinocyte and rat epithelial cells, and a translocation of β-catenin from intracellular regions to the plasma membrane with increasing cell density (38). The studies reported here suggest there is cell-cell contact mediated downregulation of IGF-IR in parental cells but not IGF-I secreting cells, despite similar and higher cell densities (Figure 2.3). The connected between increased expression of E-cadherin and β-catenin is unclear. Playford et al. report that IGF-I treatment of colorectal cancer cells rapidly disrupted the E-cadherin/β-catenin interaction and resulted in sequestration of β-catenin from the plasma membrane to the nuclear portion (148), suggesting IGF-I may impact contact-dependent growth inhibition by disruption of cell-cell contacts.

Growth factor action can occur through several different mechanisms. In autocrine signaling, growth factors are secreted by cells and released to the extracellular environment, whereby they bind to and activate growth factor receptors on the cell surface (173). However, with intracrine signaling, stimulation occurs before the growth

factor can be released to the extracellular environment via interaction with intracellular receptors (156). In recent years, there has been a growing interest in intracrine signaling, particularly with regard to the EGF (197), FGF (21, 175) and IGF (41, 112, 185) families. In the studies reported here, addition of exogenous growth factors and other effectors, such as IGFBP-3, failed to alter the barrier properties of parental cells, suggesting that intracrine, and not autocrine, actions could account for differences in cell-cell contact for the IGF-I secreting and non-IGF-I secreting cell lines. However, at this time signaling through autocrine IGF-I localized proximal to the cell surface can not be ruled out.

In conclusion, autocrine production of IGF-I, possibly through intracrine signaling, reduced cell connectivity in mammary epithelial cells. Non-IGF-I secreting cells formed a nearly exclusive transport barrier that was unaltered by exogenous factors secreted by IGF-I secreting cells. Further, parental cells expressed downregulated levels of IGF-IRs with increasing cell density. In comparison, IGF-I secreting cells exhibited increased paracellular permeability, as well as reduced expression of the cell-cell junction components, E-cadherin and β-catenin, but IGF-IR expression remained constant with increasing cell density. These results suggest an intracellular regulation of cell-cell contact, possibly through IGF-I/IGF-IR action.

2.5 Acknowledgments

We also want to express our appreciation to Pat Boyle for her technical assistance. We are grateful for financial support from the National Science Foundation (NSF Career Grant 9875626), the Commonwealth Health Research Board, and DuPont (Young Faculty Award).

Chapter 3: Surface coating and plating density impact properties of *in vitro* model endothelium

Julie D. Paye, Laura J. Delo, Kimberly F. Williams*
Department of Chemical Engineering
Virginia Polytechnic Institute & State University

* To whom correspondence should be addressed

Department of Chemical Engineering
133 Randolph Hall
Blacksburg, VA 24061
Phone: (540) 231-4851
FAX: (540) 231-5022
kfw@vt.edu

3.1 Abstract

Establishment of an *in vitro* cell model is dependent on many factors including surface coating, plating density, and culture time. The model reported here utilizes bovine aortic endothelial cells (BAEC) cultured on coated Transwell® inserts. Assessment of monolayer integrity was determined by transmonolayer electrical resistance (TER), phenol red transport, and expression and organization of occludin. BAEC were plated at different densities ($5x10^4$, $1x10^5$, $2x10^5$ cells/cm^2) on Transwell® inserts, either uncoated or coated with rat tail collagen, rat tail collagen and fibronectin, or gelatin. BAEC plated at $5x10^4$ cells/cm^2 on rat tail collagen and fibronectin (RTCF) coated inserts formed the most restrictive barrier. After 8 days of culture under these conditions, the BAEC monolayer had a peak TER of 37 ± 11 ohms-cm^2 and limited the transport of phenol red. For each surface coating, BAEC plated at $5x10^4$ cells/cm^2 had approximately three fold higher expression of occludin per cell than BAEC plated at $1x10^5$ cells/cm^2. Cells cultured on RTCF coated inserts expressed the most occludin, twice as much as cells cultured on uncoated inserts. This increased expression of occludin was accompanied by enhanced formation of tight junctions, as determined by confocal imaging. This paper outlines an *in vitro* model for endothelium transport barrier and demonstrates that increased expression of occludin is involved in this enhancement.

3.2 Introduction

Endothelial cells line the inside of blood vessels and regulate the transport of compounds from the bloodstream to the underlying tissues. Large blood vessels are composed of three concentric layers. The innermost layer (tunica intima) has intimate contact with the bloodstream and is composed of a monolayer of endothelial cells on top of subendothelial connective tissue (63). As the innermost layer of the blood vessel, endothelial cells form the primary barrier to transport from the bloodstream to the underlying tissues (64, 91, 147). Transport through this layer can occur through two pathways; passively between adjacent cells or actively through the cells. A drug transported actively through the cell must first enter the cell (endocytosis), avoid digestion within the cell, and finally be transported to the other side of the cell (exocytosis): a process known as transcytosis.

Endothelial cells attach to and communicate with each other through a series of junctions. The junction complexes closest to the bloodstream are called tight junctions. The tight junctions form a dynamic barrier between neighboring endothelial. The tight junctions are formed by interactions between intermembrane proteins, such as occludin, from neighboring cells that bind one another (36, 86). It has been suggested that occludins regulate transendothelial electrical resistance and paracellular permeability (7, 80, 86, 87, 126, 187). In addition, collagen and other extracellular compounds can directly influence the transendothelial transport of proteins such as albumin via binding interactions (37, 118, 121).

Several methods exist for characterizing the permeability of a cell monolayer *in vitro*. Transmonolayer electrical resistance (TER) has been a popular method for evaluating the barrier properties of epithelial and endothelial cells in culture (14, 34, 91). This method evaluates the ability of small charged particles to pass between adjacent cells. Another method of monitoring the permeability of cell monolayers is by measuring the transport of phenol red, a pH indicator with a molecular weight ~250 (198). One assumption inherent with both methods is that transport primarily occurs through paracellular and not intracellular transport.

In culturing endothelial cells *in vitro*, various parameters may affect the properties of the cells. For example, cells have been shown to have altered behavior when cultured on surfaces coated with different compounds (37, 61, 155, 184, 188), plated at different initial cell densities (90, 159), at different periods of culture time (13, 155) and with different cell types (80, 92, 118, 131). All of these parameters need to be optimized in order to develop a reliable and accurate *in vitro* model of the *in vivo* endothelium. Since there is interest in modeling the human endothelium, it is only natural to investigate the use of human endothelial cells *in vitro*. However, due to cost and ease of culture, bovine endothelial cells also provide an excellent model mammalian cell system.

Both of these cell types were investigated in the development of an optimized *in vitro* cell culture based model endothelium. Assessment was based on the ability of the cells to form a confluent cell layer in a timely manner that was restrictive to the transport of compounds paracellularly. Human aortic endothelial cells (HAEC) were tested but proved to be very unreliable due to issues with reproducibility of TER measurements. Human microvascular endothelial cells (HMVEC-L)m derived from the lung, performed fairly well *in vitro* but were not as easy to culture as bovine aortic endothelial cells (BAEC). BAEC formed the best barrier to transport and proved to be an easy and reliable cell type to culture. BAEC plated at $5x10^4$ cells/cm^2 plated on RTCF coated inserts formed the best barrier properties as assessed by TER measurements and phenol red transport.

3.3 Materials and Methods

3.3.1 Endothelial cell culture.

Pooled bovine aortic endothelial cells (BAEC) were purchased from Clonetics (Walkersville, MD) and grown in DMEM (Mediatech, Herndon VA) with 10% calf serum (Hyclone, Logan UT), 2 mM glutamine (Mediatech) and 50 units/ml of penicillin/streptomycin (Mediatech). BAEC were used between passages 6-10. Human aortic endothelial cells (HAEC) were purchased from Cascade Biologics (Portland, OR) and grown in the recommended media of Medium 200 and low serum growth supplement (Cascade Biologics) with the addition of 50 units/ml of penicillin/streptomycin. HAEC were isolated from a 17 year old male and received cryopreserved at passage 4. HAEC cultures were used between passages 8-10. Human microvascular endothelial cells derived from the lung (HMVEC-L) were purchased from Clonetics and grown in the recommended media of EGM-2-MV (Clonetics). HMVEC-L were isolated from a 31 year old Caucasian male and received cryopreserved at passage 4. HMVEC-L cultures were used between passages 8-10. Bovine mammary epithelial cells (MAC-T) were cultured as described previously (161). Human colon carcinoma cells (C2BBe1) were cultured in DMEM with 1.5 g/L sodium bicarbonate, 0.001mM sodium pyruvate, 10 mg/L transferrin, and 10% FBS.

3.3.2 Coating of inserts.

Inserts were coated with collagen and fibronectin as previously described (20). Briefly, rat tail collagen (BD Bioscience, Franklin Lakes, NJ) was diluted with sterile 0.02N acetic acid to yield a final concentration of 2 mg/ml. Transwell® inserts (Corning Costar, Cambridge MA) (12 mm, 0.4 μm pore size) were coated with collagen solution (106 μl) and allowed to air dry in a sterile hood for 12 hours. For inserts with collagen and fibronectin coating, superfibronectin (Sigma, St. Louis MO) was diluted with Dulbecco's Phosphate Buffered Saline (DPBS) (Mediatech) to yield a concentration of 50 μg/ml. After allowing collagen coated inserts to dry, superfibronectin solution (106 μl) was added to each Transwell® and incubated in a sterile hood for 30 min. Any remaining superfibronectin was aspirated and cells were plated.

Transwell® inserts (12 mm, 0.4 μm pore size) were coated with gelatin (Sigma) as previously described (131). Type I bovine skin gelatin was prepared as a 1 mg/ml solution and 106 μl was added to each insert. Inserts were allowed to air dry in a sterile hood for 12 hours before cell plating.

3.3.3 Transmonolayer electrical resistance.

Resistance measurements of membranes with and without cells were measured using Millicell-Electrical Resistance System (Millipore, Bedford MA) with a chop-stick style probe (35). Briefly, TER measurements were taken every two days before changing the media. The probe was sterilized in 70% ethanol for a minimum of 15 minutes and then equilibrated in sterile culture media prior to each use. Special care was taken to ensure proper orientation of the probe for each measurement and monitoring for drifting measurements in order to decrease error. Results were normalized to membranes with the appropriate coating maintained in culture without cells and to the surface area of the insert.

3.3.4 Phenol red transport.

The transport of phenol red was monitored based on a protocol described previously (198). Cells were plated on inserts at the desired concentration. Following four days in

culture, the media in the apical chamber was replaced with DMEM+ (DMEM with phenol red, 2 mM glutamine, 50 units/ml penicillin/streptomycin, and 10% calf serum). The media in the basolateral chamber was replaced with DMEM- (Phenol red free DMEM, 2 mM glutamine, 50 units/ml penicillin/streptomycin, and 10% calf serum). Cultures were incubated at 37°C for 12 hours and 1 ml samples were taken from the basolateral chamber and analyzed in a spectrophotometer at 479 nm. Apical and basolateral chambers were replaced with fresh DMEM+.

3.3.5 DNA quantification.

After completing phenol red transport studies, membranes were cut from the insert using a hypodermic needle and incubated in 500 µl trypsin (Mediatech) overnight. Following incubation, 500 µl of 2x DNA buffer (0.1 M Na_2HPO_4, 4 M NaCl, 0.004 M Na_2EDTA-$2H_2O$, pH 7.4) was added and samples were sonicated at setting 5 for 10 seconds using Model 60 Sonic Dismembrator (Fisher Scientific). Samples were combined with 1x DNA buffer (0.05 M Na_2HPO_4, 2 M NaCl, 0.002 M Na_2EDTA-$2H_2O$, pH 7.4) and Hoechst 33258 dye and analyzed using a DyNA Quant 200 (Hoefer, San Francisco, CA).

3.3.6 Western immunoblot for occludin.

Cells were grown on Transwell® inserts (12mm, 0.4 µm pore) for 8 days with media changed every 2 days. Cells were lysed and samples were collected. Briefly, membranes were washed twice with DPBS and lysed with 100 µl Laemmli buffer (1X) (Sigma). Insert membranes were gently scraped with a cell scraper (Costar) and crude lysates were removed. Samples were boiled for 10 min before loading into a pre-cast 10 well, 10% tris-glycine gel (Bio-Rad, Hercules, CA). DNA quantification was used to standardize sample loading. Gels were run for 1 hr 15 min at 100-125 V and equilibrated in transfer buffer (0.04 M tris base, 0.39 M glycine, 0.003 M SDS, 4% methanol) for 10 min. Following equilibration, gels were loaded into transfer tank and run at 50 V for 1.5 hrs to transfer samples to PVDF membranes. Membranes were then placed in blocking buffer (0.03 M tris HCl, 0.02 M tris base, 0.15 M NaCl, 0.5% Tween, 0.5% casein) with shaking overnight at room temperature. Following blocking, membranes were rinsed with TBS-T (0.03 M tris HCl, 0.02 M tris base, 0.15 M NaCl, 0.5% Tween) three times for 5 minutes

each. Membranes were then incubated in TBS-T with rabbit anti-occludin (1:5000) (Zymed, San Francisco CA) for 1 hour at room temperature. Following incubation, membranes were rinsed three time with TBS-T and incubated with HRP conjugated goat anti-rabbit (1:5000) (Zymed) for 45 min at room temperature. Membranes were then rinsed four times with TBS-T and developed with Pierce Super Signal Kit (Rockford, IL) for one minute. Blots were then exposed to Kodak X-OMAT radiography film (Sigma) and developed with Kodak chemicals. Analysis of blots was performed using Adobe Photoshop and UVP Gelworks 1D system.

3.3.7 Immunofluorescent staining and confocal imaging.

Cells were grown on Transwell® inserts (12mm, 0.4 μm pore) with media exchanged every 2 days. After 8 days of culture, cells were stained for occludin as described by the manufacturer (Zymed). Briefly, cells were fixed with neutral buffered formalin (3.7% formaldehyde, 45.8 mM Na_2HPO_4, 33.3 mM NaH_2PO_4) for 20 minutes. Membranes were then washed 3 times with DPBS and cut from the insert using a hypodermic needle. Cells were then permeabilized with 0.5% Triton in DPBS for 2 minutes and washed 3 times with DPBS. Cells were then incubated in 1:100 rabbit anti-occludin (Zymed) in DPBS for 1 hour and washed 3 times with DPBS. Cells were then incubated in 1:300 Cy3 goat anti-rabbit IgG conjugate (Zymed) in DPBS for 30 minutes in a dark area. After washing 3 times with DPBS, membranes were blotted dry and mounted with Permount (Fisher) on glass slides with cover slips with a 1.5 thickness number. Samples were viewed through a 40x water immersion lens on a Zeiss LSM 510 Laser Scanning Microscope (Zeiss, Thornwood NY) fitted with an inverted Axiovert 100 M. Samples were excited using a He/Ne laser with a wavelength of 543 nm.

3.4 Results and Discussion

3.4.1 Effect of surface coating

Since one of the main functions of the *in vivo* endothelium is to regulate transport from the bloodstream to underlying tissues (64, 139), it is important that an *in vitro* model system maintains those properties. Based on previous work by Biegel et al. (20) and Milton et al. (131), the studies presented here focused on the use of collagen, collagen-

fibronectin, and gelatin coated surfaces. The TER measurements of endothelial cells were altered by insert surface coatings (Figure 3.1). BAEC plated at 1 x 10^5 cells/cm^2 on RTCF coated membranes exhibited the highest TER with a peak resistance of 23 ± 5 ohms-cm^2 (Figure 3.1A). This peak value occurs after 8 days of culture and was similar to values found previously for HUVEC monolayers (91). Gelatin coated membranes promoted the highest TER values for HMVEC-L plated at 1 x 10^5 cells/cm^2 (Figure 3.1B) with a peak resistance of 22 ± 2 ohms-cm^2. However, when plated on RTC and RTCF coated membranes, HMVEC-L exhibited TER values even below that of uncoated membranes. HAEC plated at 1 x 10^5 cells/cm^2 on inserts coated with RTCF resulted in the highest average TER with a peak resistance value of 95 ± 66 ohms-cm^2. However, the larger error induced by HAEC cultured on RTCF precluded it from being used in further studies. It is not known why such a large standard error occurred since the same collagen and fibronectin solutions were used in the experiments with BAEC and HMVEC-L and a similar problem did not exist, but the error was reproducible. As shown in Figure 3.1C, there is little difference between the TER of HAEC plated on gelatin coated inserts and on non-coated inserts. The HAEC also appear to require more time to form a barrier to transport since, even after 16 days in culture, the TER had not peaked.

Since BAEC are easy to culture and exhibited consistent and high TER values, they were utilized in future investigations. The permeability of BAEC cultured on coated inserts was tested by monitoring the transport of phenol red from the apical media to the basolateral media. Similar to TER measurements (Figure 3.1), BAEC cultured on RTCF coated inserts formed the best barrier to the transport of phenol red (Table 3.1). RTCF coated inserts in the absence of cells formed a fairly exclusive barrier with similar permeabilities as gelatin and non-coated inserts in the presence of cells. The paracellular transport of bovine serum albumin conjugated Evans blue dye was also tested. However, there was no significant transport of albumin across membranes coated with collagen RTC and RTCF) even in the absence of cells. This may have been due to binding of Evans blue to collagen (75) although the concentrations used were previously shown not

to bind Evans blue (91). Since BAEC cultured on RTCF coated inserts formed the best transport barrier, the Evans blue albumin assay was excluded from future work.

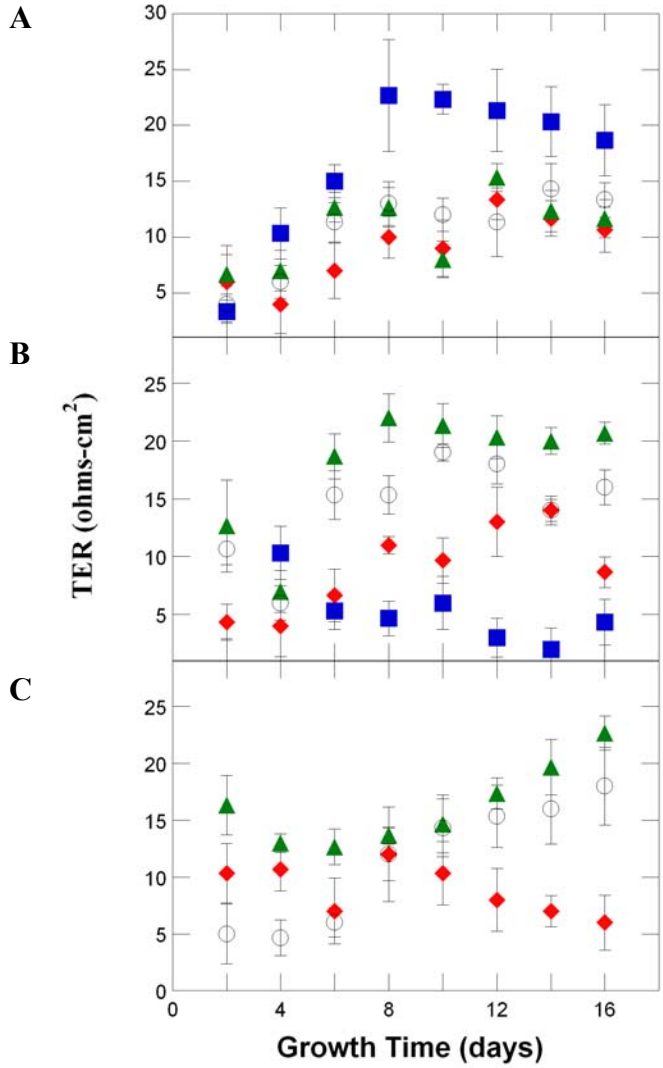

Figure 3.1: Transmonolayer electrical resistance of endothelial cells.

(A) Bovine aortic endothelial cells (BAEC), (B) human microvascular endothelial cells (HMVEC-L), and (C) human aortic endothelial cells (HAEC) were initially plated at 1 x 10^5 cells/cm^2 on rat tail collagen (RTC) (♦), rat tail collagen and fibronectin (RTCF) (■), gelatin (▲), or non (○) coated inserts. Measurements (mean ± SEM) are representative of 2 independent experiments and were normalized to coated membranes in the absence of cells and to the surface area

Table 3.1: Phenol red transported across bovine aortic endothelial cells

Absorbance (479 nm) of phenol red transported across coated and non-coated inserts in the presence and absence of cells plated at 1x105 cells/cm2. Measurements (mean ± S.E., n=3) are representative of 2 independent experiments.

Coating	With Cells (Absorbance)	No Cells (Absorbance)
Rat tail collagen	0.048 ± 0.001	0.050 ± 0.002
Rat tail collagen and fibronectin	0.044 ± 0.000	0.056 ± 0.001
Gelatin	0.054 ± 0.002	0.071± 0.002
None	0.056 ± 0.002	0.073 ± 0.002

3.4.2 Effect of cell number.

Following TER and phenol red transport measurements, BAEC plated on different surface coatings were analyzed for DNA content. As shown in Table 3.2, there was less DNA and consequently fewer cells on the inserts coated with RTCF than with any other coating. This is counterintuitive as these inserts formed the most exclusive barrier to transport. In addition, the inserts with the most number of cells (gelatin coated) formed the least exclusive transport barrier. Given this dependence on cell number, TER measurements were taken of BAEC plated at a ranged of densities (5×10^4, 1×10^5, 2×10^5 cells/cm^2) on RTCF coated inserts (Figure 3.2). Cells that were initially plated at 5×10^4 cells/cm^2 formed the most exclusive transport barrier with a peak resistance of 37 ± 11 ohms-cm^2. These results were verified by conducting phenol red transport studies with BAEC plated at different initial densities. BAEC plated at 5×10^4 cells/cm^2 prohibited the transport of phenol red to a greater extent than monolayers plated at other initial cell densities (Figure 3.3). This supports the results from DNA analysis, indicating that higher cell numbers do not correlate with improved transport barrier properties.

Table 3.2: Fluorometric DNA analysis of BAECs cultured on different surface coatings

DNA content (mean ± S.E., n=3) of BAE cells plated at $1x10^5$ cells/cm^2 on coated inserts after 8 days of culture. There is a significant different between all samples, except for between RTC and Gelatin (ANOVA $p < 0.05$).

Coating	DNA Content (μg/insert)
Rat tail collagen	6.99 ± 0.18
Rat tail collagen and fibronectin	5.52 ± 0.17
Gelatin	7.54 ± 0.18

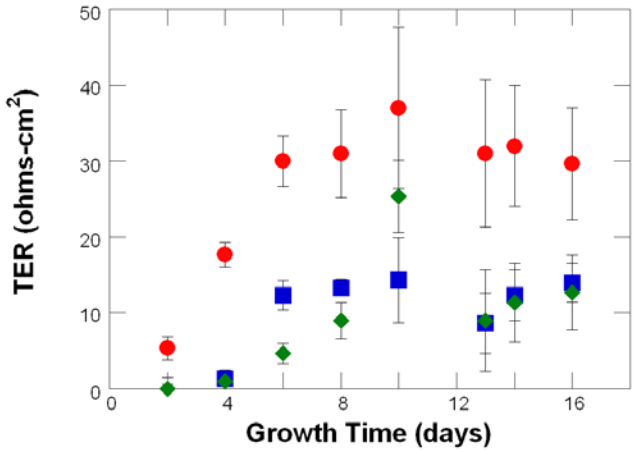

Figure 3.2: TER of BAECs plated on RTCF coated inserts at different densities

TER of BAECs plated on RTCF coated inserts at different densities $5x10^4$ (●), $1x10^5$ (■), and $2x10^5$ (♦). Measurements (mean ± S.E., n=3) were normalized to RTCF coated membranes in the absence of cells and to surface area and are representative of 2 independent experiments.

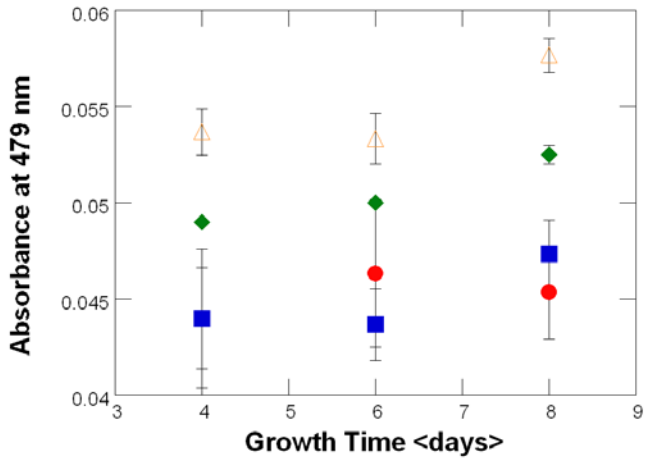

Figure 3.3:Phenol red transport across BAECs plated on RTCF coated inserts at different plating densities

Phenol red transport across BAE monolayers plated on RTCF coated inserts at different densities 5x104 (●), 1x105 (■), and 2x105 (♦) and across coated inserts in the absence of cell (△). Measurements (mean ± S.E., n=3) are representative of 2 independent experiments.

3.4.3 Western immunoblot of occludin.

In order to determine a possible mechanism for the counterintuitive increase in transport barrier formation with decreasing initial cell number, the expression of occludin, a primary tight junction protein, was investigated (Figure 3.4). Cells plated at $1x10^5$ cells/cm^2 (lanes 1- 4) expressed less occludin per cell than cells plated at $5x10^4$ cells/cm^2 (lanes 5-8) independent of the surface coating. Analysis of the western blot using densitometry (Table 3.3) confirmed that there was a significant difference in the expression of occludin for cells cultured on different surfaces and that the highest level was associated with BAEC cultured on RTCF coated inserts. There was at least a 3 fold increase in occludin expression for cells plated at $5x10^4$ cells/cm^2 than at $1x10^5$ cells/cm^2 irrespective of the coating.

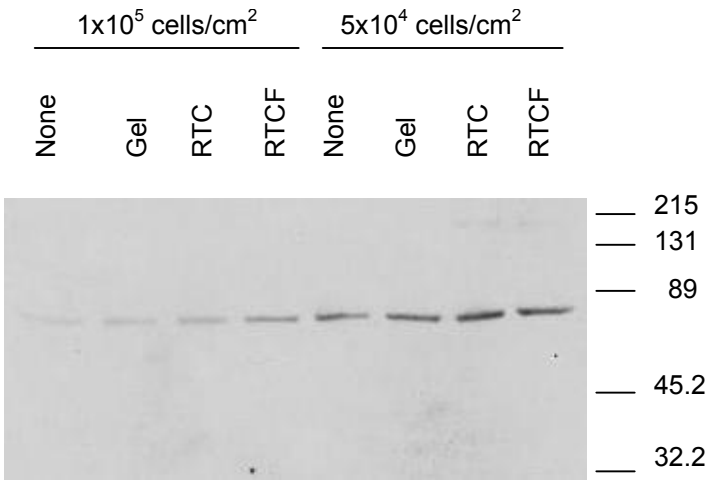

Figure 3.4 Western immunoblot for occludin using lysates from BAECs grown for 8 days on different surface coatings

BAECs plated at $1x10^5$ cells/cm^2 (lanes 1-4) and BAEC plated at $5x10^4$ cells/cm^2 (lane 5-8). Cells were plated on either non-coated inserts (lanes 1 and 5), gelatin coated inserts (lanes 2 and 6), RTC coated inserts (lanes 3 and 7), or RTCF coated inserts (lanes 4 and 8). Results are representative of 2 independent experiments.

Table 3.3: Densitometer analysis of western immunoblot for occludin

Densitometry analysis of western blot for occludin of lysates of BAE cells plated at $1x10^5$ cells/cm^2 and $5x10^4$ cells/cm^2. Results are normalized to lysate from BAE cells plated on non-coated inserts at $1x10^5$ cells/cm^2. Measurements are representative of 2 independent experiments.

	None	Gelatin	RTC	RTCF
1×10^5 (cells/cm^2)	100%	124%	148%	221%
5×10^4 (cells/cm^2)	320%	517%	646%	666%

3.4.4 Immunofluorescent staining and confocal imaging.

Since the formation of the barrier properties of epithelial and endothelial cells is dependent on the organization of the tight junctions, not only the expression of tight junction proteins, the organization of occludin was investigated through confocal imaging of cells stained with fluorescent occludin. As a control, a clone of Caco-2 cells (C2BBe1), a human epithelial cell line that is known to form organized tight junctions (39, 49), was tested. As shown in Figure 3.5A, C2BBe1 exhibited the expected peripheral staining and cobblestone morphology. Since the manufacturer of the antibody did not explicitly report reactivity with bovine cells, a bovine epithelial cell type was also tested since epithelial cells are known to form exclusive and organized tight junctions (118) than endothelial cells. As shown in Figure 3.5B, bovine epithelial cells do exhibit the expected staining and morphology, indicating the antibody works with bovine cells. When plated at 1 x 10^5 cells/cm^2 on RTCF coated inserts, BAEC did not exhibit any peripheral fluorescent staining and did not have the expected cobblestone morphology (Figure 3.5C). The entire cell, with the exception of the nucleus, was fluorescently stained and the cells appeared to be stretched out and isolated from each other. This is not indicative of good cell-cell interactions, a necessary component for the formation of an effective transport barrier. Since the barrier function of BAEC was improved when plated at 5 x 10^4 cells/cm^2 (Figure 3.3), cells plated at this density were also fluorescently stained. As shown in Figure 3.5D, the morphology of the cells is more cobblestone and some peripheral staining is evident. This indicates that the cells were in close proximity to each other and provides morphological evidence to support TER and phenol red measurements.

The optimized *in vitro* model present here utilized BAEC cultured on collagen-fibronectin coated membranes (Figure 3.1A). Under these culture conditions, good transport barrier properties, as indicated by a peak TER of 37 ± 11 ohms-cm^2, were evident after 8 days of culture (Figure 3.2). This peak value is comparable to TER values

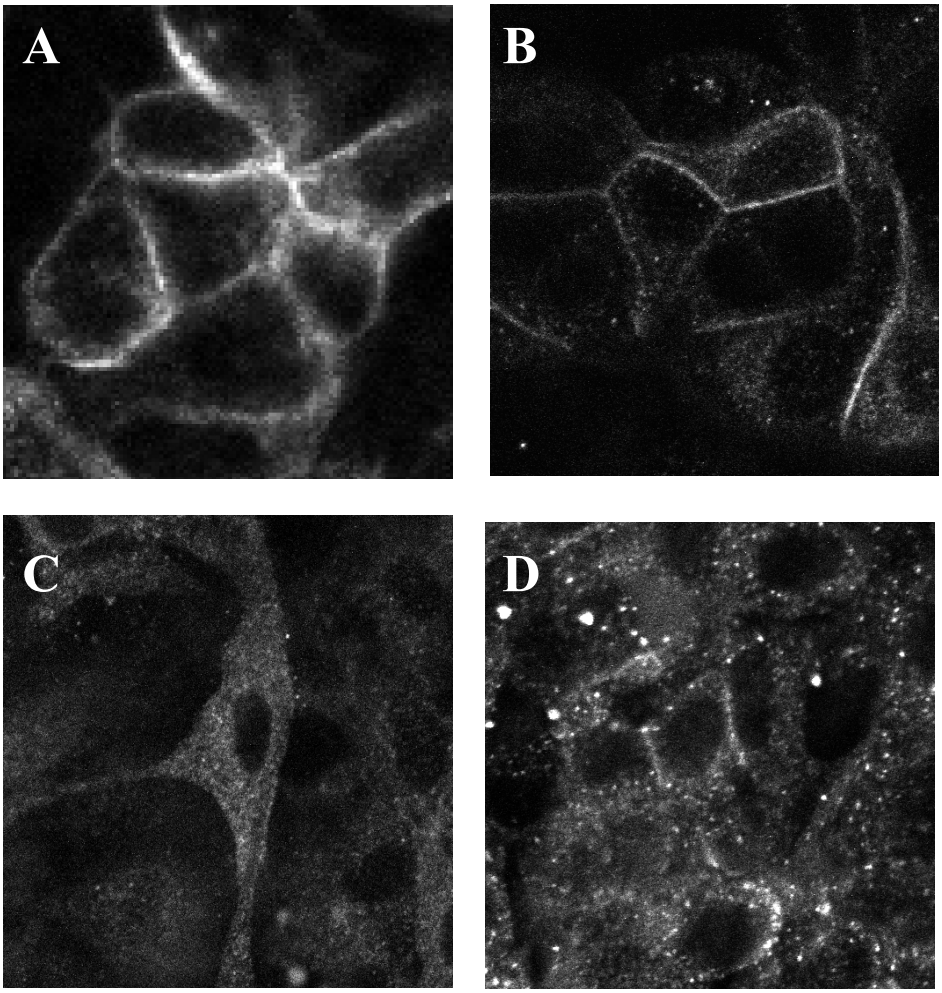

Figure 3.5: Confocal images of cells fluorescently stained for occludin

Confocal images of (A) human colon epithelial (C2BBe1) cells plated at 1x105 cells/cm2, (B) bovine mammary epithelial (MAC-T) cells plated at 5x104 cells/cm2, (C) BAECs plated on RTCF coated inserts at 1x105 cells/cm2, and (D) BAECs plated on RTCF coated inserts at 5x104 cells/cm2. Images C and D are representative of 2 independent experiments. Images are all shown at the same magnification.

reported for non-neural endothelial cells, which range from 3-33 ohms-cm^2 (61) and optimum after 8 days (131). Others, such as Del Vecchio et al. have also reported decreased permeability of sheep endothelial cells when cultured on collagen or collagen-fibronectin in comparison with endothelial cells cultured on gelatin (37). The collagen-fibronectin coating has also been reported to be the optimal coating for the establishment of *in vitro* models of the blood-brain barrier (61) and to enhance barrier function due to

increased cell adhesion (118). It appears to also be optimal for large-vessel bovine vascular cells in culture.

The use of phenol red to determine permeability has been widely used with epithelial, but not endothelial cells (198). The similar results from the TER measurements (Figure 3.2) and phenol red transport measurements (Figure 3.3) conducted in this study suggest that phenol red is a suitable method of measuring permeability for cultured endothelial cells. Further, phenol red measurements were more precise and reproducible. Both TER and phenol red measurements indicated that BAEC plated at $5x10^4$ cells/cm^2 on RTCF coated inserts formed more restrictive transport barriers. In contrast, Kazakoff *et al.* (91) found that inulin flux across HUVEC monolayers was inversely related to plating density. Their studies however were done after 48h incubation rather than 8 days as in the studies presented here. In order to determine a possible mechanism for improved barrier properties, the expression level and organization of occludin was investigated. There have been mixed reports concerning occludin expression in non-neural endothelial cells (80, 92). Hirase *et al* report weak staining for occludin in porcine aortic endothelial cells (80) while Kevil *et al* report strong intercellular occludin staining in human arterial endothelial cells (92). The cell model reported here exhibits higher occludin expression as detected by western immunoblotting, than any other culture conditions tested (Figure 3.4). This increased occludin expression level was accompanied by a cobblestone morphology and some peripheral staining (Figure 3.5D), indicating better organization. In conclusion, this study provides evidence for an improved *in vitro* endothelium based on surface coating, plating density, and culture time.

3.5 Acknowledgments

We are grateful to Dr. R. Michael Akers for his help with the cell counting and for the use of the densitometer. We also want to express our appreciation for assistance from Dr. Brian Storrie and Dr. Kristi DeCourcy in developing the protocol for fluorescently labeling the samples and viewing them using the confocal microscope. We are grateful for financial support from the National Science Foundation (NSF Career Grant 9875626 (KFW)).

Chapter 4: Delivery of insulin-like growth factor-I (IGF-I) across the endothelium: Regulation by IGF binding proteins

Julie D. Paye[1] AND Kimberly F. Williams[1*]

[1]Department of Chemical Engineering

Virginia Polytechnic Institute & State University

Blacksburg, Virginia

*Correspondence to:

Kimberly F. Williams

Department of Chemical Engineering

Virginia Polytechnic Institute & State University

133 Randolph Hall

Blacksburg, VA 24061

(540) 231-4851 (office)

(540) 231-5022 (FAX)

kfw@vt.edu

Running Head: Regulation of IGF-I Transport by IGFBPs

5 Figures

2 Tables

Contract grant sponsor: National Science Foundation; Contract grant number:BES9875626

4.1 Abstract

Delivery of growth factors via the bloodstream for the treatment of various pathological conditions may be regulated through interactions with growth factor receptors. However, a better understanding of the kinetics of growth factor binding and transport by endothelial cells is required. This report quantifies the binding, internalization, and transport kinetics involved in trafficking of insulin-like growth factor-I (IGF-I) across an *in vitro* monolayer of bovine aortic endothelial cells (BAEC). Cell culture conditions have been optimized to minimize effects of paracellular transport. Internalization and transport via IGF receptors (IGF-IR) was detected and binding analysis indicated that insulin-like growth factor binding proteins (IGFBPs), either on the cell surface or extracellular matrix, are the main vehicle for IGF-I binding in this system. There were twice as many IGFBP binding sites ($8.0 \pm 1.9 \times 10^4$ per cell) as IGF receptors (IGF-IR) ($3.9 \pm 0.6 \times 10^4$ per cell). Internalization of IGF-I by IGFBPs was not detected and IGFBP binding was shown to inhibit rather than enhance IGF-I transport. However, based on computational modeling, it is proposed that IGFBPs function as a reservoir for IGF-I, sequestering it for later release and IGF-IR-mediated transport. This reservoir function of the IGFBPs might be used to promote controlled localized delivery of IGF-I.

4.2 Introduction

Growth factors, such as insulin-like growth factor-I (IGF-I), are important regulators of cell division and tissue proliferation and, consequently, are important in embryonic development (4, 43), wound healing (144), as well as in the development and treatment of various pathological conditions (6, 42, 73, 76, 96, 98, 99, 108, 136, 137, 149, 152-154, 179, 183). In particular, low levels of insulin-like growth factor-I (IGF-I), a polypeptide member of the insulin/IGF family, have been associated with Laron syndrome (101), Gaucher disease (160), and diabetes (42, 96, 137, 152). Since intravenous infusions of IGF-I have been utilized to treat these diseases (71, 135), an understanding of the mechanisms involved in the transport of IGF-I from the bloodstream to underlying tissues may foster the development of better treatment strategies utilizing this growth factor. Endothelial cells, which line the inside of blood vessels, constitute the primary barrier

against transport from the bloodstream and thus are important in regulating the delivery of circulating IGF-I to tissues.

The actions of IGF-I are mediated by high affinity interactions with IGF cell surface receptor (IGF-IR) and with IGF binding proteins (IGFBPs). There are six known IGFBPs and they have been shown to participate, to varying degrees, in IGF-inhibiting, IGF-enhancing, and IGF-independent actions (22, 30, 32, 44, 46, 50, 70, 127-129). While several IGFBPs bind to cell surfaces with high affinity, IGFBP receptors have not yet been identified, although it has been suggested that the type V transforming growth factor β receptor and membrane-bound matrix metalloprotease-9 may also function as a receptors for IGFBP-3 (104, 105, 132).

It remains unclear how IGF-I is transported across the endothelium. IGF-I has been shown to bind to endothelial cells both *in vitro* (94) and *in vivo* (10, 23). *In vitro* studies with human umbilical vein endothelial cells (HUVECs) indicated that IGF-I was transported across the cell layer (14). However, this transport was not affected by blocking antibodies against IGF-IR or by excess IGF-I, suggesting the transport was, in their *in vitro* system, mediated by the paracellular pathway.

Since IGF-I can bind to both cell surface IGF-IRs and cell or matrix associated IGFBPs, an experimental system has been developed that minimizes paracellular transport and distinguishes between IGF-IR and IGFBP mediated binding. This allows quantification of the binding, internalization, and transport kinetics involved in trafficking of IGF-I across a monolayer of bovine aortic endothelial cells (BAEC). This reports shows that IGF-I binds primarily to non-IGF-IR sites and, once bound to these sites, is not internalized or transported. This suggests that surface IGFBPs may act as a reservoir for IGF-I within the blood vessel. Using computational modeling based on the experimental system, it was determined that both increased and decreased IGF-I transport, compared to cells in the absence of IGFBPs, is possible depending on the IGF-I delivery pulse time.

4.3 Materials and Methods

4.3.1 Materials

Pooled bovine aortic endothelial cells (BAEC) were obtained from Clonetics (Walkersville, MD). Dulbecco's modified eagles media (DMEM) was purchased from Gibco (Walkserville, MD). Dulbecco's phosphate buffered saline (DPBS), glutamine, and penicillin/streptomycin were obtained from Mediatech (Herndon, VA). Bovine calf serum was purchased from Hyclone (Logan, UT). Rat tail collagen was purchased from BD Bioscience (Franklin Lakes, NJ), superfibronectin and insulin were purchased from Sigma (St. Louis, MO), and Transwell® inserts (12 mm, 0.4 μm pore size) were purchased from Corning Costar (Cambridge, MA). Insulin-like growth factor-I (IGF-I) was obtained from Peprotech (Rocky Hill, NJ), Y60L-IGF-I was obtained from Upstate (Lake Placid, NY) and LongR3-IGF-I was obtained from GroPep (Adelaide, Australia). Compounds were radiolabeled using a chloramine-T method as described previously (2). ^{3}H-inulin was purchased from Perkin Elmer (Boston, MA).

4.3.2 Cell Culture

BAEC were grown in DMEM supplemented with 10% calf serum, 2 mM glutamine and 50 units/ml of penicillin/streptomycin. The cells tested positive for acetylated LDL uptake and negative for mycoplasma, bacteria, yeast, and fungi, as indicated by the manufacturer. BAEC cultures were used between passages 6-15.

4.3.3 Coating of inserts

Tissue culture inserts were coated with collagen and fibronectin as previously described (20). Briefly, rat tail collagen was diluted with sterile 0.02 N acetic acid to yield a final concentration of 2 mg/ml. Transwell® inserts were coated with 106 μl of 2 mg/ml collagen solution and allowed to air dry in a sterile hood for 12 hours. Superfibronectin, a recombinant form of fibronectin with enhanced adhesive properties that mimic the *in vivo* properties of fibronectin (134), was diluted with DPBS to yield a concentration of 50 μg/ml. After allowing collagen coated inserts to dry, inserts were rinsed with DPBS and 106 μl of 50 μg/ml superfibronectin was added to each Transwell®. After 30 min of

incubation in a sterile hood, any remaining superfibronectin was aspirated and cells were plated.

4.3.4 IGF-I Transport

Cells were plated on rat tail collagen and fibronectin (RTCF) coated Transwell® inserts at a plating density of $5x10^4$ cells/cm^2 and were maintained in culture with media replenished every 2-3 days. Prior to study, cells were washed with DPBS and switched to serum-free media for 12 hrs. Cells were then washed with DPBS and binding buffer (0.05% gelatin, 120 mM NaCl, 5 mM KCl, 1.2 mM $MgSO_4$, 15 mM sodium acetate, 25 mM Hepes, 10 mM Dextrose, pH 7.4) was added to the apical and basolateral chambers. Treatments (IGF-I (2 μg/ml), Y60L-IGF-I (2 μg/ml), or insulin (10 μg/ml)) were added to apical and basolateral chambers, as indicated in figures, and cells were incubated at 37°C for 20 minutes. Following incubation, ^{125}I-IGF-I, ^{125}I-Y60L-IGF-I, or ^{125}I-LongR3-IGF-I (4 ng/ml) was added to apical chambers. Cells were then incubated at 37°C for 12 hrs with samples taken every 3 hours from the basolateral chamber and replenished with binding buffer and the appropriate treatment. After 12 hours, both apical and basolateral samples were collected. Samples from all time points were subjected to degradation analysis by TCA/PTA precipitation, as described below, and counted in a COBRA II Auto-Gamma counter (Perkin Elmer Life Sciences, Downer Grove IL).

4.3.5 Paracellular Transport

Cells were plated and treated as described above for the IGF-I transport experiments. Following incubation at 37°C with treatments (IGF-I (2 μg/ml), Y60L-IGF-I (2 μg/ml), or insulin (10 μg/ml)), ^{3}H-inulin (400,000 cpm/ml) was added to apical chambers. Samples (0.5 ml) from apical and basolateral chambers were collected after 12 hrs and analyzed in a Tri-Carb 2100TR Liquid Scintillation Analyzer β-counter (Perkin Elmer Life Sciences, Downers Grove IL).

4.3.6 Binding Studies

Cells were plated on RTCF coated Transwell® inserts ($5x10^4$ cells/cm^2) and maintained in culture for 7.5 days with media replenished every 2-3 days. Cells were washed with

DPBS and serum-free media was added. Following serum starvation (12 hours), cells were washed with DPBS and binding buffer was added to the apical chamber. Cells were incubated at 4°C for 20 minutes. Following incubation, treatments (insulin, IGF-I, or Y60L-IGF-I) and ^{125}I-IGF-I (2 ng/ml) were added and cells were incubated at 4°C for 12 hrs. On ice, binding buffer was aspirated, cells were washed twice with ice cold DPBS, and lysed with 0.3 N NaOH. Samples were collected and analyzed in a COBRA II Auto-Gamma counter.

4.3.7 Analysis of Binding Results

Binding data was analyzed based on mass action kinetics (103). Briefly, kinetic equations were developed to describe binding of a ligand (L), ^{125}I-IGF-I, to a binding site (R) to form a ligand/binding site complex (C). Binding competitors (Y60L-IGF-I or insulin) were used to block one of the possible binding sites (IGF-IR or IGFBPs) throughout the binding experiments. Unlabeled IGF-I (I), a binding competitor for L that binds to R to form an inhibitor/binding site complex (X) was included in the analysis.

$$L + R \leftrightarrow C$$

$$I + R \leftrightarrow X$$

Assuming that radiolabeling of the IGF-I did not alter binding properties, ordinary differential equations were derived based on these reactions and the following equation was derived assuming steady state had been reached and that there was no ligand depletion.

$$\frac{C}{C_{max}} = \frac{1 - \dfrac{I}{K_D + I}}{1 - \dfrac{LI}{(K_D + I)(K_D + L)}}$$

where C_{max} is the maximum number of ligand/binding site complexes (when I = 0) and K_D is the dissociation constant describing binding between the ligand and the binding site. Binding data (C) was normalized to C_{max} and plotted against I. The above equation was fit to the data using MATLAB (The Mathworks, Natick MA) to determine K_D.

4.3.8 Ligand Blot

Ligand blot analysis was conducted as described previously (82). Briefly, cells were grown on Transwell® inserts for 8 days with media changed every 2 -3 days and conditioned media (CM) was collected on day 8. CM samples were concentrated using a SpeedVac® Model SC110 (Savant, Holbrook NY) and reconstituted in water. Samples were then diluted with 2x loading buffer (0.125 M TRIS, 4% SDS, 20% glycerol, 1% bromophenol blue), loaded into a 12.5% acrylamide gel, and separated at constant current. Samples were then transferred to nitrocellulose membranes and incubated overnight with ^{125}I-IGF-I. Membranes were exposed to film for 3-7 days at -70ºC.

4.3.9 Ligand Internalization

Cells were plated in 12 well plates at a plating density of $5x10^4$ cells/cm^2. After 2 days, cells were washed with DPBS and switched to serum free media. Following serum starvation (24 hrs), cells were washed with DPBS and binding buffer was added. Treatments (insulin or Y60L-IGF-I) were added and cells were incubated at 37°C for 20 minutes. Following incubation ^{125}I-IGF-I was added (4 ng/ml) at various time points, up to 10 minutes. On ice, binding buffer was then aspirated and cells were washed twice with DPBS and incubated in acid buffer (0.2 M acetic acid, 0.5 M NaCl, pH 2.5) for 10 min to remove any surface bound ligand. Following incubation, acid buffer was then collected and cells were incubated in 0.3 N NaOH for at least 1 hr to extract any internalized ligand. Samples were collected and analyzed in a COBRA II Auto-Gamma counter.

4.3.10 Analysis of Internalization Results

Internalization data was analyzed as described previously (119). Briefly, a kinetic equation was developed to describe internalization of surface ligand/binding site complexes (C_S) to form internal ligand/binding site complexes (C_I) that is dependent strictly on the internalization rate constant (k_e) and assumes no recycling or degradation within the timeframe of interest (103):

$$\frac{dC_I}{dt} = k_e * C_S$$

$$\frac{dC_I}{dt} = k_e * C_S$$

The integral of surface bound ligand (C_S) was evaluated using the trapezoid rule and plotted against internalized data (C_I) in Microsoft Excel to obtain k_e.

$$C_I = k_e \int_0^t C_S dt$$

4.3.11 Evaluation of Ligand Degradation

Samples were subjected to trichloroacetic acid (TCA) and phosphotungstic acid (PTA) precipitation as described previously (93). Briefly, TCA and PTA were added to samples to yield a final concentration of 3% and 0.3%, respectively. Samples were then vortex and incubated at 4°C for 30 minutes. Following incubation, samples were centrifuged for 3 min at 10,000 x g. Supernatants and pellets were collected and analyzed in a COBRA II Auto-Gamma counter.

4.3.12 Statistical Analysis

Statistical comparisons were conducted by two-tailed t-tests in Microsoft Excel with significance defined as $p < 0.05$.

4.3.13 Computational Model

Since it is difficult to conduct experiments that are sensitive enough to quantitatively investigate certain parameters involved in growth factor delivery, it is often advantageous to develop a mathematical model to evaluate the contributions of such parameters. The model consists of a system of 45 ordinary differential equations (Appendix A), based on mass action kinetics, which describes IGF-I transport across the cell layer via IGF-IR and IGFBP-mediated and paracellular transport. Paracellular transport was assumed to be dependent on diffusion and the porosity of the cell monolayer. Cell surface binding and dissociation rates utilized in this model were incorporated ligand diffusion from the bulk as well as forward and reverse binding rates, as described previously (54). Once internalized, IGF-I was sorted for degradation, recycling, or transport according to sorting fractions similar to those reported by French et al. for EGF (56). Parameters were

measured in this paper or obtained from the literature, with the exception of the sorting parameters, as noted in Table 5.2. The model was solved using MATLAB (version 6 release 12, The Mathworks) and the stiff ordinary differential equation solver, ode15s, with all default options except that the backward differentiation formulas option was used.

4.4 Results

4.4.1 Surface binding retards ^{125}I-IGF-I transport

Insulin-like growth factor-I (IGF-I) is known to bind to cell surface IGF-I receptors (IGF-IRs) and IGF binding proteins (IGFBPs) and these binding sites are important in regulating the delivery of IGF-I from the bloodstream to the underlying tissues. The goal of this report was to determine how competition between these binding elements (IGF-IR and IGFBPs) impacted the efficacy of delivery of intact IGF-I. In this *in vitro* system, transport of ^{125}I-IGF-I from the apical to the basolateral side of bovine aortic endothelial cells (BAEC) was quantified (Figure 4.1,Table 4.1). Surprisingly, this transport was

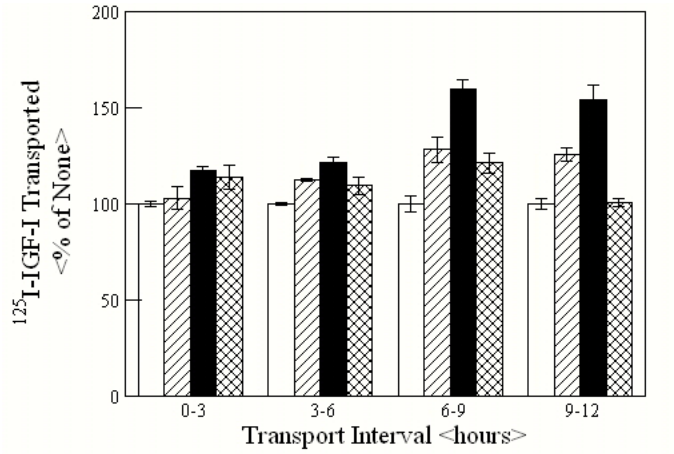

Figure 4.1: Transport of IGF-I across BAECs

125I-IGF-I transported over 12 hrs from the apical to basolateral side of bovine aortic endothelial cells (BAECs) in the absence (none) (○) or presence of binding competitors (IGF-I (2 μg/ml) (∅), Y60L-IGF-I (2 μg/ml) (●), or insulin (10 μg/ml) (⊗)) at 37°C. BAECs were plated and cultured as described in Materials and Methods. Results indicate the mean ± SEM (n = 3) and are representative of three independent experiments.

significantly enhanced ($p < 0.05$) when all binding sites (IGF-IRs and IGFBPs) were blocked by unlabeled IGF-I, suggesting that surface binding interactions retard ^{125}I-IGF-I transport *in vitro*. This phenomenon could be a result of binding to IGF-IRs and/or IGFBPs, so specific binding competitors were utilized to investigate the mechanisms involved. Inclusion of insulin, which binds to IGF-IRs but not IGFBPs (74), did not significantly affect ($p > 0.05$) the transport of ^{125}I-IGF-I. In contrast, inclusion of Y60L-IGF-I, an analog of IGF-I with significantly reduced affinity for IGF-IRs and normal affinity for IGFBPs (16), significantly enhanced ($p < 0.05$) the transport of ^{125}I-IGF-I, suggesting that IGFBP binding impeded IGF-I transport.

Table 4.1: Total IGF-I transported across BAECs over 12 hours

Cumulative amount of radiolabeled ligands transported across bovine aortic endothelial cells (BAECs) over 12 hrs at 37°C. BAECs were plated and cultured as described in Materials and Methods. Results were normalized to percentage of control (None). Results indicate the mean ± SEM (n = 3) and are representative of three independent experiments.

	^{125}I-IGF-I	^{125}I-Y60L-IGF-I	^{125}I-LongR3-IGF-I
None	100 ± 0.9 %	100 ± 2.7 %	100 ± 1.5 %
IGF-I	115 ± 2.4 %	136 ± 2.8 %	91 ± 3.2 %
Y60L	134 ± 3.0 %	135 ± 3.2 %	96 ± 1.5 %
Insulin	111 ± 4.5 %	105 ± 3.5 %	85 ± 1.4 %

To verify that these results were specific for IGF-I and that the competitors did not alter paracellular transport, inulin, a molecule with a similar molecular weight as IGF-I that does not bind cell surfaces was utilized. Similar to the IGF-I transport experiments, ^{3}H-inulin was added to the apical side of confluent BAEC monolayers and the extent of transport was determined. None of the competitors had a significant affect ($p > 0.05$) on transport via the paracellular pathway (Figure 4.2).

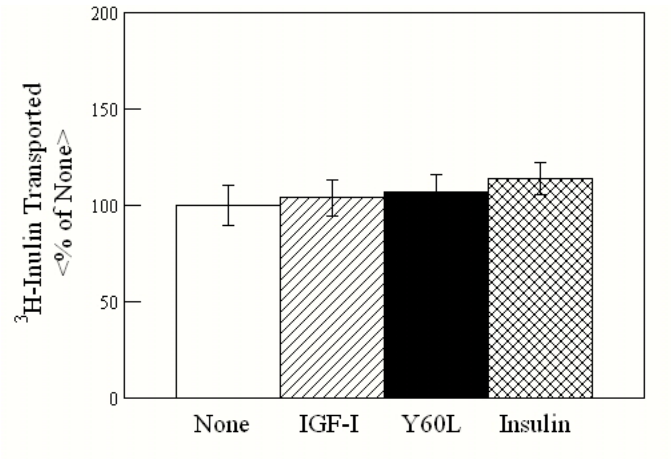

Figure 4.2: Transport of inulin across BAECs

^{3}H-inulin transported over 12 hrs from the apical to basolateral side of bovine aortic endothelial cells (BAECs) in the absence (none) (○) or presence of binding competitors (IGF-I (2 μg/ml) (∅), Y60L-IGF-I (2 μg/ml) (●), or insulin (10 μg/ml) (⊗)) at 37°C. BAECs were plated and cultured as described in Materials and Methods. Results indicate the mean ± SEM (n = 3) and are representative of three independent experiments.

Contributions of IGF-IRs and IGFBPs to the transport of ^{125}I-IGF-I were confirmed through the use of radiolabeled IGF-I analogs. Transport of ^{125}I-Y60L-IGF-I was unaffected ($p > 0.05$) by inclusion of insulin but significantly enhanced ($p < 0.05$) by inclusion of either IGF-I or Y60L-IGF-I (Figure 4.3A), supporting the hypothesis that IGFBPs retarded the transport of IGF-I. Transport of ^{125}I-LongR3-IGF-I, an analog with normal affinity for IGF-IR but essentially no affinity for IGFBPs (16, 52), was significantly ($p < 0.05$) reduced when IGF-IRs, but not IGFBPs, were blocked (Figure 4.3B).

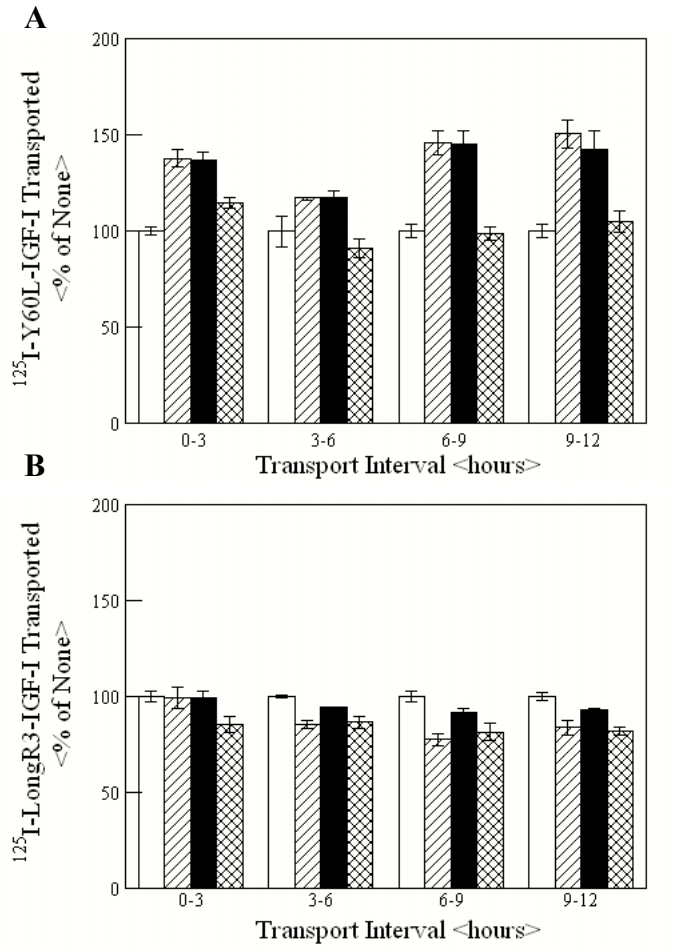

Figure 4.3: Transport of Y60L-IGF-I and LongR3-IGF-I across BAECs

^{125}I-Y60L-IGF-I (A) and ^{125}I-LongR3-IGF-I (B) transported over 12 hrs from the apical to basolateral side of bovine aortic endothelial cells (BAEC). Studies were conducted in the absence (none) (○) or presence of binding competitors (IGF-I (2 μg/ml) (∅), Y60L-IGF-I (2 μg/ml) (●), or insulin (10 μg/ml) (⊗)) at 37°C. BAECs were plated and cultured as described in Materials and Methods. Results indicate the mean ± SEM (n = 3) and are representative of three independent experiments.

4.4.2 IGFBPs dominate cell surface binding

Given the low response to the inclusion of insulin, it was suspected that receptors levels were low in this system and that IGFBPs may be the dominant binding regulators on the apical surface. To evaluate this, the relative level of binding sites on the cells was determined (Figure 4.4). Binding affinity between ^{125}I-IGF-I and IGF-IR was not significantly different from the affinity between ^{125}I-IGF-I and IGFBPs (2.4 ± 1.2 and 2.0

± 0.3 nM, respectively). However, the apical binding of IGF-I reflected twice as many IGFBP binding sites (8.0 ± 1.9 x 10^4 per cell) as IGF-IR binding sites (3.9 ± 0.6 x 10^4 per cell).

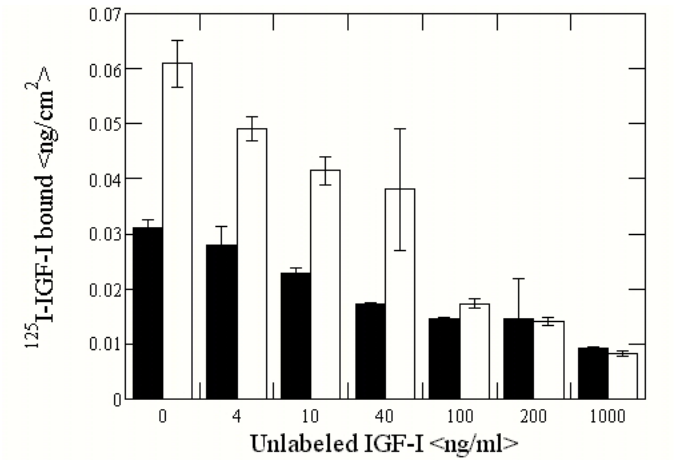

Figure 4.4: Binding of IGF-I to BAECs

Binding of ^{125}I-IGF-I to the apical surface of bovine aortic endothelial cells (BAECs) at 4°C in the presence of various concentrations of IGF-I and either Y60L-IGF-I (2 μg/ml) (■) or insulin (10 μg/ml) (□). BAECs were plated and cultured as described in Materials and Methods. Results indicate the mean ± SEM and are representative of three independent experiments.

Ligand blot analysis confirmed previous work indicating that these cells secrete IGFBP-2, 3, and 4 (Appendix G) (45). Secretion was directional since no IGFBPs were detected in the basolateral media. Further, binding studies conducted on the basolateral surface indicated significantly reduced overall binding compared to the apical surface, with approximately half as many IGFBPs sites (5.1 ± 0.6 x 10^4 per cell) and no detectable IGF-IRs sites. Quantification of binding to the separate IGFBPs was not feasible, however the overall affinity measured agrees with individual values reported in the literature (74, 191, 199).

4.4.3 IGF-IRs but not IGFBPs internalize ^{125}I-IGF-I

Since the biological activity of growth factors may be altered by cellular processes, transported ^{125}I-IGF-I was subjected to TCA/PTA precipitation to determine if ligand

degradation had occurred. Some degradation of both ^{125}I-IGF-I and ^{125}I-LongR3-IGF-I was evident (Table 2) with the percentage degraded being reduced by inclusion of IGF-I or insulin. This suggests that transport via IGF-IR leads to partial degradation of the bound ligand. There was no significant degradation of ^{125}I-IGF-I transported in the presence of insulin or of transported ^{125}I-Y60L-IGF-I beyond that detected when internalization was blocked by excess IGF-I (Table 4.2). Further, when transport studies were conducted at 4ºC, there was no significant difference in degradation between any of the treatments (data not shown), suggesting that cellular internalization was required for degradation.

Table 4.2: Degradation of IGF-I during transport

TCA/PTA precipitation of transported radiolabeled ligands across bovine aortic endothelial cells (BAECs) over 12 hrs at 37°C. BAECs were plated and cultured as described in Materials and Methods. Results were calculated as the percentage of transported sample that was TCA/PTA precipitable. Results indicate the mean ± SEM and are representative of three independent experiments.

	^{125}I-IGF-I	^{125}I-Y60L-IGF-I	^{125}I-LongR3-IGF-I
None	56 ± 6.1 %	96 ± 8.0 %	61 ± 4.9 %
IGF-I	75 ± 5.7 %	94 ± 7.7 %	83 ± 7.1 %
Y60L	54 ± 6.5 %	86 ± 13.4 %	63 ± 10.2 %
Insulin	68 ± 6.9 %	88 ± 12.8 %	74 ± 9.2 %

Endocytosis of ^{125}I-IGF-I by IGF-IR was quantified by conducting internalization experiments in the presence of Y60L-IGF-I (Figure 4.5A) and the data was analyzed using Satin analysis (119). An internalization rate constant of 0.076 ± 0.018 min^{-1} was determined. In contrast, studies conducted in the presence of insulin, which blocks binding to surface IGF-IRs, exhibited no detectable internal ^{125}I-IGF-I (Figure 4.5B), suggesting negligible endocytosis by IGBFPs.

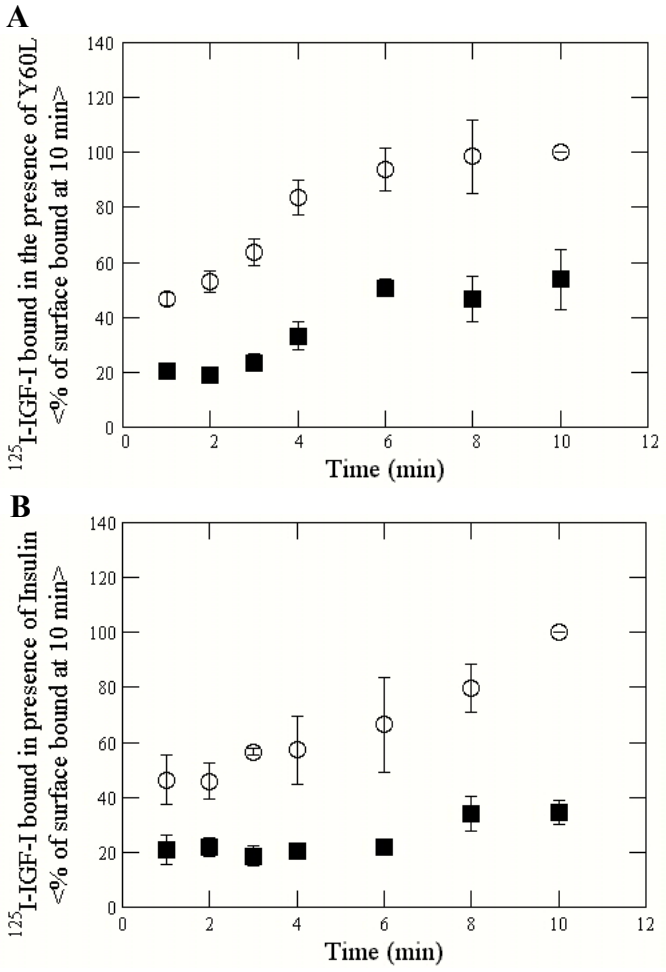

Figure 4.5: Internalization of IGF-I by BAECs

Surface (○) and internal (■) bound ^{125}I-IGF-I in the presence of Y60L-IGF-I (2 μg/ml) (A) or insulin (10 μg/ml) (B). BAECs were plated and cultured as described in Materials and Methods. Results indicate the mean ± SEM and are representative of three independent experiments.

4.5 Discussion

Delivery of growth factors across a cell monolayer, such as the endothelium, relies upon properties of the cells, such as availability of cell surface binding sites and paracellular porosity of the cell layer. For example, Maratos-Flier et al. reported that basolateral to apical transport of epidermal growth factor (EGF) across Madin-Darby canine kidney cells was inhibited when the blocking anti-EGF receptor antibody was included (122). Moreover, apical to basolateral transport of EGF did not occur and was attributed to the fact that EGF receptors were only detectable on the basolateral surface. Similarly, they reported that insulin was not transported in either direction due to a lack of expression of

insulin receptors on both apical and basolateral surfaces, suggesting that transcellular transport is dependent on the availability of surface binding sites, such as receptors.

In contrast to most growth factor systems, the actions of insulin-like growth factors (IGFs) are mediated by specific cell surface receptors as well as surface and soluble growth factor binding proteins (IGFBPs). This report shows that transport of ^{125}I-IGF-I across bovine aortic endothelial cells (BAECs) *in vitro* occurs through both paracellular and transcellular pathways and transport is largely regulated by IGFBP binding (Fig 1, Table 1). In contrast, Bastian et al. (14) reported that ^{125}I-IGF-I crosses human umbilical vein endothelial cells (HUVECs) strictly via paracellular pathways. This difference could be due to differences in IGF-IR levels on HUVECs compared to BAECs since levels vary among cell types (8, 55, 94). Differences in paracellular porosity may also contribute, since different endothelial cell types have varying permeabilities (80, 92, 118, 131) and the system reported here has been optimized to minimize paracellular transport (Chapter 3). After 2 hrs of transport, Bastian et al. report that more than 10% of the total ^{125}I-IGF-I added was transported across HUVEC monolayers (14), while in the studies reported here, less than 1% of the total ^{125}I-IGF-I added was transported across BAEC monolayers after 3 hours and approximately 3% after 12 hours. The higher porosity in their studies could have masked receptor-mediated delivery since they did detect IGF-IRs in cross-linking studies.

The binding affinity measured between ^{125}I-IGF-I and IGF-IR is similar to that reported from biosensor experiments (85), as well as endothelial cell based experiments (8, 94, 164). Similar to the insulin receptor, IGF-IRs have been shown to participate in clathrin-mediated internalization (111). Once internalized, IGF-I is reported to partially dissociate from IGF-IRs (201), and undergo partial degradation (59). This report has shown that ^{125}I-IGF-I is internalized through an IGF-IR dependent process (Fig 5a) and determined that the rate of receptor-mediated internalization is 0.076 ± 0.018 min^{-1}, which is similar to that reported by others (29). Once internalized by IGF-IR, ^{125}I-IGF-I and ^{125}I-LongR3-IGF-I are partially degraded (Table 2). The extent of this degradation will control the efficacy of therapeutic treatments with IGF-I. Since it has been reported

that the susceptibility of the ligand to acidic pH determines the sorting outcome (56, 120), it may be feasible to design a ligand analog with the capability to withstand acidic pH and thus result in efficient sorting and delivery.

In the system reported here, twice as many functional IGFBP binding sites (8.0 ± 1.9 x 10^4 per cell) as IGF-IR binding sites (3.9 ± 0.6 x 10^4 per cell) were detected. Since IGFBPs have been shown to bind to various components of extracellular matrix, such as collagen (114) and fibronectin (123) which are utilized in this culture system, matrix-bound IGFBPs may also function as reservoirs of ^{125}I-IGF-I that initially prevent cell surface binding and transport but may lead to sustained controlled delivery. Data reported here showed that these IGFBP binding sites prevent IGF-I transport, likely via competitive inhibition of IGF-IR binding and paracellular transport. This work is in agreement with a recent paper from Grulich-Henn et al., who reported substantial binding of ^{125}I-IGF-I to the extracellular matrix produced by HUVECs, which contained IGFBP-2, and suggested IGFBP-2 prevented ^{125}I-IGF-I from binding to cell surface IGF-IR. Inhibition of IGF-I transport has also been shown in other tissues. For example, Garcia et al. found that IGFBPs, most likely IGBFP-6, impeded the transport of ^{125}I-IGF-I across bovine articular cartilage (62). *In vivo*, the clearance rate of ^{125}I-IGF-I in wound chambers implanted in rats was shown to be slower than that of ^{125}I-LongR3-IGF-I, presumably due to binding to IGFBPs (15). No IGFBP-mediated internalization of IGF-I was detected (Fig 5b), but previous reports have shown that IGFBP-3 can cross the endothelial barriers (9, 12) and transport IGF-I (23), but this has only been reported in the rat heart or in cells with compromised barrier function (174). However, Schedlich et al. showed that in Chinese hamster ovary cells, intracelluar IGFBP-3 localized around the nucleus and underwent importin beta dependent uptake (165), suggesting that if IGFBP-3 was internalized, it would not contribute to the transport to of IGF-I.

The data presented here indicated that IGFBPs inhibited IGF-I transport by acting as a surface reservoir for IGF-I. However, it is possible that this reservoir of IGF-I could facilitate overall transport of IGF-I under the correct conditions. To test this, a mathematical model was developed (Chapter 5) based on parameters reported here and

subjected the system to an apical bolus of IGF-I for 60 min and apical to basolateral transport was measured for an additional 11 hrs (Figure 4.6). When IGFBPs were removed from the system, there was an initial increase in IGF-I transported during the pulse phase. However, after unbound apical IGF-I was removed from the model system, there was significantly more IGF-I delivered when IGFBPs were present, supporting the hypothesis that IGFBPs serve as a reservoir that promote long-term delivery of IGF-I. Future research exploiting this reservoir function is needed, but suggests that IGFBPs could function as a natural sustained release mechanism.

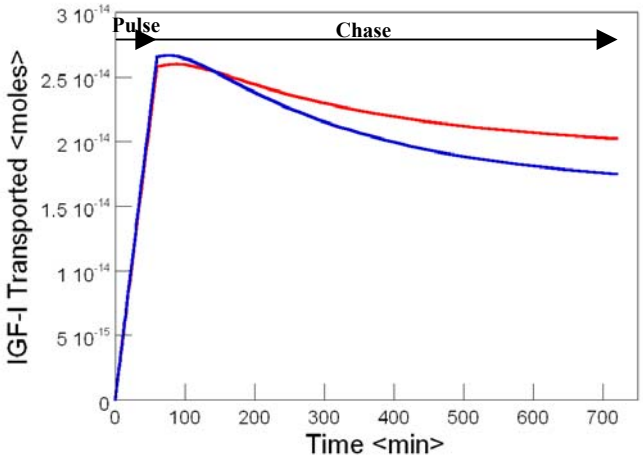

Figure 4.6: Transport of IGF-I across model endothelium

IGF-I transported from the apical to basolateral side of a model endothelium after a 60 min pulse and 11 hr chase in the presence (—) and absence (—) of cell surface IGFBPs

In conclusion, transport of ^{125}I-IGF-I across BAEC cultured on collagen and fibronectin coated Transwell® inserts occurs through both paracellular and receptor-mediated transport. Although IGFBPs were the primary IGF-I binding elements, they do not actively transport IGF-I, but likely function as a cell surface reservoir that regulates availability of IGF-I for IGF-IR-mediated and paracellular transport. While IGFBPs may initially retard transport, it is possible that they might be used to facilitate controlled sustained delivery of IGF-I.

Chapter 5: Computational Modeling of Insulin-like Growth Factor-I (IGF-I) Transport: Regulation by IGF Binding Proteins

5.1 Abstract

Insulin-like growth factor-I (IGF-I) has the potential to treat a myriad of pathological conditions, however, treatment efficacy is overshadowed by significant side effects. Computational modeling enables a mechanistic evaluation of growth factor action and can facilitate the development of better therapeutic strategies to treat various pathological conditions. A computational model of IGF-I delivery across endothelial cells has been developed based on previous experimental work that focused on regulation of IGF-I transport by IGFBPs (Chapter 4). This report demonstrates that the model can simulate the experimental data and explore the important key parameters in the transport process. The porosity of the cell layer is shown to have the largest impact on IGF-I delivery, however, since the integrity of epithelial and endothelial layers is essential to their normal physiological function, it is not feasible to design growth factors that increase cell layer permeability. Alternatively, alteration of endosome binding, and thus sorting outcome, could be achieved through development of IGF-I variants that are resistant to changes in pH and facilitate IGF-I delivery, similar EGF variants that have recently been developed. Finally, this reports demonstrates that IGFBPs can either inhibit or enhance IGF-I transport when compared to transport in the absence of IGFBPs by varying the exposure time. This illustrated the importance of examining the process as a system rather than simply as receptor-mediated phenomena.

5.2 Introduction

Insulin-like growth factor-I (IGF-I) has the potential to treat a variety of disorders, such as severe insulin resistance (99, 153), leprechaunism (6), renal failure (98), neurological disorders (108), Laron Syndrome (154), and diabetes (42, 96, 137, 152). Current strategies to treat these diseases involve intravenous infusions of supraphysiological doses of IGF-I (42, 96, 137). Since these high doses cause unwanted side effects, such as hair loss, upper respiratory infections, increased production of IGF-I antibodies, and

increased heart rate (71, 135), an understanding of the mechanisms involved in the transport of IGF-I from the bloodstream to underlying tissues may foster the development of better treatment strategies that minimize these side effects.

The actions of IGF-I are mediated by high affinity interactions with its cell surface receptor (IGF-IR) and IGF binding proteins (IGFBPs). There are six known IGFBPs and they have been shown to participate, to varying degrees, in IGF-inhibiting, IGF-enhancing, and IGF-independent actions (22, 30, 32, 44, 46, 50, 70, 127-129). While several IGFBPs bind to cell surfaces with high affinity, IGFBP receptors have not yet been identified, although it has been suggested that the type V transforming growth factor β receptor and membrane-bound matrix metalloprotease-9 may also function as a receptors for IGFBP-3 (104, 105, 132). In addition, IGFBPs can bind to various components of extracellular matrix, such as collagen and fibronectin. When localized in extracellular matrix, IGFBPs appear to inhibit binding of IGF-I to its receptor (62, 70). In Chapter 4, studies showed that binding of IGF-I to IGFBPs initially prevented delivery of IGF-I but facilitated long term localized delivery across bovine aortic endothelial cells.

Computational modeling is an important tool for exploring the mechanisms by which growth factor act, as reviewed recently by Wiley et al (196). Significant contributions have been made in the past decade that aid in an understanding of the mechanisms involved in sorting of and signaling through the EGF receptor and its family of ligands, which may facilitate the development of therapeutic strategies involving the EGF family to treat various pathological conditions. For example, models have been developed that describe sorting of EGF and several EGF analogs (56, 79, 176) and the dependence of acidic binding on sorting outcome (56). Shvartsman et al. have developed a model of EGF signaling and more recently, Resat et al. have developed a model that incorporated sorting as well as signaling events (157).

Until now, modeling of intracellular sorting and transport has focused mainly on epithelial, not endothelial, cells. Since many drugs are delivery systemically, it may prove beneficial to develop a model of drug transport across endothelial cells. Further,

few models of IGF-I action have been reported. Boroujerdi et al. developed a compartmental model of *in vivo* IGF-I metabolism (24), however the mechanisms involved in IGF-I delivery were not investigated. This paper investigates the kinetics of IGF-I sorting and transport across a model endothelium and addresses the relative importance of system parameters and the impact of IGFBPs on receptor-mediated transport.

5.3 Mathematical Model

The model describes insulin-like growth factor binding protein (IGFBP) regulation of IGF-I transport across an endothelial barrier and is based on experimental work examining apical to basolateral transport of IGF-I *in vitro* (Chapter 4). The model assumes uniform distribution of IGF-I receptors (IGF-IRs) and IGFBPs on the cell surface, however it does allow for heterogeneous apical and basolateral distributions of proteins. This research group (45) and others have shown that endothelial cells secrete multiple IGFBPs. Ligand blot analysis conducted using conditioned media from cells utilized in these studies showed the presence of IGFBP-2, 3, and 4 (Figure 2.5A); suggesting that IGFBP binding sites are a heterogeneous mixture. However, for simplicity, the IGFBPs in the system have been modeled as a single binding element and have based the properties on experimentally derived average dissociation constant (Chapter 4) and the kinetic association rate of IGFBP-3 (28), the binding protein of most interest on endothelial cells.

The model consists of a system of 45 ordinary differential equations, based on mass action kinetics, which describes IGF-I transport across the cell layer via IGF-IR and IGFBP-mediated and paracellular transport (Figure 5.1). A schematic of important kinetic reactions governing IGF-I transport is shown (Figure 5.2). Apical solution IGF-I (L_a) binds apical IGF-IRs (R_a), IGFBPs (B_a), or may be transported paracellularly (k_{para}), where it can bind with basolateral IGF-IRs (R_b) and IGFBPs (B_b). The rate of change of IGF-I/IGF-IR complexes on the apical surface (C_a) is

$$\frac{dC_a}{dt} = k_{f1} R_a L_a - k_{r1} C_a + k_{off2} X_a P(R_a) - k_{ec} C_a + k_{rec} C_{ia}(1-f_{1C})(1-f_{2C}) + k_{trans} C_{ib}(1-f_{1C})(f_{2C}) \quad (1)$$

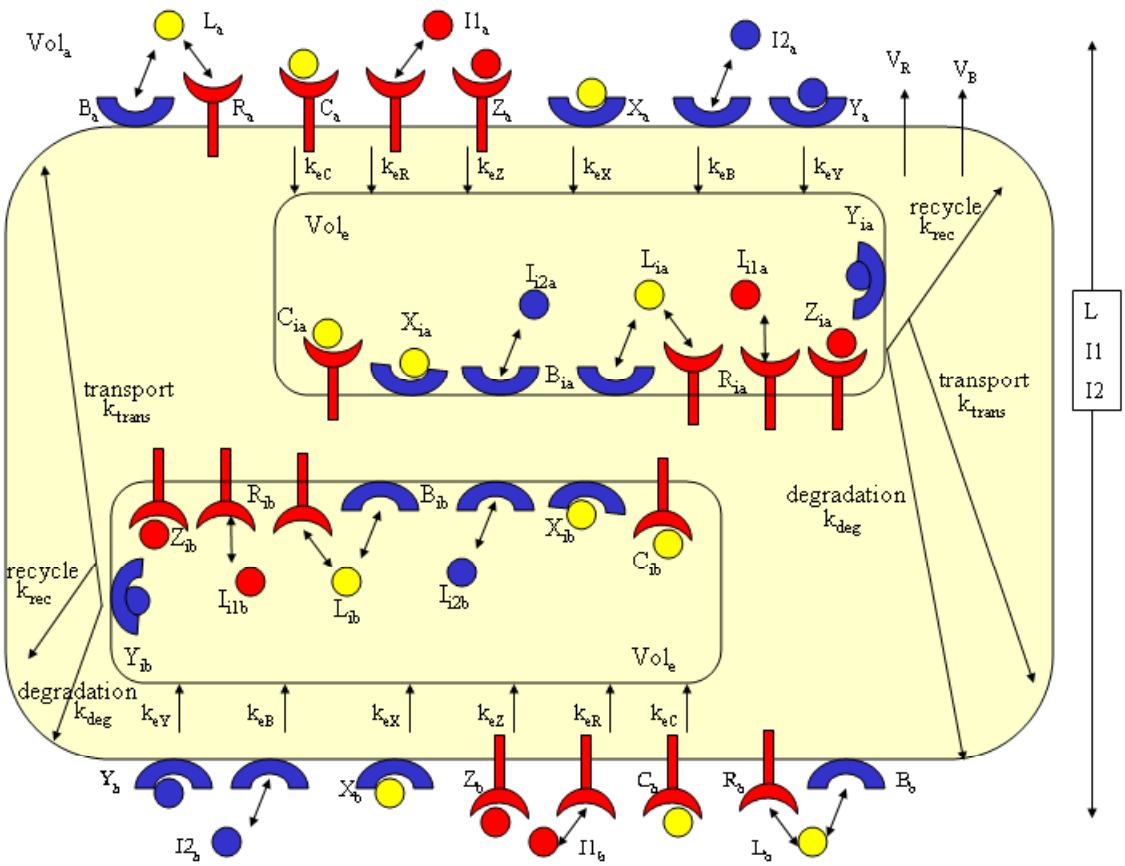

Figure 5.1: Schematic of IGF-I transport

which reflects binding ($k_{f1}R_aL_a$) and dissociation ($k_{r1}C_a$), including advantageous rebinding of IGF-I released from local IGFBPs ($k_{off2}X_aP(R_a)$), where $P(R_a)$ is the probability of IGF-I capture by IGF-IRs, as described previously (54). Also included are the internalization of surface complexes (k_{eC}), and recycling (k_{rec}) and transport (k_{trans}) of complexes from apical and basolateral endosomes (C_{ia} and C_{ib}, respectively). Endosome contents are sorted into either degradation or non-degradation (recycling or transport) pathways. The sorting parameter f_l represents the fraction of each component, such as f_{1C} for IGF-I/IGF-IR complexes, which is directed towards degradation pathways. Components directed towards non-degradation pathways, ($1-f_{1C}$) for IGF-I/IGF-IR

complexes, are again sorted for either recycling ($1-f_{2C}$) or transport pathways (f_{2C}), where f_2 represents the fraction of each non-degraded component that enters the transport pathway. It is assumed, based on previous reports investigating transferrin and IgG (166), that apical and basolateral sorting endosomes remain separate but maintain identical binding and sorting kinetics.

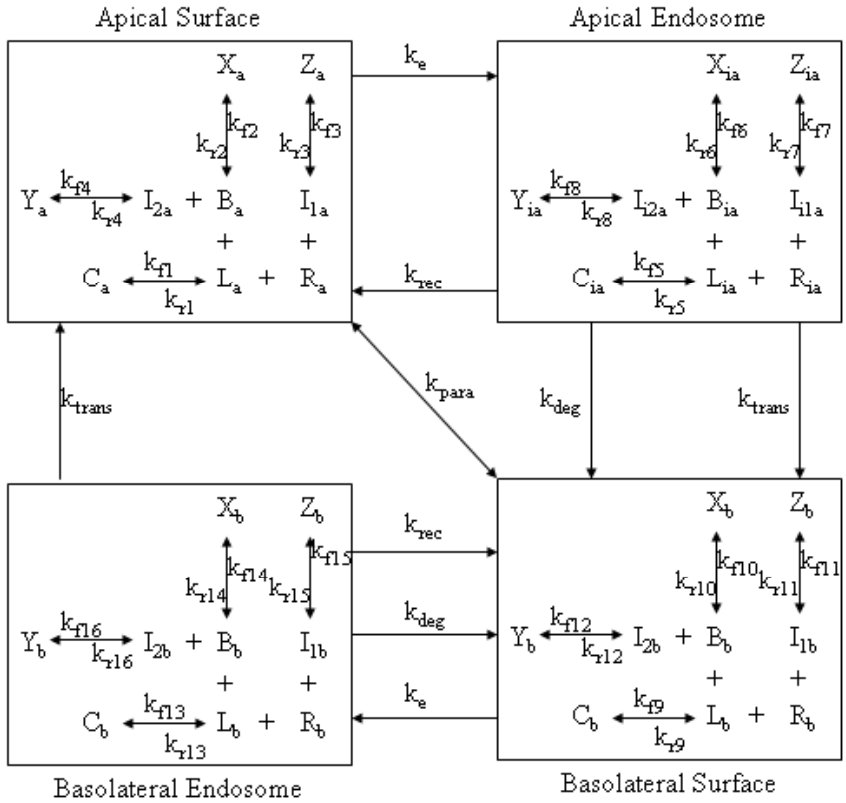

Figure 5.2: Kinetic reactions of IGF-I transport

The forward and reverse rates (Table 5.1) for cell-surface interactions are a function of ligand diffusion from the bulk to the cell surface, as well as the binding affinity between the ligand and its binding site (54). Due to the small volume of the endosomes, it is assumed that binding is not diffusion-limited so that forward and reverse rates are constants. Change in the presence of apical IGF-I/IGFBP complexes (X_a) is described by

$$\begin{aligned}\frac{dX_a}{dt} &= k_{f2}B_aL_a - k_{r2}X_a + k_{off1}C_aP(B_a) - k_{ex}X_a \\ &\quad + k_{rec}X_{ia}(1-f_{1X})(1-f_{2X}) + k_{trans}X_{ib}(1-f_{1X})(f_{2X})\end{aligned} \tag{2}$$

and is dependent upon binding ($k_{f2}B_aL_a$) and dissociation ($k_{r2}X_a$), including advantageous rebinding of IGF-I released from local IGF-IRs ($k_{off1}C_aP(B_a)$), where $P(B_a)$ is the

probability of IGF-I capture by IGFBPs. Formation of complexes also depends on internalization of surface complexes (k_{eX}) and recycling and transport of complexes from apical (X_{ia}) and basolateral endosomes (X_{ib}).

Table 5.1 Binding and dissociation rates

Binding and dissociation rates at for IGF-I, insulin, and Y60L-IGF-I to IGF-IRs and IGFBPs.

	Binding Rates	Dissociation Rates
Apical IGF-I ↔ IGF-IR	$k_{f1} = \dfrac{k_{on1}}{1 + \dfrac{k_{on1}R_a + k_{on2}B_a}{4\pi sD}}$	$k_{r1} = \dfrac{k_{off1}}{1 + \dfrac{k_{on1}R_a}{4\pi sD + k_{on2}B_a}}$
Apical IGF-I ↔ IGFBP	$k_{f2} = \dfrac{k_{on2}}{1 + \dfrac{k_{on2}B_a + k_{on1}R_a}{4\pi sD}}$	$k_{r2} = \dfrac{k_{off2}}{1 + \dfrac{k_{on2}B_a}{4\pi sD + k_{on1}R_a}}$
Apical Insulin ↔ IGF-IR	$k_{f3} = \dfrac{k_{on3}}{1 + \dfrac{k_{on3}R_a}{4\pi sD}}$	$k_{r3} = \dfrac{k_{off3}}{1 + \dfrac{k_{on3}R_a}{4\pi sD}}$
Apical Y60L-IGF-I ↔ IGFBP	$k_{f4} = \dfrac{k_{on4}}{1 + \dfrac{k_{on4}B_a}{4\pi sD}}$	$k_{r4} = \dfrac{k_{off4}}{1 + \dfrac{k_{on4}B_a}{4\pi sD}}$
Basolateral IGF-I ↔ IGF-IR	$k_{f9} = \dfrac{k_{on9}}{1 + \dfrac{k_{on9}R_b + k_{on2}B_b}{4\pi sD}}$	$k_{r9} = \dfrac{k_{off9}}{1 + \dfrac{k_{on9}R_b}{4\pi sD + k_{on10}B_b}}$
Basolateral IGF-I ↔ IGFBP	$k_{f10} = \dfrac{k_{on10}}{1 + \dfrac{k_{on10}B_b + k_{on9}R_b}{4\pi sD}}$	$k_{r10} = \dfrac{k_{off10}}{1 + \dfrac{k_{on10}B_b}{4\pi sD + k_{on9}R_b}}$
Basolateral Insulin ↔ IGF-IR	$k_{f11} = \dfrac{k_{on11}}{1 + \dfrac{k_{on11}R_b}{4\pi sD}}$	$k_{r11} = \dfrac{k_{off11}}{1 + \dfrac{k_{on11}R_b}{4\pi sD}}$
Basolateral Y60L-IGF-I ↔ IGFBP	$k_{f12} = \dfrac{k_{on12}}{1 + \dfrac{k_{on12}B_b}{4\pi sD}}$	$k_{r12} = \dfrac{k_{off12}}{1 + \dfrac{k_{on12}B_a}{4\pi sD}}$

In the endosomes, the pH of the solution decreases and the binding affinities between IGF-I (L_{ia}) and its binding sites (R_{ia} and B_{ia}) are altered. *In vitro* experiments show that at reduced pH, the binding affinity between IGF-I and IGF-IR is reduced (201), suggesting that in the acidic environment of the endosome, IGF-I will dissociate from IGF-IRs. The rate of change of IGF-I/IGF-IR complexes (C_{ia}) in the apical endosomes is

$$\begin{aligned}\frac{\mathrm{d}C_{ia}}{\mathrm{d}t} &= \mathrm{k}_{\mathrm{f5}} R_{ia} L_{ia} - \mathrm{k}_{\mathrm{r5}} C_{ia} + \mathrm{k}_{\mathrm{ec}} C_a - \mathrm{k}_{\mathrm{deg}} C_{ia} (\mathrm{f}_{1\mathrm{C}}) \\ &\quad - \mathrm{k}_{\mathrm{rec}} C_{ia} (1-\mathrm{f}_{1\mathrm{C}})(1-\mathrm{f}_{2\mathrm{C}}) - \mathrm{k}_{\mathrm{trans}} C_{ia} (1-\mathrm{f}_{1\mathrm{C}})(\mathrm{f}_{2\mathrm{C}})\end{aligned} \tag{3}$$

where (R_{ia}) is the number of free IGF-IRs in the apical endosome, and binding and dissociation rates (k_{f5} and k_{r5}) represent the altered binding in the acidic environment. Complexes are sorted for degradation (k_{deg}), recycling, or transport according to the sorting parameters f_{1C} and f_{2C}.

The time dependent change in IGF-I/IGFBP complexes in the apical endosome is

$$\begin{aligned}\frac{\mathrm{d}X_{ia}}{\mathrm{d}t} &= \mathrm{k}_{\mathrm{f6}} B_{ia} L_{ia} - \mathrm{k}_{\mathrm{r6}} X_{ia} + \mathrm{k}_{\mathrm{eX}} X_a - \mathrm{k}_{\mathrm{deg}} X_{ia} (\mathrm{f}_{1\mathrm{X}}) \\ &\quad - \mathrm{k}_{\mathrm{rec}} X_{ia} (1-\mathrm{f}_{1\mathrm{X}})(1-\mathrm{f}_{2\mathrm{X}}) - \mathrm{k}_{\mathrm{trans}} X_{ia} (1-\mathrm{f}_{1\mathrm{X}})(\mathrm{f}_{2\mathrm{X}})\end{aligned} \tag{4}$$

where (B_{ia}) is the number of free IGFBPs in the apical endosome and binding and dissociation rates (kf_{r6} and k_{r6}) represent the altered binding in the acidic environment. Complexes are sorted for degradation, recycling, or transport according to the sorting parameters f_{1X} and f_{2X}.

Transport of IGF-I from apical solution (L_a) to basolateral solution (L_b) depends on IGF-I binding to IGF-IRs and IGFBPs, internalization and sorting of these components, as well as paracellular transport of IGF-I. The time-dependent change in unbound IGF-I (L_{ia}) in the apical endosome is given by

$$\begin{aligned}\frac{\mathrm{d}L_{ia}}{\mathrm{d}t} &= \frac{\mathrm{n}}{\mathrm{N}_{\mathrm{av}}\mathrm{Vol}_{\mathrm{e}}}[-\mathrm{k}_{\mathrm{f5}} R_{ia} L_{ia} + \mathrm{k}_{\mathrm{r5}} C_{ia} - \mathrm{k}_{\mathrm{f6}} B_{ia} L_{ia} \\ &\quad + \mathrm{k}_{\mathrm{r6}} X_{ia}] - \mathrm{k}_{\mathrm{deg}} L_{ia} (\mathrm{f}_{1\mathrm{L}}) \\ &\quad - \mathrm{k}_{\mathrm{rec}} L_{ia} (1-\mathrm{f}_{1\mathrm{L}})(1-\mathrm{f}_{2\mathrm{L}}) - \mathrm{k}_{\mathrm{trans}} L_{ia} (1-\mathrm{f}_{1\mathrm{L}})(\mathrm{f}_{2\mathrm{L}})\end{aligned} \tag{5}$$

and IGF-I is sorted for degradation, recycling and transport according to the sorting parameters f_{1L} and f_{2L}. Paracellular transport (k_{para}) was assumed to be dependent on

diffusive transport and the porosity of the membrane (ε). The porosity was determined based on experimental results that investigated the transport of ^{125}I-IGF-I in the presence of excess IGF-I, which blocked binding sites, leaving only the paracellular pathway available for transport (Chapter 4). Delivery of non-degraded IGF-I from apical (L_a) to basolateral (L_b) solution is represented by

$$\begin{aligned}\frac{dL_a}{dt} = \frac{n}{N_{av}Vol_a}[&-k_{f1}R_aL_a + k_{r1}C_a - k_{f2}B_aL_a + k_{r2}X_a \\ &+ k_{off1}C_a(1-P(B_a)) + k_{off2}X_a(1-P(R_a))] \\ &- k_{para}L_a + k_{para}L_b \\ &+ k_{rec}L_{ia}(1-f_{1L})(1-f_{2L}) + k_{trans}L_{ib}(1-f_{1L})(f_{2L})\end{aligned} \tag{6}$$

$$\begin{aligned}\frac{dL_b}{dt} = \frac{n}{N_{av}Vol_b}[&-k_{f9}R_bL_b + k_{r9}C_b - k_{f10}B_bL_b \\ &+ k_{r10}X_b + k_{off9}C_b(1-P(B_b)) + k_{off10}X_b(1-P(R_b))] \\ &- k_{para}L_b + k_{para}L_a \\ &+ k_{rec}L_{ib}(1-f_{1L})(1-f_{2L}) + k_{trans}L_{ia}(1-f_{1L})(f_{2L})\end{aligned} \tag{7}$$

which in addition to the apical kinetics described above, includes binding ($k_{f9}R_bL_b$ and $k_{f10}B_bL_b$) of basolateral IGF-I (L_b) to free basolateral surface IGF-IR (R_b) and IGFBPs (B_b), respectively, and dissociation of IGF-I/IGF-IR ($k_{r9}C_b$) and IGF-I/IGFBP ($k_{r10}X_b$) complexes. It is assumed that degradation products are released basolaterally since little degradation was detected in the apical solution (data not shown). The rate of change in degradation products is

$$\frac{dL_{deg}}{dt} = k_{deg}L_{ia}(f_{1L}) + k_{deg}L_{ib}(f_{1L}) \tag{8}$$

The model also considers the use of competitive binding inhibitors and their effect on overall transport. Apical competitors for IGF-IRs (I_{1a}), such as insulin or longR^3-IGF-I, are assumed to be processed similar to IGF-I. The rate of change in apical IGF-IR competitors is

$$\begin{aligned}\frac{dI_{1a}}{dt} = \frac{n}{N_{av}Vol_a}[&-k_{f3}R_aI_{1a} + k_{r3}Z_a] - k_{para}I_{1a} \\ &+ k_{para}I_{1b} + k_{rec}I_{i1a}(1-f_{1I1})(1-f_{2I1}) \\ &+ k_{trans}I_{i1b}(1-f_{1I1})(f_{2I1})\end{aligned} \tag{9}$$

and includes binding ($k_{f3}R_aI_{1a}$), dissociation ($k_{r3}Z_a$), and paracellular transport of apical (I_{1a}) and basolateral (I_{1b}) competitors, which are sorted for degradation, recycling and transport according to the sorting parameters f_{1I1} and f_{2I1}. Similarly, competitors are IGFBPs (I_{2a} and I_{2b}), such as Y60L-IGF-I, are assumed to be processed similar to IGF-I and IGF-I/IGFBP complexes. The time dependent change in apical IGFBP competitors is given by

$$\begin{aligned}\frac{dI_{2a}}{dt} = \frac{n}{N_{av}Vol_a}[-k_{f4}B_aI_{2a} + k_{r4}Y_a] - k_{para}I_{2a} \\ + k_{para}I_{2b} + k_{rec}I_{i2a}(1-f_{1I2})(1-f_{2I2}) \\ + k_{trans}I_{i2b}(1-f_{1I2})(f_{2I2})\end{aligned} \quad (10)$$

and includes binding ($k_{f4}B_aI_{2a}$), dissociation ($k_{r4}Y_a$), and paracellular transport of apical (I_{2a}) and basolateral (I_{2b}) competitors, which are sorted for degradation, recycling and transport according to the sorting parameters f_{1I2} and f_{2I2}.

5.4 Model Parameters

The cell surface binding and dissociation rates (Table 5.1) utilized in this model are dependent on ligand diffusion from the bulk as well as forward and reverse binding rates (Table 5.2), as described previously (54). The binding affinities (K_D) of IGF-I for IGF-IRs and IGFBPs at pH 7.4 were previously measured in an experimental system (Chapter 4), where $K_D = k_{off} / k_{on}$. Values for binding constants describing IGF-I binding to IGF-IR (k_{on1} and k_{on9}) (85) and IGFBP-3 (k_{on2} and k_{on10}) (28) at pH 7.4 have been reported using surface plasmon resonance. The experimental K_D values measured in Chapter 4 and literature values for binding constants were used to determine the dissociation constants (k_{off1}, k_{off9}, k_{off2}, k_{off10}). At pH 5.8, it has previously been shown that 72% of IGF-I that bound cell surface IGFBPs at pH 7.4 also bound at pH 5.8 (53). Taken together with binding constants reported for IGF-I and IGFBP-3 at pH 5.8 (k_{on6} and k_{on14}) (28), the model reported here was used to fit a value for acidic dissociation (k_{off6} and k_{off14}). Since Bevan et al. report that the dissociation, but not association, constant of insulin is predominantly altered at acidic pH (19) and, given the homology between insulin, IGF-I, and their receptors, it is assumed that the association constant for IGF-I and IGF-IR is the same at pH 7.4 and pH 5.8. Zapf et al. reported that approximately

Table 5.2 Model parameters

Parameter	Value	Significance
k_{on1}, k_{on9}	2.8×10^7 M^{-1} min^{-1}	Association of IGF-I and IGF-IR, pH 7.4
k_{off1}, k_{off9}	0.068 min^{-1}	Dissociation of IGF-I and IGF-IR, pH 7.4
k_{on2}, k_{on10}	2.2×10^7 M^{-1} min^{-1}	Association of IGF-I and IGFBP, pH 7.4
k_{off2}, k_{off10}	0.053 min^{-1}	Dissociation of IGF-I and IGFBP, pH 7.4
k_{on3}, k_{on11}	2.8×10^7 M^{-1} min^{-1}	Association of insulin and IGF-IR, pH 7.4
k_{off3}, k_{off11}	6.8 min^{-1}	Dissociation of insulin and IGF-IR, pH 7.4
k_{on4}, k_{on12}	2.2×10^7 M^{-1} min^{-1}	Association of Y60L and IGFBP, pH 7.4
k_{off4}, k_{off12}	0.053 min^{-1}	Dissociation of Y60L and IGFBP, pH 5.8
k_{on5}, k_{on13}	2.8×10^7 M^{-1} min^{-1}	Association of IGF-I and IGF-IR, pH 5.8
k_{off5}, k_{off13}	0.20 min^{-1}	Dissociation of IGF-I and IGF-IR, pH 5.8
k_{on6}, k_{on14}	4.0×10^7 M^{-1} min^{-1}	Association of IGF-I and IGFBP, pH 5.8
k_{off6}, k_{off14}	0.13 min^{-1}	Dissociation of IGF-I and IGFBP, pH 5.8
k_{on7}, k_{on15}	2.8×10^7 M^{-1} min^{-1}	Association of insulin and IGF-IR, pH 5.8
k_{off7}, k_{off15}	20 min^{-1}	Dissociation of insulin and IGF-IR, pH 5.8
k_{on8}, k_{on16}	4.0×10^7 M^{-1} min^{-1}	Association of Y60L and IGFBP, pH 5.8
k_{off8}, k_{off16}	0.13 min^{-1}	Dissociation of Y60L and IGFBP, pH 5.8
k_{eR}	0.007 min^{-1}	Internalization rate for free IGF-IR
k_{eB}	0 min^{-1}	Internalization rate for free IGFBPs
k_{eC}	0.076 min^{-1}	Internalization rate for IGF-I / IGF-IR complexes
k_{eX}	0 min^{-1}	Internalization rate for IGF-I / IGFBP complexes
k_{eZ}	0.076 min^{-1}	Internalization rate for insulin / IGF-IR complexes
k_{eY}	0 min^{-1}	Internalization rate for IGF-I / IGFBP complexes
k_{trans}	0.11 min^{-1}	Transport rate constant
k_{rec}	0.11 min^{-1}	Recycling rate constant
k_{deg}	0.02 min^{-1}	Degradation rate constant
f_{1R}, f_{2R}	0.25, 0.25	Fraction of free IGF-IRs degraded or transported, respectively
f_{1B}, f_{2B}	0.25, 0.25	Fraction of free IGFBPs degraded or transported, respectively
f_{1L}, f_{2L}	0.75, 0.25	Fraction of free IGF-I degraded or transported, respectively
f_{1C}, f_{2C}	0.25, 0.75	Fraction of IGF-I / IGF-IR complexes degraded or transported, respectively
f_{1X}, f_{2X}	0.25, 0.25	Fraction of IGF-I / IGFBP complexes degraded or transported, respectively
f_{1I1}, f_{2I1}	0.75, 0.25	Fraction of free insulin degraded or transported, respectively
f_{1Z}, f_{2Z}	0.25, 0.75	Fraction of insulin / IGF-IR complexes degraded or transported, respectively
f_{1I2}, f_{2I2}	0.75, 0.25	Fraction of free Y60L degraded or transported, respectively

Table 2 Continued		
f_{1Y}, f_{2Y}	0.25, 0.25	Fraction of Y60L / IGFBP complexes degraded or transported, respectively
s	5.0×10^{-4} cm cell^{-1}	Cell radius
D	2.1×10^{-6} cm^2 sec^{-1}	Diffusivity
Vol_a	0.0005 L	Apical solution volume
Vol_b	0.0015 L	Basolateral solution volume
Vol_e	1.0×10^{-13} L cell^{-1}	Endosome volume
$P(R_a)$	$-3.73 + 0.743 \log (R_a)$	Advantageous rebinding to free apical IGF-IRs
$P(R_b)$	$-3.73 + 0.743 \log (R_b)$	Advantageous rebinding to free basolateral IGF-IRs
$P(B_a)$	$-3.73 + 0.743 \log (B_a)$	Advantageous rebinding to free apical IGFBPs
$P(B_b)$	$-3.73 + 0.743 \log (B_b)$	Advantageous rebinding to free basolateral IGFBPs
V_R	$k_{eR}R_a - k_{rec}R_{ia}(1-f_{1R})(1-f_{2R}) - k_{trans}R_{ib}(1-f_{1R})(f_{2R})$	Synthesis of IGF-IRs
V_B	$k_{eB}B_a - k_{rec}B_{ia}(1-f_{1B})(1-f_{2B}) - k_{trans}B_{ib}(1-f_{1B})(f_{2B})$	Synthesis of IGFBPs
k_{para}	$\varepsilon 4\pi s D N_{av}$	Paracellular transport rate

38% of IGF-I that bound cell surface IGF-IRs at pH 7.4 also bound at pH 5.8 (201). Similar to determining the acidic dissociation constant, for IGF-I and IGFBP-3, the model reported here was used to fit a value for acidic dissociation for IGF-I and IGF-IR (k_{off5} and k_{off13}).

Since Bayne et al. report that Y60L-IGF-I has similar binding affinity for human serum binding proteins (hBP) as IGF-I (16), binding (k_{on4}, k_{on8}, k_{on12}, and k_{on16}) and (k_{off4}, k_{off8}, k_{off12}, and k_{off16}) dissociation constants were assumed to be similar to those used for IGF-I. Jansson et al. report a dissociation constant for insulin and IGF-IR (k_{off3} and k_{off11}) that is approximately 100 fold higher than that for IGF-I and IGF-IR (85). Taken together with reports that there is a 100 fold increase in binding affinities (K_D) for insulin and IGF-IR as there is with IGF-I and IGF-IR (85), it assumed that insulin and IGF-I have similar association constants (k_{on3} and k_{on11}) for IGF-IR. Due to the homology between insulin and IGF-I, it is also assumed that they are equally effected by pH so that association (k_{on7} and k_{on15}) between insulin and IGF-IR is the same at pH 7.4 and pH 5.8. Further, the ratio of dissociation constants for IGF-I and IGF-IR at pH 5.8 and pH 7.4,

which is approximately 3, will remain similar for insulin, and acidic dissociation constants are determined (k_{off7} and k_{off15}).

The internalization rate of IGF-I/IGF-IR complexes was measured in Chapter 4 and a similar internalization rate of insulin/IGF-IR complexes is assumed. Since previous experimental work (Chapter 4) suggested that IGFBPs are not internalized, the internalization rates of IGFBPs, IGF-I/IGFBP complexes, Y60L/IGFBP complexes were initially set to zero. A constitutive internalization rate of 0.007 min^{-1}, similar to that reported by Hemar et al. (77), was assumed for free IGF-IRs.

The sorting parameters (k_{rec}, k_{trans}, and k_{deg}) were defined based on previous experimental work. Ghosh et al. report a recycling rate (k_{rec})of approximately 0.11 min^{-1} for transferrin and, for the model, a similar rate for transport (k_{trans}) is assumed. French et al. report degradation constants for EGF and several of its analogs (56). Based on these results, an average degradation constant of 0.02 min^{-1} was used in the model. Since it has been reported that membrane bound transferrin and IgA are sorted to recycling endosomes while fluid marker such as LDL and HRP are sorted to lysosomes (65, 107, 166), it is assumed that receptors and ligand/receptor complexes are destined for recycling or transport, while dissociated ligands are destined for degradation. French et al. report recycling fractions ($(1-f_l)$ in this model) for various EGF receptor bound ligands that range from approximately 0.5 to 0.8. The model assumes degradation sorting fractions of 0.25 for receptors and complexes and 0.75 for free ligand.

5.5 Solution of Model

The system of 45 ordinary differential equations (Appendix A) were solved using MATLAB (version 6 release 12, The Mathworks) and the stiff ordinary differential equation solver, ode15s, with all default options except that the backward differentiation formulas option was used (Appendix B).

5.6 Results and Discussion

The primary goal of this research was to determine how the transport mechanisms, such as binding, internalization, and sorting, impacted overall delivery of IGF-I. To assess this, a mathematical model was developed based on previous experimental data (Chapter 4) to determine the contributions of the parameters to overall delivery. Results from this model showed similar trends as the experimental data (Figure 3), suggesting the model is an adequate *in silica* representation of *in vitro* endothelium.

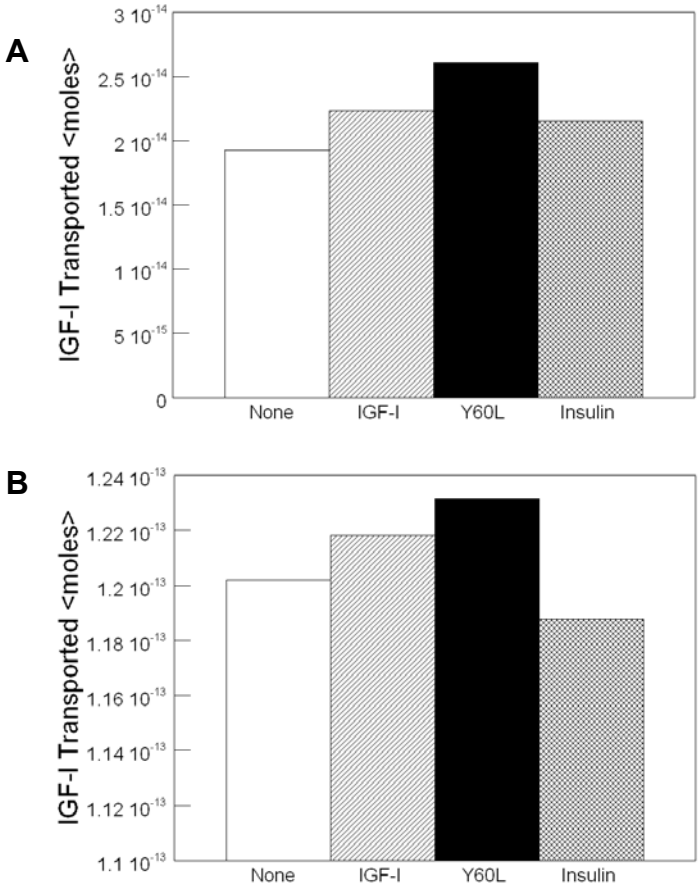

Figure 5.3: In vitro and in silica transport of IGF-I

IGF-I transported in the absence (none) (○) or presence of binding competitors (IGF-I (2 μg/ml) (∅), Y60L-IGF-I (2 μg/ml) (●), or insulin (10 μg/ml) (⊗)) over 12 hrs from the apical to basolateral side of (A) bovine aortic endothelial cells (BAECs) or (B) model endothelium.

It has previously been shown that there was significant transport of IGF-I through the paracellular pathway of bovine aortic endothelial cells cultured on rat tail collagen and fibronectin coated inserts (Chapter 4). Since this kinetic parameter was fit to the data and not measure directly, this research sought to evaluate the effects of cell layer porosity on the transport of IGF-I. The maximum delivery of IGF-I was reached when the porosity varied between 0.6 and 1.0 and an impermeable cell layer (0.0 porosity) still allowed transport of IGF-I, through IGF-IR mediated processes, that was 11% of maximum (Figure 4). The porosity used in this model, 0.25, allowed delivery of IGF-I that was 93% of the maximum. Since paracellular transport is dependent on molecular size, it is reasonable that there would be a porosity at which there is no longer a barrier to free diffusion, 0.6 for the case of IGF-I.

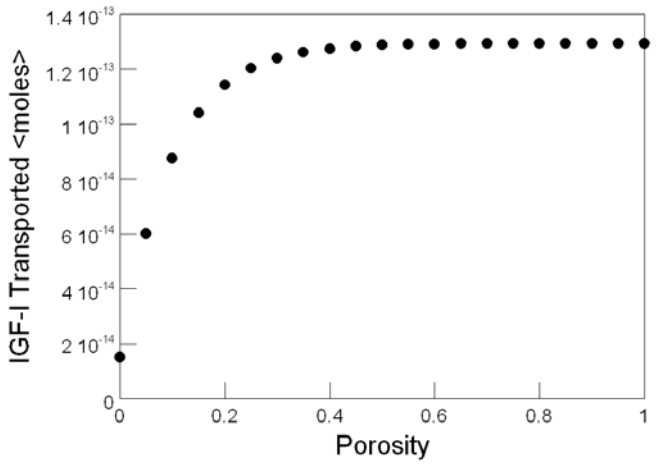

Figure 5.4: Affect of porosity on IGF-I transport

IGF-I transported from the apical to basolateral side of a model endothelium with varying porosity

Since there was no detectable internalization of IGFBPs in the experimental system, such as that reported by for different cell types (53), the model was used to varying the internalization rates of free IGFBPs and IGF-I / IGFBP complexes between the base case, where there was no internalization (k_{eB},k_{eX} = 0), to rates similar to that measured for IGF-I / IGF-IR internalization (0.76 min $^{-1}$). There was a decrease, in the amount of IGF-I transported when free IGFBPs were allowed to internalize and an increase when IGF-I / IGBFP complexes were allowed to internalize (Figure 5.5). Since the sorting

parameters used in the base case of the model assumed preferential recycling of IGFBPs, either free or in complex, IGFBPs internalized from the apical surface are mostly returned to the apical surface. However, once returned to the apical surface, IGF-I may then be released and transported paracellular. The decrease detected when free IGFBPs were allowed to internalize was due to sequestration of IGF-I away from IGF-IRs in the endosomes, resulting in apical recycling rather than basolateral transport of IGF-I.

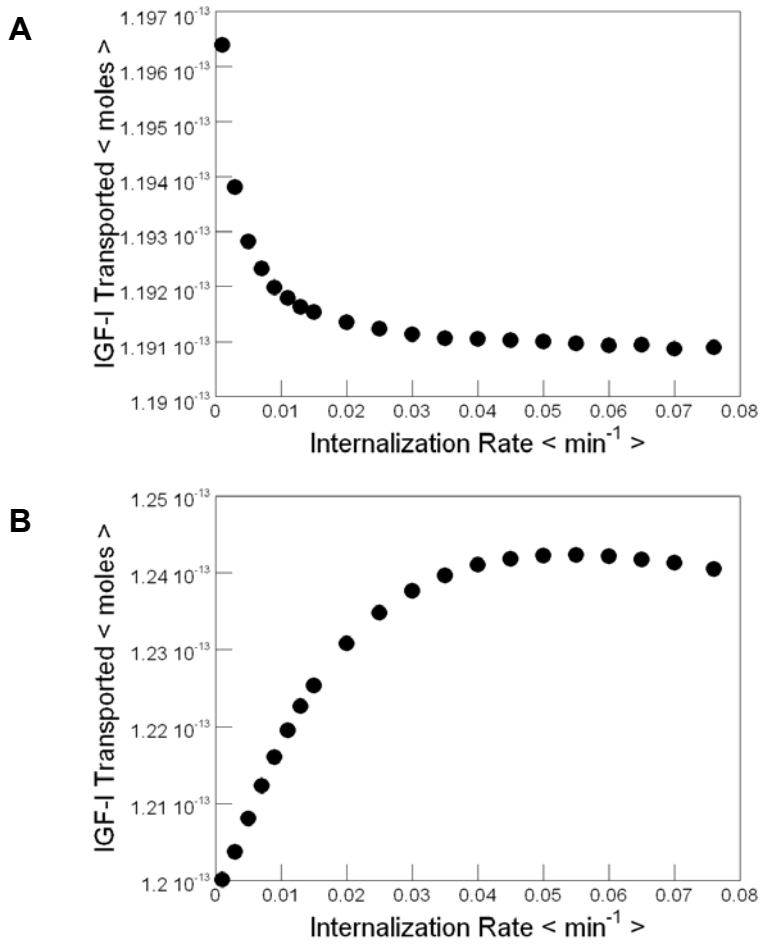

Figure 5.5: Effect of IGFBP internalization on IGF-I transport

IGF-I transported from the apical to basolateral side of a model endothelium with varying internalization rates for (A) free IGFBPs and (B) IGF-I/IGFBP complexes

Delivery of therapeutics, such as growth factors, is an active transport process that relies on cell-mediated uptake, sorting, and delivery. The sorting of growth factors,

such as EGF, depends on their ability to bind their receptors in the acidic environment of the endosomes. The receptor for EGF can also bind with high affinity to similar molecules, such as transforming growth factor-α (TGF-α) . At normal physiological pH, mouse EGF (mEGF), human EGF (hEGF), and TGF-α have very similar binding kinetics (56). However, at acidic pH, such as that found in endosomes, the ratio of binding affinities of TGF-α at pH 6 and pH 7.4 is 9 times that of mEGF. These differences in binding lead to a difference in sorting kinetics for each EGF receptor ligand (56, 120). Similarly, Bevan et al. report that analogues of insulin with enhanced

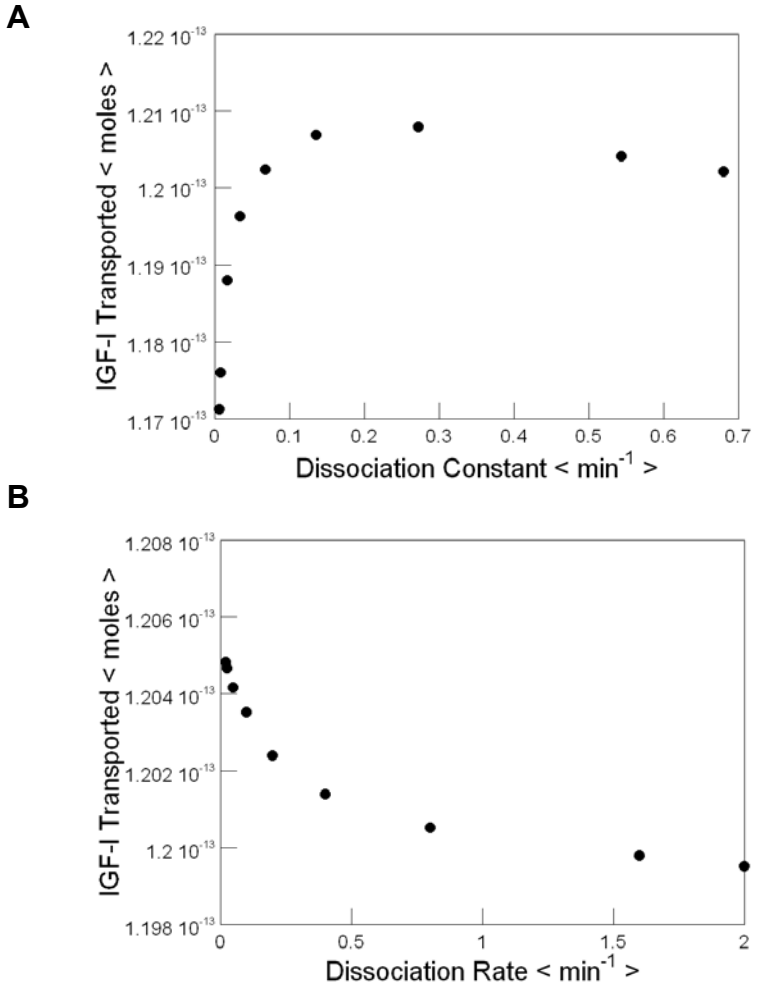

Figure 5.6: Affect of dissociation from IGF-IR on IGF-I transport

IGF-I transported from the apical to basolateral side of a model endothelium with varying dissociation rates for IGF-I and IGF-IR at (A) pH 7.4 and (B) pH 5.8

receptor binding at acidic pH undergo less degradation (39% and 25%) *in vivo* than insulin (55%) (17). They also report that insulin undergoes maximum degradation at pH 6, the conditions found in endosomes. The binding affinities of IGF-I for IGF-IR and IGFBPs at acidic pH have not been reported, however, Zapf et al. reported that at pH 7.4, binding of IGF-I to Rat-1 fibroblasts and HIRc B cells, presumably to IGF-IRs, was approximately 80% of maximal binding and at pH 6.0, binding was nearly 30% of maximum (201). In addition, Forsten et al. reported that binding of IGF-I to IGFBPs at pH 5.8 was 72% of that at pH 7.4 (53)

To determine the effect of binding affinities on overall delivery of IGF-I, the dissociation constants (k_{off}) for IGF-I to each binding site at pH 7.4 and pH 5.8 were varied. Counter to what might be expected, increased dissociation of IGF-I from IGF-IRs at pH 7.4 resulted in increased transport of IGF-I through the paracellular pathway (Figure 5.6A). In contrast, increased dissociation at pH 5.8 resulted in decreased delivery of IGF-I due to increased degradation of free IGF-I (Figure 5.6B). Similarly, increased dissociation of IGF-I from IGFBPs at pH 7.4 resulted in enhanced delivery of IGF-I (Figure 5.7A), due to increased IGF-I available for IGF-IR mediated and paracellular transport. However, changes in the dissociation of IGF-I from IGFBPs at pH 5.8 did not substantially alter delivery of IGF-I (Figure 5.7B) since there were no IGFBPs present in the endosomes.

Computational models have been utilized to expand the knowledge base of the mechanisms by which growth factor act, as recently reviewed by Wiley et al (196). Significant contributions have been made in the past decade that aid in an understanding of the mechanisms involved in sorting and signaling of the EGF receptor and its family of ligands, which may facilitate the development of therapeutic strategies involving the EGF family to treat various pathological conditions. Models have been developed that describe sorting of EGF and several EGF analogs (56, 79, 176) and the dependence of acidic binding on sorting outcome (56). Starbuck and Lauffenburger reported that increased dissociation of EGF from EGF receptors resulted in decreased cell proliferation, supporting results that indicated that increased dissociation prevents

interaction with binding sites and promotes paracellular transport (Figure 5.6 and Figure 5.7)

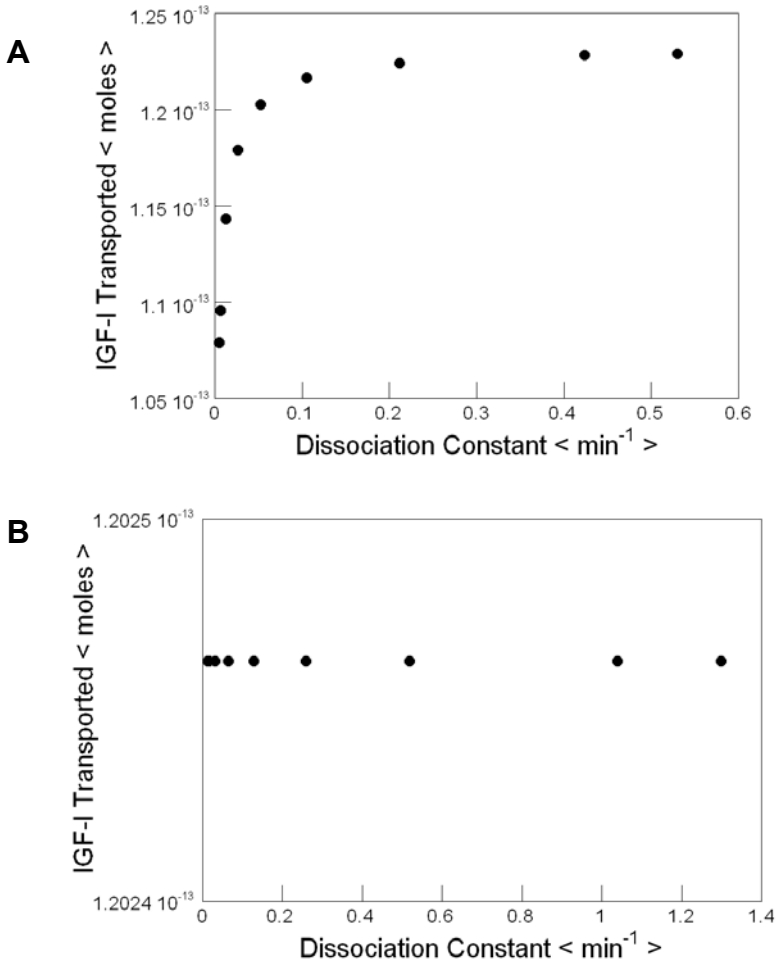

Figure 5.7: Affect of dissociation from IGFBPs on IGF-I transport

IGF-I transported from the apical to basolateral side of a model endothelium with varying dissociation rates for IGF-I and IGFBPs at (A) pH 7.4 and (B) pH 5.8

The degradation (Figure 5.8) and transport (Figure 5.9) sorting fractions for IGFBPs, IGF-I / IGFBP complexes, and IGF-I / IGF-IR complexes were varied to determine their contributions to IGF-I delivery. Since there were no IGFBPs present in the endosomes, varying the sorting fractions for IGFBPs and IGF-I / IGFBP complexes did not affect transport of IGF-I (Figure 5.8A and Figure 5.9A). However, increasing the degradation sorting fraction for IGF-I / IGF-IR complexes decreased IGF-I delivery

(Figure 5.8B) while increasing the transport sorting fraction for these complexes promoted delivery (Figure 5.9B). Since the degradation rate constant is an order of magnitude smaller than the transport and recycling rates, as the delivery of IGF-I becomes more dependent on the degradation rate, there is a decrease in total IGF-I transported and an intracellular accumulation of IGF-I / IGF-IR complexes.

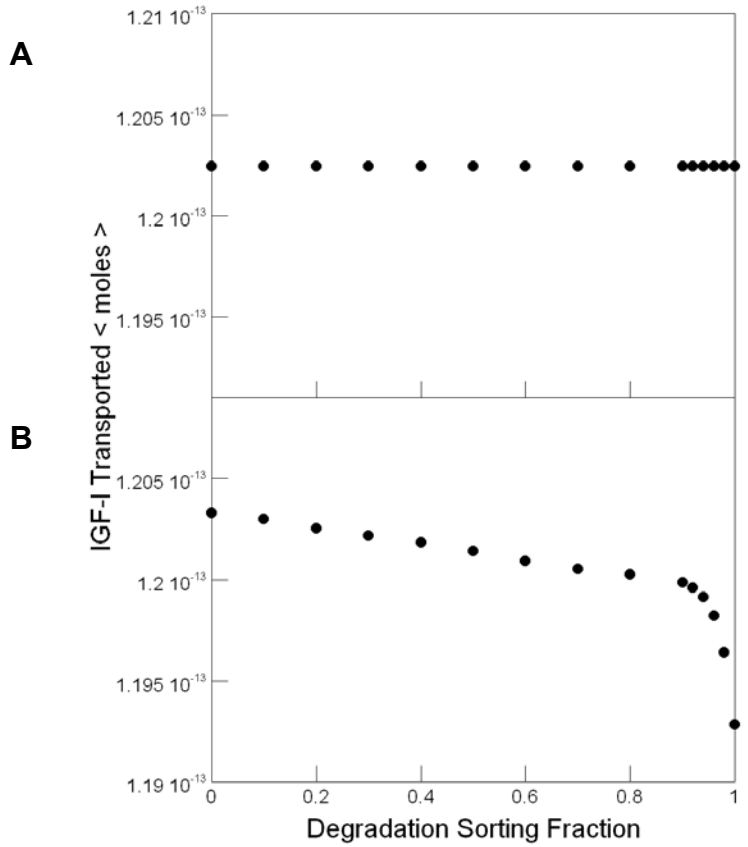

Figure 5.8: Affect of degradation sorting fractions on IGF-I transport

IGF-I transported from the apical to basolateral side of a model endothelium with varying degradation sorting fractions for (A) IGFBPs and IGF-I/IGFBP complexes and (B) IGF-I/IGF-IR complexes

.

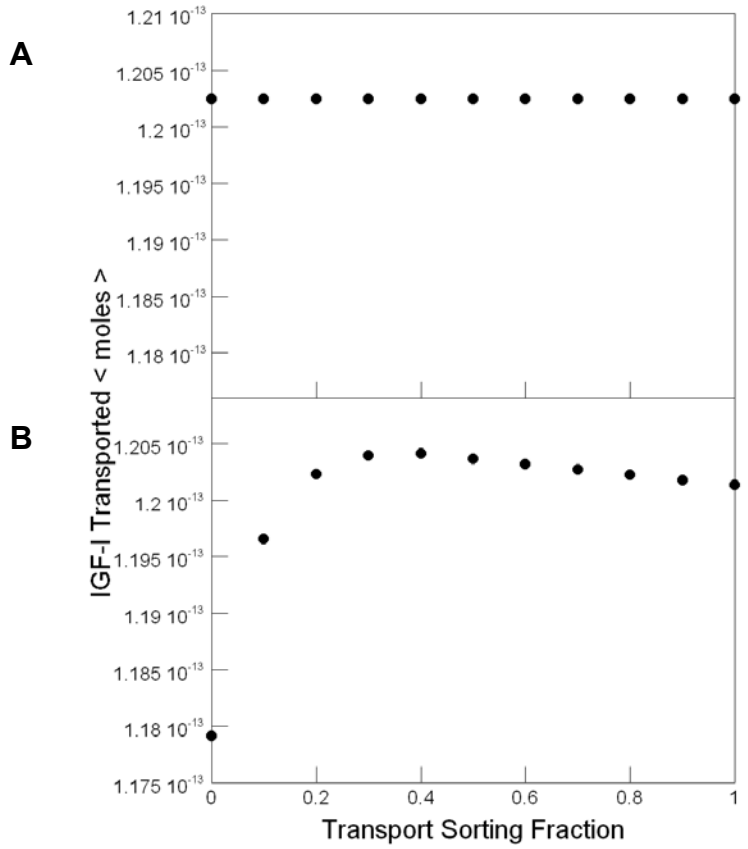

Figure 5.9: Affect of transport sorting fractions on IGF-I transport

IGF-I transported from the apical to basolateral side of a model endothelium with varying transport sorting fractions for (A) IGFBPs and IGF-I/IGFBP complexes and (B) IGF-I/IGF-IR complexes

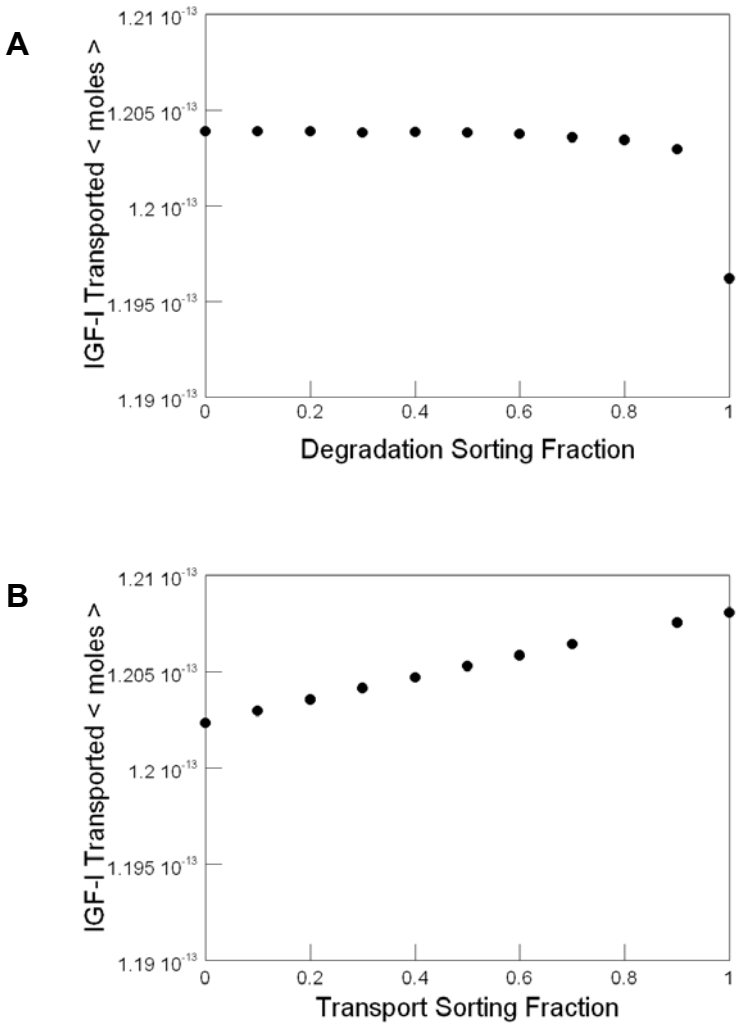

Figure 5.10: Combined affects of IGFBP internalization and sorting fractions on IGF-I transport

IGF-I transported from the apical to basolateral side of a model endothelium with varying degradation (A) and transport (B) sorting fractions for IGFBPs and IGF-I / IGFBPs when internalization is allowed at levels similar to IGF-IRs

To evaluate the affect of sorting fraction when IGFBPs are internalized, such as that found in other cell types, the internalization rate of free IGFBPs was defined similar to free IGF-IRs and IGF-I / IGFBP complexes were allowed to internalize at a similar rate as IGF-I / IGF-IRs. Similar to IGF-I / IGF-IR complexes (Figure 5.8B), when the degradation sorting fraction for IGF-I / IGFBP complexes increased, there was an initial gradual decrease in IGF-I transported followed by a dramatic decrease as transport became less dependent on the recycling rate constant and more dependent on

the slower degradation rate (Figure 5.10A). In addition, when as the transport sorting fraction increased, the amount of IGF-I transport also increased.

Computational models may also be utilized to identify key parameters to target when developing engineered growth factors for the treatment of diseases. The parameter in this model that impacted IGF-I delivery the most was the porosity of the cell layer (Figure 5.4). However, since the integrity of epithelial and endothelial layers is essential to their function, it is not feasible to design growth factors that increase cell layer permeability. Alternatively, the sorting factions (Figure 5.8, Figure 5.9) and internalization rates (Figure 5.10) are reasonable targets for the design of engineered growth factors. Since the sorting fractions are dictated by binding affinities in the acidic environment of the endosomes, it may be beneficial to design and analogs of IGF-I that are more resistant to changes in pH. Lauffenburger et al. have developed EGF variants whose binding affinities for EGF receptors are less sensitive to changes in pH (102). These variants were sorted preferentially into recycling rather than degradation pathways and exhibit increased mitogenic potency in comparison with wild type EGF, suggesting a similar approach may be feasible for IGF-I.

Chapter 4 showed data that indicated that IGFBPs inhibited IGF-I transport by acting as a surface reservoir for IGF-I. However, it is possible that this reservoir of IGF-I could facilitate overall transport of IGF-I under the correct conditions. To test this, the model system was subjected to an apical bolus of IGF-I for 60 min and apical to basolateral transport was measured for an additional 11 hrs (Figure 4.6). When IGFBPs were removed from the system, there was an initial increase in IGF-I transported during the pulse phase. However, after unbound apical IGF-I was removed from the model system, there was significantly more IGF-I delivered when IGFBPs were present, supporting the hypothesis that IGFBPs serve as a reservoir that promote long-term delivery of IGF-I. This research sought to determine the affect of pulse duration of this promoting characteristic of IGFBPs to further characterize the reservoir function of the IGFBPs. To achieve this, simulations were run using various pulse durations and the transport of IGF-I in the presence and absence of IGFBPs was recorded. Pulse

durations of less than 6 hrs resulted in enhanced delivery of IGF-I in the presence of IGFBPs, above that for delivery in the absence of IGFBPs (Figure 5.11). This suggests cell or matrix associated IGFBPs will enhance IGF-I delivery when physiological fluctuations in serum IGF-I levels are less than 6 hrs in duration.

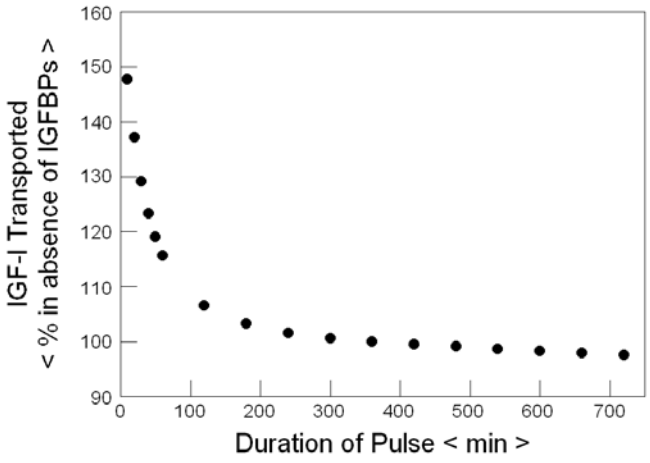

Figure 5.11: Affect of pulse duration of the function of IGFBPs as an IGF-I reservoir

IGF-I transported from the apical to basolateral side of a model endothelium in the presence of surface IGFBPs after a pulse of IGF-I with varying duration. Pulse period was followed by chase period such that the total observation time was 12 hours. Results are normalized to transport of IGF-I in the absence of IGFBPs

Chapter 6: Conclusions and Future Work

Growth factors, such as insulin-like growth factor-I (IGF-I), are important regulators of cell division and tissue proliferation and, consequently, play a vital role in embryonic development (4, 43), wound healing (144), as well as in the development and treatment of various pathological conditions (6, 42, 73, 76, 96, 98, 99, 108, 136, 137, 149, 152-154, 179, 183). The role of IGF-I in these pathological conditions varies. For instance, many tumors over express IGF-I or other family members, such as IGF-II and IGF-IR, (73, 76, 136, 149, 179, 183) and high serum levels of IGF-I have been associated with an increased risk of developing cancer (60, 170). On the other hand, IGF-I has the potential to treat a variety of disorders, such as severe insulin resistance (99, 153), leprechaunism (6), renal failure (98), neurological disorders (108), Laron Syndrome (154), and diabetes (42, 96, 137, 152). The main objectives of this research was to demonstrate that 1) autocrine production of IGF-I, such as that found in tumor cells, alters epithelial cell layer permeability which could facilitate metastasis and 2) transport of IGF-I across endothelial cells is regulated by IGFBPs.

To meet the first objective, parental and IGF-I secreting bovine mammary epithelial cells were tested for cell layer permeability, tight and adherens junction proteins, IGF-IR, and one of its downstream signaling components (Akt). Parental cells (MAC-T) formed nearly exclusive barriers to the transport of phenol barriers while both IGF-I secreting cells (TK-IGF-I and SV40-IGF-I) formed poor barriers (Figure 2.2). In comparison with parental cells, IGF-I secreting cells had high levels of IGF-IRs, but low levels of the junction components E-cadherin, β-catenin (Figure 2.7), and occludin (Appendix E). The differences in parental and IGF-I secreting cells was not due to extracellular stimuli since inclusion of IGF-I (Figure 2.4), IGFBP-3 (Figure 2.5), or coculture (Table 2.1) with SV40-IGF-I cells did not alter the barrier properties of parental cells. Further work needs to be conducted to determine the intracellular mechanisms involved in disruption of the junction components in IGF-I secreting cells. Western immunoblots should be conducted to identify key signaling components mediating signaling from the IGF-IR and junction proteins as well as the levels of E-

cadherin and β-catenin following continuous incubation of IGF-I. In addition, identification of the subcellular distribution of IGF-IRs and β-catenin should be conducted, perhaps through confocal imaging or cell fractionation.

The second objective focused on exogenous rather than endogenous IGF-I and the role of IGFBPs and IGF-IRs in ligand transcytosis. Since Bastian et al. report predominantly paracellular transport of IGF-I in both epithelial (13) and endothelial (14) cells, culture conditions were optimized to develop an *in vitro* model endothelial system that minimized paracellular transport and was more representative of *in vivo* endothelium. Of the three types of endothelial cells tested, bovine aortic endothelial cells (BAECs) formed the best and more consistent transport barriers (Figure 3.1). In addition, various surface coating and initial plating densities were tested and BAECs initially plated at 5 x 10^4 cells/cm^2 on rat tail collagen and fibronectin (RTCF) inserts and cultured for 8 days form the best transport barriers (Figure 3.2). Western immunoblots (Figure 3.4) indicated that BAECs cultured under these conditions expressed more occludin, a key regulator of paracellular transport, than BAECs cultured on other surfaces or at other initial plating densities. Future work should be conducted to investigate different surface coatings such as laminin and various cell types, particularly HUVECs.

Once paracellular transport was optimized in this *in vitro* model endothelium, experiments were conducted to determine the mechanisms involved in transport of IGF-I. Transport studies showed that, although there was still significant paracellular transport, IGFBPs inhibited and IGF-IRs promoted transport of IGF-I (Figure 4.1). Binding studies determined that IGF-I has similar binding affinity for both binding sites (IGFBPs and IGF-IRs) but there were twice as many IGFBP binding sites as IGF-IR sites (Figure 4.4). Although IGFBPs bind more IGF-I, the complexes formed are not internalized (Figure 4.5B). In contrast, IGF-I / IGF-IR complexes are internalized with a rate constant of 0.076 min^{-1}. Further work needs to be conducted to determine the location of IGFBP binding sites, matrix vs. cell surface, and the distribution of IGFBP species between these locations. A computational model was developed to identify key

parameters to target when developing engineered growth factors for the treatment of diseases. The most influential parameter was the porosity of the cell layer (Figure 5.4). However, since the integrity of epithelial and endothelial layers is essential to their function, it is not feasible to design growth factors that increase cell layer permeability. Alternatively, the sorting factions (Figure 5.8 and Figure 5.9) and internalization rates (Figure 5.10) are reasonable targets for the design of engineered growth factors. Since the sorting fractions are dictated by binding affinities in the acidic environment of the endosomes, it may be beneficial to design and analog of IGF-I that is more resistant to changes in pH.

To obtain a more rigorous computational model of this transport process, further experiments need to be conducted to determine the binding and dissociation constants for all ligand and binding sites at pH 7.4 and pH 5.8. The model can also be updated to include the affects of IGFBPs in solution and the individual contributions of each IGFBP species. In addition, sorting fractions for all components need to be measured directly and the model may be modified to include early and late endosome and lysosomes. It may also prove beneficial to conduct similar studies with HUVECs to determine the mechanisms causing differences in IGF-I transport compared to the BAEC system or with colon epithelial cells, such as Caco-2, as a model for oral delivery of IGF-I. Further considerations could involve the use of a bioreactor, such as the Cellmax® capillary system, that could incorporate pulsatile shear flow as well as co-culture with smooth muscle cells, to better model the *in vivo* vascular environment.

References

1. **Adams TE, Epa VC, Garrett TP, and Ward CW.** Structure and function of the type 1 insulin-like growth factor receptor. *Cell Mol Life Sci* 57: 1050-1093., 2000.

2. **Akers RM, McFadden TB, Beal WE, Guidry AJ, and Farrell HM.** Radioimmunoassay for measurement of bovine alpha-lactalbumin in serum, milk and tissue culture media. *J Dairy Res* 53: 419-429, 1986.

3. **Ali S.** Transferrin trojan horses as a rational approach for the biological delivery of therapeutic peptide domains. *J Biol Chem* 274: 24066-24073, 1999.

4. **Allan GJ, Flint DJ, and Patel K.** Insulin-like growth factor axis during embryonic development. *Reproduction* 122: 31-39, 2001.

5. **Andre F, Rigot V, Thimonier J, Montixi C, Parat F, Pommier G, Marvaldi J, and Luis J.** Integrins and E-cadherin cooperate with IGF-I to induce migration of epithelial colonic cells. *Int J Cancer* 83: 497-505., 1999.

6. **Backeljauw PF, Alves C, Eidson M, Cleveland W, Underwood LE, and Davenport ML.** Effect of intravenous insulin-like growth factor I in two patients with leprechaunism. *Pediatr Res* 36: 749-754, 1994.

7. **Balda MS, Whitney JA, Flores C, Gonzalez S, Cereijido M, and Matter K.** Functional dissociation of paracellular permeability and transepithelial electrical resistance and disruption of the apical-basolateral intramembrane diffusion barrier by expression of a mutant tight junction membrane protein. *J Cell Biol* 134: 1031-1049, 1996.

8. **Banskota NK, Carpentier JL, and King GL.** Processing and release of insulin and insulin-like growth factor I by macro- and microvascular endothelial cells. *Endocrinology* 119: 1904-1913, 1986.

9. **Bar RS, Boes M, Clemmons DR, Busby WH, Sandra A, Dake BL, and Booth BA.** Insulin differentially alters transcapillary movement of intravascular IGFBP-1, IGFBP-2 and endothelial cell IGF-binding proteins in the rat heart. *Endocrinology* 127: 497-499, 1990.

10. **Bar RS, Boes M, Dake BL, Sandra A, Bayne M, Cascieri M, and Booth BA.** Tissue localization of perfused endothelial cell IGF binding protein is markedly altered by association with IGF-I. *Endocrinology* 127: 3243-3245, 1990.

11. **Bar RS, Boes M, and Yorek M.** Processing of insulin-like growth factors I and II by capillary and large vessel endothelial cells. *Endocrinology* 118: 1072-1080, 1986.

12. **Bar RS, Clemmons DR, Boes M, Busby WH, Booth BA, Dake BL, and Sandra A.** Transcapillary permeability and subendothelial distribution of endothelial and amniotic fluid insulin-like growth factor binding proteins in the rat heart. *Endocrinology* 127: 1078-1086, 1990.

13. **Bastian SE, Walton PE, Ballard FJ, and Belford DA.** Transport of IGF-I across epithelial cell monolayers. *J Endocrinol* 162: 361-369, 1999.

14. **Bastian SE, Walton PE, and Belford DA.** Paracellular transport of insulin-like growth factor-I (IGF-I) across human umbilical vein endothelial cell monolayers. *J Cell Physiol* 170: 290-298, 1997.

15. **Bastian SE, Walton PE, and Belford DA.** Transport of circulating IGF-I and LR3IGF-I from blood to extracellular wound fluid sites in rats. *J Endocrinol* 164: 77-86, 2000.

16. **Bayne ML, Applebaum J, Chicchi GG, Miller RE, and Cascieri MA.** The roles of tyrosines 24, 31, and 60 in the high affinity binding of insulin-like growth factor-I to the type 1 insulin-like growth factor receptor. *J Biol Chem* 265: 15648-15652, 1990.

17. **Beavon IR.** The E-cadherin-catenin complex in tumour metastasis: structure, function and regulation. *Eur J Cancer* 36: 1607-1620, 2000.

18. **Bereket A, Lang CH, and Wilson TA.** Alterations in the growth hormone-insulin-like growth factor axis in insulin dependent diabetes mellitus. *Horm Metab Res* 31: 172-181, 1999.

19. **Bevan AP, Seabright PJ, Tikerpae J, Posner BI, Smith GD, and Siddle K.** The role of insulin dissociation from its endosomal receptor in insulin degradation. *Mol Cell Endocrinol* 164: 145-157, 2000.

20. **Biegel D and Pachter JS.** Growth of brain microvessel endothelial cells on collagen gels: applications to the study of blood-brain barrier physiology and CNS inflammation. *In Vitro Cell Dev Biol Anim* 30A: 581-588, 1994.

21. **Bilak MM, Hossain WA, and Morest DK.** Intracellular fibroblast growth factor produces effects different from those of extracellular application on development of avian cochleovestibular ganglion cells in vitro. *J Neurosci Res* 71: 629-647, 2003.

22. **Blum WF, Jenne EW, Reppin F, Kietzmann K, Ranke MB, and Bierich JR.** Insulin-like growth factor I (IGF-I)-binding protein complex is a better mitogen than free IGF-I. *Endocrinology* 125: 766-772, 1989.

23. **Boes M, Dake BL, Booth BA, Sandra A, Bateman M, Knudtson KL, and Bar RS.** IGF-I and IGFBP-3 transport in the rat heart. *Am J Physiol Endocrinol Metab* 284: E237-239, 2003.

24. **Boroujerdi MA, Sonksen PH, and Jones RH.** A compartmental model for simulation of IGF-I kinetics and metabolism. *Methods Inf Med* 33: 514-521, 1994.

25. **Braga V.** Cell-cell adhesion and signalling. *Curr Opin Cell Biol* 14: 546, 2002.

26. **Bremnes RM, Veve R, Hirsch FR, and Franklin WA.** The E-cadherin cell-cell adhesion complex and lung cancer invasion, metastasis, and prognosis. *Lung Cancer* 36: 115-124, 2002.

27. **Burroughs KD, Oh J, Barrett JC, and DiAugustine RP.** Phosphatidylinositol 3-kinase and mek1/2 are necessary for insulin-like growth factor-I-induced vascular endothelial growth factor synthesis in prostate epithelial cells: a role for hypoxia-inducible factor-1? *Mol Cancer Res* 1: 312-322, 2003.

28. **Cassino TR.** *Quantification of the binding of insulin-like growth factor-I (IGF-I) and IGF binding protein-3 (IGFBP-3) using surface plasmon resonance* (MS Thesis). Blacksburg, Virginia: Virginia Polytechnic Institute & State University, 2002.

29. **Chow JC, Condorelli G, and Smith RJ.** Insulin-like growth factor-I receptor internalization regulates signaling via the shc/mitogen-activated protein kinase pathway, but not the insulin receptor substrate-1 pathway. *J Biol Chem* 273: 4672-4680, 1998.

30. **Clemmons DR and Gardner LI.** A factor contained in plasma is required for IGF binding protein-1 to potentiate the effect of IGF-I on smooth muscle cell DNA synthesis. *J Cell Physiol* 145: 129-135, 1990.

31. **Conacci-Sorrell M, Zhurinsky J, and Ben-Ze'ev A.** The cadherin-catenin adhesion system in signaling and cancer. *J Clin Invest* 109: 987-991, 2002.

32. **Conover CA and Powell DR.** Insulin-like growth factor (IGF)-binding protein-3 blocks IGF-I-induced receptor down-regulation and cell desensitization in cultured bovine fibroblasts. *Endocrinology* 129: 710-716., 1991.

33. **Coschigano KT, Clemmons D, Bellush LL, and Kopchick JJ.** Assessment of growth parameters and life span of GHR/BP gene-disrupted mice. *Endocrinology* 141: 2608-2613, 2000.

34. **Dehouck B, Fenart L, Dehouck MP, Pierce A, Torpier G, and Cecchelli R.** A new function for the LDL receptor: transcytosis of LDL across the blood-brain barrier. *J Cell Biol* 138: 877-889., 1997.

35. **Dehouck MP, Meresse S, Delorme P, Fruchart JC, and Cecchelli R.** An easier, reproducible, and mass-production method to study the blood- brain barrier in vitro. *J Neurochem* 54: 1798-1801, 1990.

36. **Dejana E, Corada M, and Lampugnani MG.** Endothelial cell-to-cell junctions. *Faseb J* 9: 910-918, 1995.

37. **Del Vecchio PJ, Siflinger-Birnboim A, Shepard JM, Bizios R, Cooper JA, and Malik AB.** Endothelial monolayer permeability to macromolecules. *Fed Proc* 46: 2511-2515, 1987.

38. **Dietrich C, Scherwat J, Faust D, and Oesch F.** Subcellular localization of beta-catenin is regulated by cell density. *Biochem Biophys Res Commun* 292: 195-199, 2002.

39. **Dodane V, Amin Khan M, and Merwin JR.** Effect of chitosan on epithelial permeability and structure. *Int J Pharm* 182: 21-32., 1999.

40. **Dowd CJ, Cooney CL, and Nugent MA.** Heparan sulfate mediates bFGF transport through basement membrane by diffusion with rapid reversible binding. *J Biol Chem* 274: 5236-5244., 1999.

41. **Dubois V, Couissi D, Schonne E, Schneider YJ, Remacle C, and Trouet A.** Estrogen and insulin modulation of intracellular insulin-like growth factor binding proteins in human breast cancer cells: possible involvement in lysosomal hydrolases oversecretion. *Biochem Biophys Res Commun* 192: 295-301, 1993.

42. **Dunger DB and Acerini CL.** Does recombinant human insulin-like growth factor-1 have a role in the treatment of diabetes? *Diabet Med* 14: 723-731, 1997.

43. **Dunker N and Krieglstein K.** Targeted mutations of transforming growth factor-beta genes reveal important roles in mouse development and adult homeostasis. *Eur J Biochem* 267: 6982-6988, 2000.

44. **Elgin RG, Busby WH, Jr., and Clemmons DR.** An insulin-like growth factor (IGF) binding protein enhances the biologic response to IGF-I. *Proc Natl Acad Sci U S A* 84: 3254-3258, 1987.

45. **Elhadj S, Akers RM, and Forsten-Williams K.** Chronic pulsatile shear stress alters insulin-like growth factor-I (IGF-I) binding protein release in vitro. *Ann Biomed Eng* 31: 163-170, 2003.

46. **Fawcett J and Rabkin R.** The processing of insulin-like growth factor-I (IGF-I) by a cultured kidney cell line is altered by IGF-binding protein-3. *Endocrinology* 136: 1340-1347., 1995.

47. **Federici M, Porzio O, Zucaro L, Giovannone B, Borboni P, Marini MA, Lauro D, and Sesti G.** Increased abundance of insulin/IGF-I hybrid receptors in adipose tissue from NIDDM patients. *Mol Cell Endocrinol* 135: 41-47, 1997.

48. **Federici M, Zucaro L, Porzio O, Massoud R, Borboni P, Lauro D, and Sesti G.** Increased expression of insulin/insulin-like growth factor-I hybrid receptors in skeletal muscle of noninsulin-dependent diabetes mellitus subjects. *J Clin Invest* 98: 2887-2893, 1996.

49. **Ferruzza S, Scarino ML, Rotilio G, Ciriolo MR, Santaroni P, Muda AO, and Sambuy Y.** Copper treatment alters the permeability of tight junctions in cultured human intestinal Caco-2 cells. *Am J Physiol* 277: G1138-1148., 1999.

50. **Ferry Jr RJ, Cerri RW, and Cohen P.** Insulin-like growth factor binding proteins: new proteins, new functions. *Horm Res* 51: 53-67, 1999.

51. **Fisher KD, Ulbrich K, Subr V, Ward CM, Mautner V, Blakey D, and Seymour LW.** A versatile system for receptor-mediated gene delivery permits increased entry of DNA into target cells, enhanced delivery to the nucleus and elevated rates of transgene expression. *Gene Ther* 7: 1337-1343., 2000.

52. **Forbes BE, Hartfield PJ, McNeil KA, Surinya KH, Milner SJ, Cosgrove LJ, and Wallace JC.** Characteristics of binding of insulin-like growth factor (IGF)-I and IGF-II analogues to the type 1 IGF receptor determined by BIAcore analysis. *Eur J Biochem* 269: 961-968, 2002.

53. **Forsten KE, Akers RM, and San Antonio JD.** Insulin-like growth factor (IGF) binding protein-3 regulation of IGF-I is altered in an acidic extracellular environment. *J Cell Physiol* 189: 356-365., 2001.

54. **Forsten KE and Lauffenburger DA.** The role of low-affinity interleukin-2 receptors in autocrine ligand binding: alternative mechanisms for enhanced binding effect. *Mol Immunol* 31: 739-751, 1994.

55. **Frank HJ, Pardridge WM, Morris WL, Rosenfeld RG, and Choi TB.** Binding and internalization of insulin and insulin-like growth factors by isolated brain microvessels. *Diabetes* 35: 654-661, 1986.

56. **French AR, Tadaki DK, Niyogi SK, and Lauffenburger DA.** Intracellular trafficking of epidermal growth factor family ligands is directly influenced by the pH sensitivity of the receptor/ligand interaction. *J Biol Chem* 270: 4334-4340, 1995.

57. **Friedl J, Puhlmann M, Bartlett DL, Libutti SK, Turner EN, Gnant MF, and Alexander HR.** Induction of permeability across endothelial cell monolayers by tumor necrosis factor (TNF) occurs via a tissue factor-dependent mechanism: relationship between the procoagulant and permeability effects of TNF. *Blood* 100: 1334-1339, 2002.

58. **Frystyk J, Bek T, Flyvbjerg A, Skjaerbaek C, and Orskov H.** The relationship between the circulating IGF system and the presence of retinopathy in Type 1 diabetic patients. *Diabet Med* 20: 269-276, 2003.

59. **Furlanetto RW.** Receptor-mediated endocytosis and lysosomal processing of insulin-like growth factor I by mitogenically responsive cells. *Endocrinology* 122: 2044-2053, 1988.

60. **Furstenberger G and Senn HJ.** Insulin-like growth factors and cancer. *Lancet Oncol* 3: 298-302, 2002.

61. **Garberg P.** In vitro models of the blood-brain barrier. *ATLA* 26: 821-847, 1998.

62. **Garcia AM, Szasz N, Trippel SB, Morales TI, Grodzinsky AJ, and Frank EH.** Transport and binding of insulin-like growth factor I through articular cartilage. *Arch Biochem Biophys* 415: 69-79, 2003.

63. **Gartner LP and Hiatt JL.** Circulatory System. In: *Color Atlas of Histology* (2nd ed.), edited by Coryell P. Baltimore: Williams & Wilkins, 1994, p. 144-160.

64. **Ghinea N and Milgrom E.** Transport of protein hormones through the vascular endothelium. *J Endocrinol* 145: 1-9, 1995.

65. **Ghosh RN, Gelman DL, and Maxfield FR.** Quantification of low density lipoprotein and transferrin endocytic sorting HEp2 cells using confocal microscopy. *J Cell Sci* 107 (Pt 8): 2177-2189, 1994.

66. **Gibson A, Futter CE, Maxwell S, Allchin EH, Shipman M, Kraehenbuhl JP, Domingo D, Odorizzi G, Trowbridge IS, and Hopkins CR.** Sorting mechanisms regulating membrane protein traffic in the apical transcytotic pathway of polarized MDCK cells. *J Cell Biol* 143: 81-94, 1998.

67. **Gospodarowicz D, Delgado D, and Vlodavsky I.** Permissive effect of the extracellular matrix on cell proliferation in vitro. *Proc Natl Acad Sci U S A* 77: 4094-4098, 1980.

68. **Gottardi CJ and Gumbiner BM.** Adhesion signaling: how beta-catenin interacts with its partners. *Curr Biol* 11: R792-794, 2001.

69. **Gray H.** *Gray's Anatomy*. New York: Barnes & Noble Books, 1901.

70. **Grulich-Henn J, Ritter J, Mesewinkel S, Heinrich U, Bettendorf M, and Preissner KT.** Transport of insulin-like growth factor-I across endothelial cell monolayers and its binding to the subendothelial matrix. *Exp Clin Endocrinol Diabetes* 110: 67-73, 2002.

71. **Guevara-Aguirre J, Vasconez O, Martinez V, Martinez AL, Rosenbloom AL, Diamond FB, Jr., Gargosky SE, Nonoshita L, and Rosenfeld RG.** A randomized, double blind, placebo-controlled trial on safety and efficacy of recombinant human insulin-like growth factor-I in children with growth hormone receptor deficiency. *J Clin Endocrinol Metab* 80: 1393-1398, 1995.

72. **Guvakova MA and Surmacz E.** Overexpressed IGF-I receptors reduce estrogen growth requirements, enhance survival, and promote E-cadherin-mediated cell-cell adhesion in human breast cancer cells. *Exp Cell Res* 231: 149-162, 1997.

73. **Happerfield LC, Miles DW, Barnes DM, Thomsen LL, Smith P, and Hanby A.** The localization of the insulin-like growth factor receptor 1 (IGFR-1) in benign and malignant breast tissue. *J Pathol* 183: 412-417, 1997.

74. **Heding A, Gill R, Ogawa Y, De Meyts P, and Shymko RM.** Biosensor measurement of the binding of insulin-like growth factors I and II and their analogues to the insulin-like growth factor-binding protein-3. *J Biol Chem* 271: 13948-13952, 1996.

75. **Heinle H and Lindner V.** The binding of Evans blue to collagen and elastin in elastic tissue. *Arch Int Physiol Biochim* 92: 13-17., 1984.

76. **Hellawell GO, Turner GD, Davies DR, Poulsom R, Brewster SF, and Macaulay VM.** Expression of the type 1 insulin-like growth factor receptor is up-regulated in primary prostate cancer and commonly persists in metastatic disease. *Cancer Res* 62: 2942-2950, 2002.

77. **Hemar A, Lieb M, Subtil A, DiSanto JP, and Dautry-Varsat A.** Endocytosis of the beta chain of interleukin-2 receptor requires neither interleukin-2 nor the gamma chain. *Eur J Immunol* 24: 1951-1955, 1994.

78. **Henderson BR and Fagotto F.** The ins and outs of APC and beta-catenin nuclear transport. *EMBO Rep* 3: 834-839, 2002.

79. **Herbst JJ, Opresko LK, Walsh BJ, Lauffenburger DA, and Wiley HS.** Regulation of postendocytic trafficking of the epidermal growth factor receptor through endosomal retention. *J Biol Chem* 269: 12865-12873, 1994.

80. **Hirase T, Staddon JM, Saitou M, Ando-Akatsuka Y, Itoh M, Furuse M, Fujimoto K, Tsukita S, and Rubin LL.** Occludin as a possible determinant of tight junction permeability in endothelial cells. *J Cell Sci* 110: 1603-1613, 1997.

81. **Holleran WM, Ginns EI, Menon GK, Grundmann JU, Fartasch M, McKinney CE, Elias PM, and Sidransky E.** Consequences of beta-glucocerebrosidase deficiency in epidermis. Ultrastructure and permeability barrier alterations in Gaucher disease. *J Clin Invest* 93: 1756-1764, 1994.

82. **Hossenlopp P, Seurin D, Segovia-Quinson B, Hardouin S, and Binoux M.** Analysis of serum insulin-like growth factor binding proteins using western blotting: use of the method for titration of the binding proteins and competitive binding studies. *Anal Biochem* 154: 138-143, 1986.

83. **Hsieh ET, Shepherd FA, and Tsao MS.** Co-expression of epidermal growth factor receptor and transforming growth factor-alpha is independent of ras mutations in lung adenocarcinoma. *Lung Cancer* 29: 151-157, 2000.

84. **Huynh HT, Robitaille G, and Turner JD.** Establishment of bovine mammary epithelial cells (MAC-T): an in vitro model for bovine lactation. *Exp Cell Res* 197: 191-199., 1991.

85. **Jansson M, Hallen D, Koho H, Andersson G, Berghard L, Heidrich J, Nyberg E, Uhlen M, Kordel J, and Nilsson B.** Characterization of ligand binding of a soluble human insulin-like growth factor I receptor variant suggests a ligand-induced conformational change. *J Biol Chem* 272: 8189-8197, 1997.

86. **Jiang WG, Bryce RP, Horrobin DF, and Mansel RE.** Regulation of tight junction permeability and occludin expression by polyunsaturated fatty acids. *Biochem Biophys Res Commun* 244: 414-420, 1998.

87. **Jiang WG, Martin TA, Matsumoto K, Nakamura T, and Mansel RE.** Hepatocyte growth factor/scatter factor decreases the expression of occludin and transendothelial resistance (TER) and increases paracellular permeability in human vascular endothelial cells. *J Cell Physiol* 181: 319-329, 1999.

88. **Jones JI, Gockerman A, Busby WH, Jr., Wright G, and Clemmons DR.** Insulin-like growth factor binding protein 1 stimulates cell migration and binds to the alpha 5 beta 1 integrin by means of its Arg-Gly-Asp sequence. *Proc Natl Acad Sci U S A* 90: 10553-10557, 1993.

89. **Jones SM and Kazlauskas A.** Growth factor-dependent signaling and cell cycle progression. *Chem Rev* 101: 2413-2423, 2001.

90. **Kaji T, Yamada A, Miyajima S, Yamamoto C, Fujiwara Y, Wight T, and Kinsella M.** Cell density-dependent regulation of proteoglycan sythesis by transforming growth factor-$\beta_1$in cultured bovine aortic endothelial cells. *JBC* 275: 1463-1470, 2000.

91. **Kazakoff PW, McGuire TR, Hoie EB, Cano M, and Iversen PL.** An *in vitro* model for endothelial permeability: assessment of monolayer integrity. *In Vitro Cellular & Developmental Biology - Animal* 31: 846-852, 1995.

92. **Kevil CG, Payne DK, Mire E, and Alexander JS.** Vascular permeability factor/vascular endothelial cell growth factor-mediated permeability occurs through disorganization of endothelial junctional proteins. *J Biol Chem* 273: 15099-15103, 1998.

93. **Kil SJ, Hobert M, and Carlin C.** A leucine-based determinant in the epidermal growth factor receptor juxtamembrane domain is required for the efficient transport of ligand-receptor complexes to lysosomes. *J Biol Chem* 274: 3141-3150., 1999.

94. **King GL, Goodman AD, Buzney S, Moses A, and Kahn CR.** Receptors and growth-promoting effects of insulin and insulinlike growth factors on cells from bovine retinal capillaries and aorta. *J Clin Invest* 75: 1028-1036, 1985.

95. **Kleeff J, Shi X, Bode HP, Hoover K, Shrikhande S, Bryant PJ, Korc M, Buchler MW, and Friess H.** Altered expression and localization of the tight junction protein ZO-1 in primary and metastatic pancreatic cancer. *Pancreas* 23: 259-265., 2001.

96. **Kolaczynski JW and Caro JF.** Insulin-like growth factor-1 therapy in diabetes: physiologic basis, clinical benefits, and risks. *Ann Intern Med* 120: 47-55, 1994.

97. **Kolodziejczyk J, Gertler A, Leibovich H, Rzasa J, and Gregoraszczuk EL.** Synergistic action of growth hormone and insulin-like growth factor I (IGF-I) on proliferation and estradiol secretion in porcine granulosa and theca cells cultured alone or in coculture. *Theriogenology* 60: 559-570, 2003.

98. **Kopple JD.** The rationale for the use of growth hormone or insulin-like growth factor I in adult patients with renal failure. *Miner Electrolyte Metab* 18: 269-275, 1992.

99. **Kuzuya H, Matsuura N, Sakamoto M, Makino H, Sakamoto Y, Kadowaki T, Suzuki Y, Kobayashi M, Akazawa Y, Nomura M, and et al.** Trial of insulinlike growth factor I therapy for patients with extreme insulin resistance syndromes. *Diabetes* 42: 696-705, 1993.

100. **Lahm H, Amstad P, Wyniger J, Yilmaz A, Fischer JR, Schreyer M, and Givel JC.** Blockade of the insulin-like growth-factor-I receptor inhibits growth of human colorectal cancer cells: evidence of a functional IGF-II-mediated autocrine loop. *Int J Cancer* 58: 452-459, 1994.

101. **Laron Z.** Somatomedin-1 (insulin-like growth factor-I) in clinical use. Facts and potential. *Drugs* 45: 1-8, 1993.

102. **Lauffenburger DA, Chu L, French AR, Oehrtman G, Reddy C, Wells A, Niyogi SK, and Wiley HS.** Engineering dynamics of growth factors and other theapeutic ligands. *Biotechnol Bioeng* 52: 61-80, 1996.

103. **Lauffenburger DA and Linderman JJ.** *Receptors*. New York: Oxford, 1993.

104. **Leal SM, Huang SS, and Huang JS.** Interactions of high affinity insulin-like growth factor-binding proteins with the type V transforming growth factor-beta receptor in mink lung epithelial cells. *J Biol Chem* 274: 6711-6717., 1999.

105. **Leal SM, Liu Q, Huang SS, and Huang JS.** The type V transforming growth factor beta receptor is the putative insulin-like growth factor-binding protein 3 receptor. *J Biol Chem* 272: 20572-20576., 1997.

106. **Lee KW and Cohen P.** Nuclear effects: unexpected intracellular actions of insulin-like growth factor binding protein-3. *J Endocrinol* 175: 33-40, 2002.

107. **Leung SM, Ruiz WG, and Apodaca G.** Sorting of membrane and fluid at the apical pole of polarized Madin-Darby canine kidney cells. *Mol Biol Cell* 11: 2131-2150., 2000.

108. **Lewis ME, Neff NT, Contreras PC, Stong DB, Oppenheim RW, Grebow PE, and Vaught JL.** Insulin-like growth factor-I: potential for treatment of motor neuronal disorders. *Exp Neurol* 124: 73-88, 1993.

109. **Li G, Schaider H, Satyamoorthy K, Hanakawa Y, Hashimoto K, and Herlyn M.** Downregulation of E-cadherin and Desmoglein 1 by autocrine hepatocyte growth factor during melanoma development. *Oncogene* 20: 8125-8135, 2001.

110. **Li W, Fawcett J, Widmer HR, Fielder PJ, Rabkin R, and Keller GA.** Nuclear transport of insulin-like growth factor-I and insulin-like growth factor binding protein-3 in opossum kidney cells. *Endocrinology* 138: 1763-1766., 1997.

111. **Lin FT, Daaka Y, and Lefkowitz RJ.** beta-arrestins regulate mitogenic signaling and clathrin-mediated endocytosis of the insulin-like growth factor I receptor. *J Biol Chem* 273: 31640-31643, 1998.

112. **Lin SB, Hsieh SH, Hsu HL, Lai MY, Kan LS, and Au LC.** Antisense oligodeoxynucleotides of IGF-II selectively inhibit growth of human hepatoma cells overproducing IGF-II. *J Biochem (Tokyo)* 122: 717-722, 1997.

113. **Liou GI, Matragoon S, Samuel S, Behzadian MA, Tsai NT, Gu X, Roon P, Hunt DM, Hunt RC, Caldwell RB, and Marcus DM.** MAP kinase and beta-catenin signaling in HGF induced RPE migration. *Mol Vis* 8: 483-493, 2002.

114. **Liu B, Weinzimer SA, Gibson TB, Mascarenhas D, and Cohen P.** Type Ialpha collagen is an IGFBP-3 binding protein. *Growth Horm IGF Res* 13: 89-97, 2003.

115. **Liu YC, Leu CM, Wong FH, Fong WS, Chen SC, Chang C, and Hu C.** Autocrine stimulation by insulin-like growth factor I is involved in the growth, tumorigenicity and chemoresistance of human esophageal carcinoma cells. *J Biomed Sci* 9: 665-674, 2002.

116. **Longo KA, Kennell JA, Ochocinska MJ, Ross SE, Wright WS, and MacDougald OA.** Wnt signaling protects 3T3-L1 preadipocytes from apoptosis through induction of insulin-like growth factors. *J Biol Chem* 277: 38239-38244, 2002.

117. **Lui WY, Wong CH, Mruk DD, and Cheng CY.** TGF-beta3 regulates the blood-testis barrier dynamics via the p38 mitogen activated protein (MAP) kinase pathway: an in vivo study. *Endocrinology* 144: 1139-1142, 2003.

118. **Lum H and Malik AB.** Regulation of vascular endothelial barrier function. *Am J Physiol* 267: L223-241, 1994.

119. **Lund K, Opresko L, Starbuck C, Walsh B, and Wiley H.** Quantitative analysis of the endocytic system involved in hormone- induced receptor internalization. *J Biol Chem* 265: 15713-15723, 1990.

120. **Maeda K, Kato Y, and Sugiyama Y.** pH-dependent receptor/ligand dissociation as a determining factor for intracellular sorting of ligands for epidermal growth factor receptors in rat hepatocytes. *J Control Release* 82: 71-82, 2002.

121. **Malik AB, Lynch JJ, and Cooper JA.** Endothelial barrier function. *J Invest Dermatol* 93: 62S-67S, 1989.

122. **Maratos-Flier E, Kao CY, Verdin EM, and King GL.** Receptor-mediated vectorial transcytosis of epidermal growth factor by Madin-Darby canine kidney cells. *J Cell Biol* 105: 1595-1601, 1987.

123. **Martin JA, Miller BA, Scherb MB, Lembke LA, and Buckwalter JA.** Co-localization of insulin-like growth factor binding protein 3 and fibronectin in human articular cartilage. *Osteoarthritis Cartilage* 10: 556-563, 2002.

124. **Mauro L, Bartucci M, Morelli C, Ando S, and Surmacz E.** Igf-i receptor-induced cell-cell adhesion of mcf-7 breast cancer cells requires the expression of junction protein zo-1. *J Biol Chem* 276: 39892-39897., 2001.

125. **Mauro L, Salerno M, Morelli C, Boterberg T, Bracke ME, and Surmacz E.** Role of the IGF-I receptor in the regulation of cell-cell adhesion: implications in cancer development and progression. *J Cell Physiol* 194: 108-116, 2003.

126. **McCarthy KM, Skare IB, Stankewich MC, Furuse M, Tsukita S, Rogers RA, Lynch RD, and Schneeberger EE.** Occludin is a functional component of the tight junction. *J Cell Sci* 109: 2287-2298, 1996.

127. **McCusker RH, Busby WH, Dehoff MH, Camacho-Hubner C, and Clemmons DR.** Insulin-like growth factor (IGF) binding to cell monolayers is directly modulated by the addition of IGF-binding proteins. *Endocrinology* 129: 939-949, 1991.

128. **McCusker RH, Camacho-Hubner C, Bayne ML, Cascieri MA, and Clemmons DR.** Insulin-like growth factor (IGF) binding to human fibroblast and glioblastoma cells: the modulating effect of cell released IGF binding proteins (IGFBPs). *J Cell Physiol* 144: 244-253, 1990.

129. **McCusker RH and Clemmons DR.** Use of lanthanum to accurately quantify insulin-like growth factor binding to proteins on cell surfaces. *J Cell Biochem* 66: 256-267., 1997.

130. **McRoberts JA and Riley NE.** Regulation of T84 cell monolayer permeability by insulin-like growth factors. *Am J Physiol* 262: C207-213., 1992.

131. **Milton SG and Knutson VP.** Comparison of the function of the tight junctions of endothelial cells and epithelial cells in regulating the movement of electrolytes and macromolecules across the cell monolayer. *J Cell Physiol* 144: 498-504, 1990.

132. **Mira E, Manes S, Lacalle RA, Marquez G, and Martinez AC.** Insulin-like growth factor I-triggered cell migration and invasion are mediated by matrix metalloproteinase-9. *Endocrinology* 140: 1657-1664, 1999.

133. **Monsky WL, Fukumura D, Gohongi T, Ancukiewcz M, Weich HA, Torchilin VPY, Fan, and Jain RK.** Augmentation of transvascular transport of macromolecules and nanoparticles in tumors using vascular endothelial growth factor. *Cancer Research* 49: 4129-4135, 1999.

134. **Morla A, Zhang Z, and Ruoslahti E.** Superfibronectin is a functionally distinct form of fibronectin. *Nature* 367: 193-196., 1994.

135. **Morrow LA, O'Brien MB, Moller DE, Flier JS, and Moses AC.** Recombinant human insulin-like growth factor-I therapy improves glycemic control and insulin action in the type A syndrome of severe insulin resistance. *J Clin Endocrinol Metab* 79: 205-210., 1994.

136. **Moschos SJ and Mantzoros CS.** The role of the IGF system in cancer: from basic to clinical studies and clinical applications. *Oncology* 63: 317-332, 2002.

137. **Moses AC, Young SC, Morrow LA, O'Brien M, and Clemmons DR.** Recombinant human insulin-like growth factor I increases insulin sensitivity and improves glycemic control in type II diabetes. *Diabetes* 45: 91-100, 1996.

138. **Nguyen DA and Neville MC.** Tight junction regulation in the mammary gland. *J Mammary Gland Biol Neoplasia* 3: 233-246., 1998.

139. **Niles WD and Malik AB.** Endocytosis and exocytosis events regulate vesicle traffic in endothelial cells. *J Membr Biol* 167: 85-101, 1999.

140. **Nugent MA and Edelman ER.** Kinetics of basic fibroblast growth factor binding to its receptor and heparan sulfate proteoglycan: a mechanism for cooperactivity. *Biochemistry* 31: 8876-8883, 1992.

141. **Nwariaku FE, Liu Z, Zhu X, Turnage RH, Sarosi GA, and Terada LS.** Tyrosine phosphorylation of vascular endothelial cadherin and the regulation of microvascular permeability. *Surgery* 132: 180-185, 2002.

142. **Oft M, Heider KH, and Beug H.** TGFbeta signaling is necessary for carcinoma cell invasiveness and metastasis. *Curr Biol* 8: 1243-1252, 1998.

143. **Oh Y, Muller HL, Lamson G, and Rosenfeld RG.** Insulin-like growth factor (IGF)-independent action of IGF-binding protein-3 in Hs578T human breast cancer cells. Cell surface binding and growth inhibition. *J Biol Chem* 268: 14964-14971, 1993.

144. **O'Kane S and Ferguson MW.** Transforming growth factor beta s and wound healing. *Int J Biochem Cell Biol* 29: 63-78, 1997.

145. **Onoda N, Ohmura E, Tsushima T, Ohba Y, Emoto N, Isozaki O, Sato Y, Shizume K, and Demura H.** Autocrine role of insulin-like growth factor (IGF)-I in a human thyroid cancer cell line. *Eur J Cancer* 28A: 1904-1909, 1992.

146. **Pennisi PA, Barr V, Nunez NP, Stannard B, and Le Roith D.** Reduced expression of insulin-like growth factor I receptors in MCF-7 breast cancer cells leads to a more metastatic phenotype. *Cancer Res* 62: 6529-6537, 2002.

147. **Phelps JE and DePaola N.** Spatial variations in endothelial barrier function in disturbed flows in vitro. *Am J Physiol Heart Circ Physiol* 278: H469-476, 2000.

148. **Playford MP, Bicknell D, Bodmer WF, and Macaulay VM.** Insulin-like growth factor 1 regulates the location, stability, and transcriptional activity of beta-catenin. *Proc Natl Acad Sci U S A* 97: 12103-12108, 2000.

149. **Pollak M.** Insulin-like growth factor physiology and cancer risk. *Eur J Cancer* 36: 1224-1228., 2000.

150. **Pomilio M, Mohn A, Verrotti A, and Chiarelli F.** Endothelial dysfunction in children with type 1 diabetes mellitus. *J Pediatr Endocrinol Metab* 15: 343-361, 2002.

151. **Pricci F, Pugliese G, Romano G, Romeo G, Locuratolo N, Pugliese F, Mene P, Galli G, Casini A, Rotella CM, and Di Mario U.** Insulin-like growth factors I and II stimulate extracellular matrix production in human glomerular mesangial cells. Comparison with transforming growth factor-beta. *Endocrinology* 137: 879-885, 1996.

152. **Quattrin T, Thrailkill K, Baker L, Litton J, Dwigun K, Rearson M, Poppenheimer M, Giltinan D, Gesundheit N, and Martha P, Jr.** Dual hormonal replacement with insulin and recombinant human insulin-like growth factor I in IDDM. Effects on glycemic control, IGF-I levels, and safety profile. *Diabetes Care* 20: 374-380., 1997.

153. **Quin JD, Checkley A, Gallagher A, Jones J, MacCuish AC, and Miell JP.** Response of insulin-like growth factor (IGF)-binding protein-1 (IGFBP- 1) and IGFBP-3 to IGF-I treatment in severe insulin resistance. *J Endocrinol* 141: 177-182, 1994.

154. **Ranke MB, Wollmann HA, and Savage MO.** Experience with insulin-like growth factor I (IGF-I) treatment of growth hormone insensitivity syndrome (GHIS). *J Pediatr Endocrinol Metab* 12 Suppl 1: 259-266, 1999.

155. **Raub TJ, Kuentzel SL, and Sawada GA.** Permeability of bovine brain microvessel endothelial cells in vitro: barrier tightening by a factor released from astroglioma cells. *Exp Cell Res* 199: 330-340, 1992.

156. **Re RN.** Toward a theory of intracrine hormone action. *Regul Pept* 106: 1-6, 2002.

157. **Resat H, Ewald JA, Dixon DA, and Wiley HS.** An integrated model of epidermal growth factor receptor trafficking and signal transduction. *Biophys J* 85: 730-743, 2003.

158. **Reuss B, Dono R, and Unsicker K.** Functions of fibroblast growth factor (FGF)-2 and FGF-5 in astroglial differentiation and blood-brain barrier permeability: evidence from mouse mutants. *J Neurosci* 23: 6404-6412, 2003.

159. **Richardson TP, Trinkaus-Randall V, and Nugent MA.** Regulation of basic fibroblast growth factor binding and activity by cell density and heparan sulfate. *J Biol Chem* 274: 13534-13540, 1999.

160. **Rite S, Baldellou A, Giraldo P, Labarta JI, Giralt M, Rubio-Felix D, Guallar A, Perez-Calvo JI, Mayayo E, Ferrandez A, and Pocovi M.** Insulin-like growth factors in childhood-onset Gaucher disease. *Pediatr Res* 52: 109-112, 2002.

161. **Robinson RM, Akers RM, and Forsten KE.** Real-time detection of insulin-like growth factor-1 stimulation of the MAC-T bovine mammary epithelial cell line. *Endocrine* 13: 345-352., 2000.

162. **Romagnolo D, Akers RM, Byatt JC, Wong EA, and Turner JD.** Regulation of expression of IGF-I-induced IGFBP-3 and IGF-I-receptor by constitutive vs regulated expression of recombinant IGF-I in transfected mammary epithelial cells. *Endocrine Journal* 2: 375-384, 1994.

163. **Romagnolo D, Akers RM, Wong EA, Boyle PL, McFadden TB, and Turner JD.** Overexpression of ovine insulin-like growth factor-I stimulates autonomous autocrine or paracrine growth in bovine mammary-derived epithelial cells. *Mol Endocrinol* 6: 1774-1780, 1992.

164. **Schalch DS, Sessions CM, Farley AC, Masakawa A, Emler CA, and Dills DG.** Interaction of insulin-like growth factor I/somatomedin-C with cultured rat chondrocytes: receptor binding and internalization. *Endocrinology* 118: 1590-1597, 1986.

165. **Schedlich LJ, Le Page SL, Firth SM, Briggs LJ, Jans DA, and Baxter RC.** Nuclear import of insulin-like growth factor-binding protein-3 and -5 is mediated by the importin beta subunit. *J Biol Chem* 275: 23462-23470., 2000.

166. **Sheff D, Darn E, Hull M, and Mellman I.** The receptor recycling pathway contains two distinct populations of early endosomes with different sorting functions. *The Journal of Cell Biology* 145: 123-139, 1999.

167. **Shoubridge CA and Read LC.** Preferential intestinal delivery of long[Arg3] insulin-like growth factor (LR3IGF-I) over IGF-I in preweaning and adult rats. *Endocrinology* 144: 1887-1893, 2003.

168. **Shvartsman SY, Wiley HS, Deen WM, and Lauffenburger DA.** Spatial range of autocrine signaling: modeling and computational analysis. *Biophys J* 81: 1854-1867., 2001.

169. **Sinaga E, Jois SD, Avery M, Makagiansar IT, Tambunan US, Audus KL, and Siahaan TJ.** Increasing paracellular porosity by E-cadherin peptides: discovery of bulge and groove regions in the EC1-domain of E-cadherin. *Pharm Res* 19: 1170-1179, 2002.

170. **Smith GD, Gunnell D, and Holly J.** Cancer and insulin-like growth factor-I. A potential mechanism linking the environment with cancer risk. *Bmj* 321: 847-848, 2000.

171. **Soler AP, Miller RD, Laughlin KV, Carp NZ, Klurfeld DM, and Mullin JM.** Increased tight junctional permeability is associated with the development of colon cancer. *Carcinogenesis* 20: 1425-1431., 1999.

172. **Sperinde GV and Nugent MA.** Mechanisms of fibroblast growth factor 2 intracellular processing: a kinetic analysis of the role of heparan sulfate proteoglycans. *Biochemistry* 39: 3788-3796, 2000.

173. **Sporn MB and Roberts AB.** Autocrine secretion--10 years later. *Ann Intern Med* 117: 408-414, 1992.

174. **Spranger J, Buhnen J, Jansen V, Krieg M, Meyer-Schwickerath R, Blum WF, Schatz H, and Pfeiffer AF.** Systemic levels contribute significantly to increased intraocular IGF-I, IGF-II and IGF-BP3 [correction of IFG-BP3] in proliferative diabetic retinopathy. *Horm Metab Res* 32: 196-200, 2000.

175. **Stachowiak MK, Moffett J, Maher P, Tucholski J, and Stachowiak EK.** Growth factor regulation of cell growth and proliferation in the nervous system. A new intracrine nuclear mechanism. *Mol Neurobiol* 15: 257-283, 1997.

176. **Starbuck C and Lauffenburger DA.** Mathematical model for the effects of epidermal growth factor receptor trafficking dynamics on fibroblast proliferation responses. *Biotechnol Prog* 8: 132-143, 1992.

177. **Stevenson BR and Keon BH.** The tight junction: morphology to molecules. *Ann Rev Cell Dev Biol* 14: 89-109, 1998.

178. **Sugiyama Y, Kusuhara H, and Suzuki H.** Kinetic and biochemical analysis of carrier-mediated efflux of drugs through the blood-brain and blood-cerebrospinal fluid barriers: importance in the drug delivery to the brain. *J Control Release* 62: 179-186., 1999.

179. **Surmacz E.** Function of the IGF-I receptor in breast cancer. *J Mammary Gland Biol Neoplasia* 5: 95-105, 2000.

180. **Suzuki K, Saito J, Yanai R, Yamada N, Chikama T, Seki K, and Nishida T.** Cell-matrix and cell-cell interactions during corneal epithelial wound healing. *Prog Retin Eye Res* 22: 113-133, 2003.

181. **Tan XD, Chang H, Qu XW, Caplan M, Gonzalez-Crussi F, and Hsueh W.** Platelet-activating factor increases mucosal permeability in rat intestine via tyrosine phosphorylation of E-cadherin. *Br J Pharmacol* 129: 1522-1529, 2000.

182. **Timar J, Csuka O, Orosz Z, Jeney A, and Kopper L.** Molecular pathology of tumor metastasis. I. Predictive pathology. *Pathol Oncol Res* 7: 217-230, 2001.

183. **Toropainen E, Lipponen P, and Syrjanen K.** Expression of insulin-like growth factor I (IGF-I) in female breast cancer as related to established prognostic factors and long-term prognosis. *Eur J Cancer* 9: 1443-1448, 1995.

184. **Underwood PA and Bennett FA.** The effect of extracellular matrix molecules on the in vitro behavior of bovine endothelial cells. *Exp Cell Res* 205: 311-319., 1993.

185. **Van der Ven LT, Van Buul-Offers SC, Gloudemans T, Roholl PJ, Sussenbach JS, and Den Otter W.** Histamine-stimulated expression of insulin-like growth factors in human glioma cells. *Br J Cancer* 75: 1091-1097, 1997.

186. **Venkiteswaran K, Xiao K, Summers S, Calkins CC, Vincent PA, Pumiglia K, and Kowalczyk AP.** Regulation of endothelial barrier function and growth by VE-cadherin, plakoglobin, and beta-catenin. *Am J Physiol Cell Physiol* 283: C811-821, 2002.

187. **Vestweber D.** Molecular mechanisms that control endothelial cell contacts. *J Pathol* 190: 281-291., 2000.

188. **Villars F, Conrad V, Rouais F, Lefebvre F, Amedee J, and Bordenave L.** Ability of various inserts to promote endothelium cell culture for the establishment of coculture models. *Cell Biol Toxicol* 12: 207-214., 1996.

189. **Vleminckx K and Kemler R.** Cadherins and tissue formation: integrating adhesion and signaling. *Bioessays* 21: 211-220, 1999.

190. **Vlodavsky I, Folkman J, Sullivan R, Fridman R, Ishai-Michaeli R, Sasse J, and Klagsbrun M.** Endothelial cell-derived basic fibroblast growth factor: synthesis and deposition into subendothelial extracellular matrix. *Proc Natl Acad Sci U S A* 84: 2292-2296, 1987.

191. **Vorwerk P, Hohmann B, Oh Y, Rosenfeld RG, and Shymko RM.** Binding properties of insulin-like growth factor binding protein-3 (IGFBP-3), IGFBP-3 N- and C-terminal fragments, and structurally related proteins mac25 and connective tissue growth factor measured using a biosensor. *Endocrinology* 143: 1677-1685, 2002.

192. **Wang E, Brown PS, Aroeti B, Chapin SJ, Mostov KE, and Dunn KW.** Apical and basolateral endocytic pathways of MDCK cells meet in acidic common endosomes distinct from a nearly-neutral apical recycling endosome. *Traffic* 1: 480-493., 2000.

193. **Ward CW, Garrett TP, McKern NM, Lou M, Cosgrove LJ, Sparrow LG, Frenkel MJ, Hoyne PA, Elleman TC, Adams TE, Lovrecz GO, Lawrence LJ, and Tulloch PA.** The three dimensional structure of the type I insulin-like growth factor receptor. *Mol Pathol* 54: 125-132, 2001.

194. **Weinzimer SA, Gibson TB, Collett-Solberg PF, Khare A, Liu B, and Cohen P.** Transferrin is an insulin-like growth factor-binding protein-3 binding protein. *J Clin Endocrinol Metab* 86: 1806-1813., 2001.

195. **West MR, Ferguson DJ, Hart VJ, Sanjar S, and Man Y.** Maintenance of the epithelial barrier in a bronchial epithelial cell line is dependent on functional E-cadherin local to the tight junctions. *Cell Commun Adhes* 9: 29-44, 2002.

196. **Wiley HS, Shvartsman SY, and Lauffenburger DA.** Computational modeling of the EGF-receptor system: a paradigm for systems biology. *Trends Cell Biol* 13: 43-50, 2003.

197. **Wiley HS, Woolf MF, Opresko LK, Burke PM, Will B, Morgan JR, and Lauffenburger DA.** Removal of the membrane-anchoring domain of epidermal growth factor leads to intracrine signaling and disruption of mammary epithelial cell organization. *J Cell Biol* 143: 1317-1328., 1998.

198. **Wills NK.** Epithelial cell culture. In: *Epithelial transport*, edited by Wills NK, Reuss L and Lewis SA. New York: Chapman & Hall, 1996, p. 251-252.

199. **Wong MS, Fong CC, and Yang M.** Biosensor measurement of the interaction kinetics between insulin-like growth factors and their binding proteins. *Biochim Biophys Acta* 1432: 293-301, 1999.

200. **Zabner J, Winter MC, Shasby S, Ries D, and Shasby DM.** Histamine decreases E-cadherin-based adhesion to increase permeability of human airway epithelium. *Chest* 123: 385S, 2003.

201. **Zapf A, Hsu D, and Olefsky JM.** Comparison of the intracellular itineraries of insulin-like growth factor-I and insulin and their receptors in Rat-1 fibroblasts. *Endocrinology* 134: 2445-2452, 1994.

Appendix A: Equations for Mathematical Model

The following is the complete set of equations for the model. The corresponding dedimensionlized equations are shown in gray. Baseline parameter values and their meaning can be found in Table 5.2.

1

$$\frac{\mathrm{d}R_a}{\mathrm{d}t} = -\mathrm{k}_{\mathrm{f1}} R_a L_a + \mathrm{k}_{\mathrm{r1}} C_a - \mathrm{k}_{\mathrm{f3}} R_a I_{1a} + \mathrm{k}_{\mathrm{r3}} Z_a - \mathrm{k}_{\mathrm{off2}} X_a \mathrm{P}(R_a) + \mathrm{V}_{\mathrm{R}}$$
$$- \mathrm{k}_{\mathrm{er}} R_a + \mathrm{k}_{\mathrm{rec}} R_{ia} (1-\mathrm{f}_{1\mathrm{R}})(1-\mathrm{f}_{2\mathrm{R}}) + \mathrm{k}_{\mathrm{trans}} R_{ib} (1-\mathrm{f}_{1\mathrm{R}})(\mathrm{f}_{2\mathrm{R}})$$

$$\frac{\mathrm{d}\alpha_1}{\mathrm{d}\tau} = -\frac{\lambda_1\eta_1}{1+\lambda_1+\lambda_2} + \frac{\mu_1\beta_1(1+\lambda_2)}{1+\lambda_1+\lambda_2} - \frac{\lambda_3\theta_2}{1+\lambda_3} + \frac{\mu_3\gamma_1}{1+\lambda_3} - \frac{\mu_2\beta_2}{\omega}\mathrm{P}(R_a) + \upsilon_1$$
$$-\rho_1\alpha_1 + \rho_9\delta_1(1-\mathrm{f}_{1\mathrm{R}})(1-\mathrm{f}_{2\mathrm{R}}) + \rho_7\delta_3(1-\mathrm{f}_{1\mathrm{R}})(\mathrm{f}_{2\mathrm{R}})$$

2

$$\frac{\mathrm{d}B_a}{\mathrm{d}t} = -\mathrm{k}_{\mathrm{f2}} B_a L_a + \mathrm{k}_{\mathrm{r2}} X_a - \mathrm{k}_{\mathrm{f4}} B_a I_{2a} + \mathrm{k}_{\mathrm{r4}} Y_a - \mathrm{k}_{\mathrm{off1}} C_a \mathrm{P}(B_a) + \mathrm{V}_{\mathrm{B}}$$
$$- \mathrm{k}_{\mathrm{eB}} B_a + \mathrm{k}_{\mathrm{rec}} B_{ia} (1-\mathrm{f}_{1\mathrm{B}})(1-\mathrm{f}_{2\mathrm{B}}) + \mathrm{k}_{\mathrm{trans}} B_{ib} (1-\mathrm{f}_{1\mathrm{B}})(\mathrm{f}_{2\mathrm{B}})$$

$$\frac{\mathrm{d}\alpha_2}{\mathrm{d}\tau} = -\frac{\lambda_2\eta_1\omega}{1+\lambda_1+\lambda_2} + \frac{\mu_2\beta_2(1+\lambda_1)}{1+\lambda_1+\lambda_2} - \frac{\lambda_4\sigma_1}{1+\lambda_4} + \frac{\mu_4\gamma_2}{1+\lambda_4} - \mu_1\beta_1\omega\mathrm{P}(B_a) + \upsilon_2$$
$$-\rho_2\alpha_2 + \rho_9\delta_2(1-\mathrm{f}_{1\mathrm{B}})(1-\mathrm{f}_{2\mathrm{B}}) + \rho_7\delta_4(1-\mathrm{f}_{1\mathrm{B}})(\mathrm{f}_{2\mathrm{B}})$$

3

$$\frac{\mathrm{d}R_b}{\mathrm{d}t} = -\mathrm{k}_{\mathrm{f9}} R_b L_b + \mathrm{k}_{\mathrm{r9}} C_b - \mathrm{k}_{\mathrm{f11}} R_b I_{1b} + \mathrm{k}_{\mathrm{r11}} Z_b - \mathrm{k}_{\mathrm{off10}} X_b \mathrm{P}(R_b)$$
$$- \mathrm{k}_{\mathrm{er}} R_b + \mathrm{k}_{\mathrm{rec}} R_{ib} (1-\mathrm{f}_{1\mathrm{R}})(1-\mathrm{f}_{2\mathrm{R}}) + \mathrm{k}_{\mathrm{trans}} R_{ia} (1-\mathrm{f}_{1\mathrm{R}})(\mathrm{f}_{2\mathrm{R}})$$

$$\frac{\mathrm{d}\alpha_3}{\mathrm{d}\tau} = -\frac{\lambda_9\eta_3}{1+\lambda_9+\lambda_{10}} + \frac{\mu_9\beta_3(1+\lambda_{10})}{1+\lambda_9+\lambda_{10}} - \frac{\lambda_{11}\theta_3}{1+\lambda_{11}} + \frac{\mu_{11}\gamma_3}{1+\lambda_{11}} - \frac{\mu_{10}\beta_4}{\omega}\mathrm{P}(R_b)$$
$$-\rho_1\alpha_3 + \rho_9\delta_3(1-\mathrm{f}_{1\mathrm{R}})(1-\mathrm{f}_{2\mathrm{R}}) + \rho_7\delta_1(1-\mathrm{f}_{1\mathrm{R}})(\mathrm{f}_{2\mathrm{R}})$$

4

$$\frac{\mathrm{d}B_b}{\mathrm{d}t} = -\mathrm{k}_{\mathrm{f10}} B_b L_b + \mathrm{k}_{\mathrm{r10}} X_b - \mathrm{k}_{\mathrm{f12}} B_b I_{2b} + \mathrm{k}_{\mathrm{r12}} Y_b - \mathrm{k}_{\mathrm{off9}} C_b \mathrm{P}(B_b)$$
$$- \mathrm{k}_{\mathrm{eB}} B_b + \mathrm{k}_{\mathrm{rec}} B_{ib} (1-\mathrm{f}_{\mathrm{1B}})(1-\mathrm{f}_{\mathrm{2B}}) + \mathrm{k}_{\mathrm{trans}} B_{ia} (1-\mathrm{f}_{\mathrm{1B}})(\mathrm{f}_{\mathrm{2B}})$$

$$\frac{\mathrm{d}\alpha_4}{\mathrm{d}\tau} = -\frac{\lambda_{10}\eta_3\omega}{1+\lambda_9+\lambda_{10}} + \frac{\mu_{10}\beta_4(1+\lambda_9)}{1+\lambda_9+\lambda_{10}} - \frac{\lambda_{12}\sigma_3}{1+\lambda_{12}} + \frac{\mu_{12}\gamma_4}{1+\lambda_{12}} - \mu_9\beta_3\omega\mathrm{P}(B_b)$$
$$- \rho_2\alpha_4 + \rho_9\delta_4(1-\mathrm{f}_{\mathrm{1B}})(1-\mathrm{f}_{\mathrm{2B}}) + \rho_7\delta_2(1-\mathrm{f}_{\mathrm{1B}})(\mathrm{f}_{\mathrm{2B}})$$

5

$$\frac{\mathrm{d}C_a}{\mathrm{d}t} = \mathrm{k}_{\mathrm{f1}} R_a L_a - \mathrm{k}_{\mathrm{r1}} C_a + \mathrm{k}_{\mathrm{off2}} X_a \mathrm{P}(R_a) - \mathrm{k}_{\mathrm{ec}} C_a$$
$$+ \mathrm{k}_{\mathrm{rec}} C_{ia} (1-\mathrm{f}_{\mathrm{1C}})(1-\mathrm{f}_{\mathrm{2C}}) + \mathrm{k}_{\mathrm{trans}} C_{ib} (1-\mathrm{f}_{\mathrm{1C}})(\mathrm{f}_{\mathrm{2C}})$$

$$\frac{\mathrm{d}\beta_1}{\mathrm{d}\tau} = \frac{\lambda_1\eta_1}{1+\lambda_1+\lambda_2} - \frac{\mu_1\beta_1(1+\lambda_2)}{1+\lambda_1+\lambda_2} + \frac{\mu_2\beta_2}{\omega}\mathrm{P}(R_a) - \rho_3\beta_1$$
$$+ \rho_9\varepsilon_1(1-\mathrm{f}_{\mathrm{1C}})(1-\mathrm{f}_{\mathrm{2C}}) + \rho_7\varepsilon_3(1-\mathrm{f}_{\mathrm{1C}})(\mathrm{f}_{\mathrm{2C}})$$

6

$$\frac{\mathrm{d}X_a}{\mathrm{d}t} = \mathrm{k}_{\mathrm{f2}} B_a L_a - \mathrm{k}_{\mathrm{r2}} X_a + \mathrm{k}_{\mathrm{off1}} C_a \mathrm{P}(B_a) - \mathrm{k}_{\mathrm{ex}} X_a$$
$$+ \mathrm{k}_{\mathrm{rec}} X_{ia} (1-\mathrm{f}_{\mathrm{1X}})(1-\mathrm{f}_{\mathrm{2X}}) + \mathrm{k}_{\mathrm{trans}} X_{ib} (1-\mathrm{f}_{\mathrm{1X}})(\mathrm{f}_{\mathrm{2X}})$$

$$\frac{\mathrm{d}\beta_2}{\mathrm{d}\tau} = \frac{\lambda_2\eta_1\omega}{1+\lambda_1+\lambda_2} - \frac{\mu_2\beta_2(1+\lambda_1)}{1+\lambda_1+\lambda_2} + \mu_1\beta_1\omega\mathrm{P}(B_a) - \rho_4\beta_2$$
$$+ \rho_9\varepsilon_2(1-\mathrm{f}_{\mathrm{1X}})(1-\mathrm{f}_{\mathrm{2X}}) + \rho_7\varepsilon_4(1-\mathrm{f}_{\mathrm{1X}})(\mathrm{f}_{\mathrm{2X}})$$

7

$$\frac{\mathrm{d}C_b}{\mathrm{d}t} = \mathrm{k}_{\mathrm{f9}} R_b L_b - \mathrm{k}_{\mathrm{r9}} C_b + \mathrm{k}_{\mathrm{off10}} X_b \mathrm{P}(R_b) - \mathrm{k}_{\mathrm{ec}} C_b$$
$$+ \mathrm{k}_{\mathrm{rec}} C_{ib} (1-\mathrm{f}_{\mathrm{1C}})(1-\mathrm{f}_{\mathrm{2C}}) + \mathrm{k}_{\mathrm{trans}} C_{ia} (1-\mathrm{f}_{\mathrm{1C}})(\mathrm{f}_{\mathrm{2C}})$$

$$\frac{\mathrm{d}\beta_3}{\mathrm{d}\tau} = \frac{\lambda_9\eta_3}{1+\lambda_9+\lambda_{10}} - \frac{\mu_9\beta_3(1+\lambda_{10})}{1+\lambda_9+\lambda_{10}} + \frac{\mu_{10}\beta_4}{\omega}\mathrm{P}(R_b) - \rho_3\beta_3$$
$$+ \rho_9\varepsilon_3(1-\mathrm{f}_{\mathrm{1C}})(1-\mathrm{f}_{\mathrm{2C}}) + \rho_7\varepsilon_1(1-\mathrm{f}_{\mathrm{1C}})(\mathrm{f}_{\mathrm{2C}})$$

8

$$\frac{\mathrm{d}X_b}{\mathrm{d}t} = \mathrm{k}_{\mathrm{f10}} B_b L_b - \mathrm{k}_{\mathrm{r10}} X_b + \mathrm{k}_{\mathrm{off9}} C_b \mathrm{P}(B_b) - \mathrm{k}_{\mathrm{ex}} X_b$$
$$+ \mathrm{k}_{\mathrm{rec}} X_{ib} (1 - \mathrm{f}_{1\mathrm{X}})(1 - \mathrm{f}_{2\mathrm{X}}) + \mathrm{k}_{\mathrm{trans}} X_{ia} (1 - \mathrm{f}_{1\mathrm{X}})(\mathrm{f}_{2\mathrm{X}})$$

$$\frac{\mathrm{d}\beta_4}{\mathrm{d}\tau} = \frac{\lambda_{10}\eta_3\omega}{1+\lambda_9+\lambda_{10}} - \frac{\mu_{10}\beta_4(1+\lambda_9)}{1+\lambda_9+\lambda_{10}} + \mu_9\beta_3\omega\mathrm{P}(B_b) - \rho_4\beta_4$$
$$+ \rho_9\varepsilon_4(1-\mathrm{f}_{1\mathrm{X}})(1-\mathrm{f}_{2\mathrm{X}}) + \rho_7\varepsilon_2(1-\mathrm{f}_{1\mathrm{X}})(\mathrm{f}_{2\mathrm{X}})$$

9

$$\frac{\mathrm{d}Z_a}{\mathrm{d}t} = \mathrm{k}_{\mathrm{f3}} R_a I_{1a} - \mathrm{k}_{\mathrm{r3}} Z_a - \mathrm{k}_{\mathrm{eZ}} Z_a + \mathrm{k}_{\mathrm{rec}} Z_{ia} (1 - \mathrm{f}_{1\mathrm{Z}})(1 - \mathrm{f}_{2\mathrm{Z}}) + \mathrm{k}_{\mathrm{trans}} Z_{ib} (1 - \mathrm{f}_{1\mathrm{Z}})(\mathrm{f}_{2\mathrm{Z}})$$

$$\frac{\mathrm{d}\gamma_1}{\mathrm{d}\tau} = \frac{\lambda_3\theta_1}{1+\lambda_3} - \frac{\mu_3\gamma_1}{1+\lambda_3} - \rho_5\gamma_1 + \rho_9\varsigma_1(1-\mathrm{f}_{1\mathrm{Z}})(1-\mathrm{f}_{2\mathrm{Z}}) + \rho_7\varsigma_3(1-\mathrm{f}_{1\mathrm{Z}})(\mathrm{f}_{2\mathrm{Z}})$$

10

$$\frac{\mathrm{d}Y_a}{\mathrm{d}t} = \mathrm{k}_{\mathrm{f4}} B_a I_{2a} - \mathrm{k}_{\mathrm{r4}} Y_a - \mathrm{k}_{\mathrm{eY}} Y_a + \mathrm{k}_{\mathrm{rec}} Y_{ia} (1 - \mathrm{f}_{1\mathrm{Y}})(1 - \mathrm{f}_{2\mathrm{Y}}) + \mathrm{k}_{\mathrm{trans}} Y_{ib} (1 - \mathrm{f}_{1\mathrm{Y}})(\mathrm{f}_{2\mathrm{Y}})$$

$$\frac{\mathrm{d}\gamma_2}{\mathrm{d}\tau} = \frac{\lambda_4\sigma_1}{1+\lambda_4} - \frac{\mu_4\gamma_2}{1+\lambda_4} - \rho_6\gamma_2 + \rho_9\varsigma_2(1-\mathrm{f}_{1\mathrm{Y}})(1-\mathrm{f}_{2\mathrm{Y}}) + \rho_7\varsigma_4(1-\mathrm{f}_{1\mathrm{Y}})(\mathrm{f}_{2\mathrm{Y}})$$

11

$$\frac{\mathrm{d}Z_b}{\mathrm{d}t} = \mathrm{k}_{\mathrm{f11}} R_b I_{1b} - \mathrm{k}_{\mathrm{r11}} Z_b - \mathrm{k}_{\mathrm{eZ}} Z_b + \mathrm{k}_{\mathrm{rec}} Z_{ib} (1 - \mathrm{f}_{1\mathrm{Z}})(1 - \mathrm{f}_{2\mathrm{Z}}) + \mathrm{k}_{\mathrm{trans}} Z_{ia} (1 - \mathrm{f}_{1\mathrm{Z}})(\mathrm{f}_{2\mathrm{Z}})$$

$$\frac{\mathrm{d}\gamma_3}{\mathrm{d}\tau} = \frac{\lambda_{11}\theta_3}{1+\lambda_{11}} - \frac{\mu_{11}\gamma_3}{1+\lambda_{11}} - \rho_5\gamma_3 + \rho_9\varsigma_3(1-\mathrm{f}_{1\mathrm{Z}})(1-\mathrm{f}_{2\mathrm{Z}}) + \rho_7\varsigma_1(1-\mathrm{f}_{1\mathrm{Z}})(\mathrm{f}_{2\mathrm{Z}})$$

12

$$\frac{\mathrm{d}Y_b}{\mathrm{d}t} = \mathrm{k}_{\mathrm{f12}} B_b I_{2b} - \mathrm{k}_{\mathrm{r12}} Y_b - \mathrm{k}_{\mathrm{eY}} Y_b + \mathrm{k}_{\mathrm{rec}} Y_{ib} (1 - \mathrm{f}_{1\mathrm{Y}})(1 - \mathrm{f}_{2\mathrm{Y}}) + \mathrm{k}_{\mathrm{trans}} Y_{ia} (1 - \mathrm{f}_{1\mathrm{Y}})(\mathrm{f}_{2\mathrm{Y}})$$

$$\frac{\mathrm{d}\gamma_4}{\mathrm{d}\tau} = \frac{\lambda_{12}\sigma_3}{1+\lambda_{12}} - \frac{\mu_{12}\gamma_4}{1+\lambda_{12}} - \rho_6\gamma_4 + \rho_9\varsigma_4(1-\mathrm{f}_{1\mathrm{Y}})(1-\mathrm{f}_{2\mathrm{Y}}) + \rho_7\varsigma_2(1-\mathrm{f}_{1\mathrm{Y}})(\mathrm{f}_{2\mathrm{Y}})$$

13

$$\frac{\mathrm{d}R_{ia}}{\mathrm{d}t} = -\mathrm{k}_{\mathrm{f5}} R_{ia} L_{ia} + \mathrm{k}_{\mathrm{r5}} C_{ia} - \mathrm{k}_{\mathrm{f7}} R_{ia} I_{i1a} + \mathrm{k}_{\mathrm{r7}} Z_{ia} + \mathrm{k}_{\mathrm{eR}} R_a$$
$$- \mathrm{k}_{\mathrm{deg}} R_{ia} (\mathrm{f}_{\mathrm{1R}}) - \mathrm{k}_{\mathrm{rec}} R_{ia} (1-\mathrm{f}_{\mathrm{1R}})(1-\mathrm{f}_{\mathrm{2R}}) - \mathrm{k}_{\mathrm{trans}} R_{ia} (1-\mathrm{f}_{\mathrm{1R}})(\mathrm{f}_{\mathrm{2R}})$$

$$\frac{\mathrm{d}\delta_1}{\mathrm{d}\tau} = -\lambda_5 \eta_2 + \mu_5 \varepsilon_1 - \lambda_7 \theta_2 + \mu_7 \varsigma_1 + \rho_1 \alpha_1$$
$$- \rho_{10} \delta_1 (\mathrm{f}_{\mathrm{1R}}) - \rho_9 \delta_1 (1-\mathrm{f}_{\mathrm{1R}})(1-\mathrm{f}_{\mathrm{2R}}) - \rho_7 \delta_1 (1-\mathrm{f}_{\mathrm{1R}})(\mathrm{f}_{\mathrm{2R}})$$

14

$$\frac{\mathrm{d}B_{ia}}{\mathrm{d}t} = -\mathrm{k}_{\mathrm{f6}} B_{ia} L_{ia} + \mathrm{k}_{\mathrm{r6}} X_{ia} - \mathrm{k}_{\mathrm{f8}} B_{ia} I_{i2a} + \mathrm{k}_{\mathrm{r8}} Y_{ia} + \mathrm{k}_{\mathrm{eB}} B_a$$
$$- \mathrm{k}_{\mathrm{deg}} B_{ia} (\mathrm{f}_{\mathrm{1B}}) - \mathrm{k}_{\mathrm{rec}} B_{ia} (1-\mathrm{f}_{\mathrm{1B}})(1-\mathrm{f}_{\mathrm{2B}}) - \mathrm{k}_{\mathrm{trans}} B_{ia} (1-\mathrm{f}_{\mathrm{1B}})(\mathrm{f}_{\mathrm{2B}})$$

$$\frac{\mathrm{d}\delta_2}{\mathrm{d}\tau} = -\lambda_6 \eta_2 \omega + \mu_6 \varepsilon_2 - \lambda_8 \sigma_2 + \mu_8 \varsigma_2 + \rho_2 \alpha_2$$
$$- \rho_{10} \delta_2 (\mathrm{f}_{\mathrm{1B}}) - \rho_9 \delta_2 (1-\mathrm{f}_{\mathrm{1B}})(1-\mathrm{f}_{\mathrm{2B}}) - \rho_7 \delta_2 (1-\mathrm{f}_{\mathrm{1B}})(\mathrm{f}_{\mathrm{2B}})$$

15

$$\frac{\mathrm{d}R_{ib}}{\mathrm{d}t} = -\mathrm{k}_{\mathrm{f13}} R_{ib} L_{ib} + \mathrm{k}_{\mathrm{r13}} C_{ib} - \mathrm{k}_{\mathrm{f7}} R_{ib} I_{i1b} + \mathrm{k}_{\mathrm{r1}} Z_{ib} + \mathrm{k}_{\mathrm{eR}} R_b$$
$$- \mathrm{k}_{\mathrm{deg}} R_{ib} (\mathrm{f}_{\mathrm{1R}}) - \mathrm{k}_{\mathrm{rec}} R_{ib} (1-\mathrm{f}_{\mathrm{1R}})(1-\mathrm{f}_{\mathrm{2R}}) - \mathrm{k}_{\mathrm{trans}} R_{ib} (1-\mathrm{f}_{\mathrm{1R}})(\mathrm{f}_{\mathrm{2R}})$$

$$\frac{\mathrm{d}\delta_3}{\mathrm{d}\tau} = -\lambda_{13} \eta_4 + \mu_5 \varepsilon_3 - \lambda_1 \theta_4 + \mu_7 \varsigma_3 + \rho_1 \alpha_3$$
$$- \rho_{10} \delta_3 (\mathrm{f}_{\mathrm{1R}}) - \rho_9 \delta_3 (1-\mathrm{f}_{\mathrm{1R}})(1-\mathrm{f}_{\mathrm{2R}}) - \rho_7 \delta_3 (1-\mathrm{f}_{\mathrm{1R}})(\mathrm{f}_{\mathrm{2R}})$$

16

$$\frac{\mathrm{d}B_{ib}}{\mathrm{d}t} = -\mathrm{k}_{\mathrm{f14}} B_{ib} L_{ib} + \mathrm{k}_{\mathrm{r14}} X_{ib} - \mathrm{k}_{\mathrm{f16}} B_{ib} I_{i2b} + \mathrm{k}_{\mathrm{r16}} Y_{ib} + \mathrm{k}_{\mathrm{eB}} B_b$$
$$- \mathrm{k}_{\mathrm{deg}} B_{ib} (\mathrm{f}_{\mathrm{1B}}) - \mathrm{k}_{\mathrm{rec}} B_{ib} (1-\mathrm{f}_{\mathrm{1B}})(1-\mathrm{f}_{\mathrm{2B}}) - \mathrm{k}_{\mathrm{trans}} B_{ib} (1-\mathrm{f}_{\mathrm{1B}})(\mathrm{f}_{\mathrm{2B}})$$

$$\frac{\mathrm{d}\delta_4}{\mathrm{d}\tau} = -\lambda_{14} \eta_4 \omega + \mu_6 \varepsilon_4 - \lambda_{16} \sigma_4 + \mu_8 \varsigma_4 + \rho_2 \alpha_4$$
$$- \rho_{10} \delta_4 (\mathrm{f}_{\mathrm{1B}}) - \rho_9 \delta_4 (1-\mathrm{f}_{\mathrm{1B}})(1-\mathrm{f}_{\mathrm{2B}}) - \rho_7 \delta_4 (1-\mathrm{f}_{\mathrm{1B}})(\mathrm{f}_{\mathrm{2B}})$$

17

$$\frac{\mathrm{d}C_{ia}}{\mathrm{d}t} = \mathrm{k}_{\mathrm{f5}} R_{ia} L_{ia} - \mathrm{k}_{\mathrm{r5}} C_{ia} + \mathrm{k}_{\mathrm{ec}} C_a - \mathrm{k}_{\mathrm{deg}} C_{ia}(\mathrm{f}_{1\mathrm{C}}) - \mathrm{k}_{\mathrm{rec}} C_{ia}(1-\mathrm{f}_{1\mathrm{C}})(1-\mathrm{f}_{2\mathrm{C}}) - \mathrm{k}_{\mathrm{trans}} C_{ia}(1-\mathrm{f}_{1\mathrm{C}})(\mathrm{f}_{2\mathrm{C}})$$

$$\frac{\mathrm{d}\varepsilon_1}{\mathrm{d}\tau} = \lambda_5 \eta_2 - \mu_5 \varepsilon_1 + \rho_3 \beta_1 - \rho_{10} \varepsilon_1 (\mathrm{f}_{1\mathrm{C}}) - \rho_9 \varepsilon_1 (1-\mathrm{f}_{1\mathrm{C}})(1-\mathrm{f}_{2\mathrm{C}}) - \rho_7 \varepsilon_1 (1-\mathrm{f}_{1\mathrm{C}})(\mathrm{f}_{2\mathrm{C}})$$

18

$$\frac{\mathrm{d}X_{ia}}{\mathrm{d}t} = \mathrm{k}_{\mathrm{f6}} B_{ia} L_{ia} - \mathrm{k}_{\mathrm{r6}} X_{ia} + \mathrm{k}_{\mathrm{eX}} X_a - \mathrm{k}_{\mathrm{deg}} X_{ia}(\mathrm{f}_{1\mathrm{X}}) - \mathrm{k}_{\mathrm{rec}} X_{ia}(1-\mathrm{f}_{1\mathrm{X}})(1-\mathrm{f}_{2\mathrm{X}}) - \mathrm{k}_{\mathrm{trans}} X_{ia}(1-\mathrm{f}_{1\mathrm{X}})(\mathrm{f}_{2\mathrm{X}})$$

$$\frac{\mathrm{d}\varepsilon_2}{\mathrm{d}\tau} = \lambda_6 \eta_2 \omega - \mu_6 \varepsilon_2 + \rho_4 \beta_2 - \rho_{10} \varepsilon_2 (\mathrm{f}_{1\mathrm{X}}) - \rho_9 \varepsilon_2 (1-\mathrm{f}_{1\mathrm{X}})(1-\mathrm{f}_{2\mathrm{X}}) - \rho_7 \varepsilon_2 (1-\mathrm{f}_{1\mathrm{X}})(\mathrm{f}_{2\mathrm{X}})$$

19

$$\frac{\mathrm{d}C_{ib}}{\mathrm{d}t} = \mathrm{k}_{\mathrm{f13}} R_{ib} L_{ib} - \mathrm{k}_{\mathrm{r13}} C_{ib} + \mathrm{k}_{\mathrm{ec}} C_b - \mathrm{k}_{\mathrm{deg}} C_{ib}(\mathrm{f}_{1\mathrm{C}}) - \mathrm{k}_{\mathrm{rec}} C_{ib}(1-\mathrm{f}_{1\mathrm{C}})(1-\mathrm{f}_{2\mathrm{C}}) - \mathrm{k}_{\mathrm{trans}} C_{ib}(1-\mathrm{f}_{1\mathrm{C}})(\mathrm{f}_{2\mathrm{C}})$$

$$\frac{\mathrm{d}\varepsilon_3}{\mathrm{d}\tau} = \lambda_{13} \eta_2 - \mu_5 \varepsilon_1 + \rho_3 \beta_1 - \rho_{10} \varepsilon_1 (\mathrm{f}_{1\mathrm{C}}) - \rho_9 \varepsilon_1 (1-\mathrm{f}_{1\mathrm{C}})(1-\mathrm{f}_{2\mathrm{C}}) - \rho_7 \varepsilon_1 (1-\mathrm{f}_{1\mathrm{C}})(\mathrm{f}_{2\mathrm{C}})$$

20

$$\frac{\mathrm{d}X_{ib}}{\mathrm{d}t} = \mathrm{k}_{\mathrm{f14}} B_{ib} L_{ib} - \mathrm{k}_{\mathrm{r14}} X_{ib} + \mathrm{k}_{\mathrm{eX}} X_b - \mathrm{k}_{\mathrm{deg}} X_{ib}(\mathrm{f}_{1\mathrm{X}}) - \mathrm{k}_{\mathrm{rec}} X_{ib}(1-\mathrm{f}_{1\mathrm{X}})(1-\mathrm{f}_{2\mathrm{X}}) - \mathrm{k}_{\mathrm{trans}} X_{ib}(1-\mathrm{f}_{1\mathrm{X}})(\mathrm{f}_{2\mathrm{X}})$$

$$\frac{\mathrm{d}\varepsilon_4}{\mathrm{d}\tau} = \lambda_{14} \eta_4 \omega - \mu_6 \varepsilon_4 + \rho_4 \beta_4 - \rho_{10} \varepsilon_4 (\mathrm{f}_{1\mathrm{X}}) - \rho_9 \varepsilon_4 (1-\mathrm{f}_{1\mathrm{X}})(1-\mathrm{f}_{2\mathrm{X}}) - \rho_7 \varepsilon_4 (1-\mathrm{f}_{1\mathrm{X}})(\mathrm{f}_{2\mathrm{X}})$$

21

$$\frac{\mathrm{d}Z_{ia}}{\mathrm{d}t} = \mathrm{k}_{\mathrm{f7}} R_{ia} I_{i1a} - \mathrm{k}_{\mathrm{r7}} Z_{ia} + \mathrm{k}_{\mathrm{eZ}} Z_a - \mathrm{k}_{\mathrm{deg}} Z_{ia}(\mathrm{f}_{1\mathrm{Z}}) - \mathrm{k}_{\mathrm{rec}} Z_{ia}(1-\mathrm{f}_{1\mathrm{Z}})(1-\mathrm{f}_{2\mathrm{Z}}) - \mathrm{k}_{\mathrm{trans}} Z_{ia}(1-\mathrm{f}_{1\mathrm{Z}})(\mathrm{f}_{2\mathrm{Z}})$$

$$\frac{\mathrm{d}\varsigma_1}{\mathrm{d}\tau} = \lambda_7 \theta_2 - \mu_7 \varsigma_1 + \rho_5 \gamma_1 - \rho_{10} \varsigma_1 (\mathrm{f}_{1\mathrm{Z}}) - \rho_9 \varsigma_1 (1-\mathrm{f}_{1\mathrm{Z}})(1-\mathrm{f}_{2\mathrm{Z}}) - \rho_7 \varsigma_1 (1-\mathrm{f}_{1\mathrm{Z}})(\mathrm{f}_{2\mathrm{Z}})$$

22

$$\frac{\mathrm{d}Y_{ia}}{\mathrm{d}t} = \mathrm{k}_{\mathrm{f8}} B_{ia} I_{i2a} - \mathrm{k}_{\mathrm{r8}} Y_{ia} + \mathrm{k}_{\mathrm{eY}} Y_a - \mathrm{k}_{\mathrm{deg}} Y_{ia}(\mathrm{f}_{1\mathrm{Y}}) - \mathrm{k}_{\mathrm{rec}} Y_{ia}(1-\mathrm{f}_{1\mathrm{Y}})(1-\mathrm{f}_{2\mathrm{Y}}) - \mathrm{k}_{\mathrm{trans}} Y_{ia}(1-\mathrm{f}_{1\mathrm{Y}})(\mathrm{f}_{2\mathrm{Y}})$$

$$\frac{\mathrm{d}\varsigma_2}{\mathrm{d}\tau} = \lambda_8 \sigma_2 - \mu_8 \varsigma_2 + \rho_6 \gamma_2 - \rho_{10} \varsigma_2 (\mathrm{f}_{1\mathrm{Y}}) - \rho_9 \varsigma_2 (1-\mathrm{f}_{1\mathrm{Y}})(1-\mathrm{f}_{2\mathrm{Y}}) - \rho_7 \varsigma_2 (1-\mathrm{f}_{1\mathrm{Y}})(\mathrm{f}_{2\mathrm{Y}})$$

23

$$\frac{\mathrm{d}Z_{ib}}{\mathrm{d}t} = \mathrm{k}_{\mathrm{f15}} R_{ib} I_{i1b} - \mathrm{k}_{\mathrm{r15}} Z_{ib} + \mathrm{k}_{\mathrm{eZ}} Z_b - \mathrm{k}_{\mathrm{deg}} Z_{ib}(\mathrm{f}_{1\mathrm{Z}}) - \mathrm{k}_{\mathrm{rec}} Z_{ib}(1-\mathrm{f}_{1\mathrm{Z}})(1-\mathrm{f}_{2\mathrm{Z}}) - \mathrm{k}_{\mathrm{trans}} Z_{ib}(1-\mathrm{f}_{1\mathrm{Z}})(\mathrm{f}_{2\mathrm{Z}})$$

$$\frac{\mathrm{d}\varsigma_3}{\mathrm{d}\tau} = \lambda_{15}\theta_4 - \mu_7\varsigma_3 + \rho_5\gamma_3 - \rho_{10}\varsigma_3(\mathrm{f}_{1\mathrm{Z}}) - \rho_9\varsigma_3(1-\mathrm{f}_{1\mathrm{Z}})(1-\mathrm{f}_{2\mathrm{Z}}) - \rho_7\varsigma_3(1-\mathrm{f}_{1\mathrm{Z}})(\mathrm{f}_{2\mathrm{Z}})$$

24

$$\frac{\mathrm{d}Y_{ib}}{\mathrm{d}t} = \mathrm{k}_{\mathrm{f16}} B_{ib} I_{i2b} - \mathrm{k}_{\mathrm{r16}} Y_{ib} + \mathrm{k}_{\mathrm{eY}} Y_b - \mathrm{k}_{\mathrm{deg}} Y_{ib}(\mathrm{f}_{1\mathrm{Y}}) - \mathrm{k}_{\mathrm{rec}} Y_{ib}(1-\mathrm{f}_{1\mathrm{Y}})(1-\mathrm{f}_{2\mathrm{Y}}) - \mathrm{k}_{\mathrm{trans}} Y_{ib}(1-\mathrm{f}_{1\mathrm{Y}})(\mathrm{f}_{2\mathrm{Y}})$$

$$\frac{\mathrm{d}\varsigma_4}{\mathrm{d}\tau} = \lambda_{16}\sigma_4 - \mu_8\varsigma_4 + \rho_6\gamma_4 - \rho_{10}\varsigma_4(\mathrm{f}_{1\mathrm{Y}}) - \rho_9\varsigma_4(1-\mathrm{f}_{1\mathrm{Y}})(1-\mathrm{f}_{2\mathrm{Y}}) - \rho_7\varsigma_4(1-\mathrm{f}_{1\mathrm{Y}})(\mathrm{f}_{2\mathrm{Y}})$$

25

$$\frac{\mathrm{d}L_a}{\mathrm{d}t} = \frac{\mathrm{n}}{\mathrm{N}_{\mathrm{av}}\mathrm{Vol}_{\mathrm{a}}}[-\mathrm{k}_{\mathrm{f1}} R_a L_a + \mathrm{k}_{\mathrm{r1}} C_a - \mathrm{k}_{\mathrm{f2}} B_a L_a + \mathrm{k}_{\mathrm{r2}} X_a + \mathrm{k}_{\mathrm{off1}} C_a(1-\mathrm{P}(B_a)) + \mathrm{k}_{\mathrm{off2}} X_a(1-\mathrm{P}(R_a))]$$
$$- \mathrm{k}_{\mathrm{para}} L_a + \mathrm{k}_{\mathrm{para}} L_b + \mathrm{k}_{\mathrm{rec}} L_{ia}(1-\mathrm{f}_{1\mathrm{L}})(1-\mathrm{f}_{2\mathrm{L}}) + \mathrm{k}_{\mathrm{trans}} L_{ib}(1-\mathrm{f}_{1\mathrm{L}})(\mathrm{f}_{2\mathrm{L}})$$

$$\frac{\mathrm{d}\eta_1}{\mathrm{d}\tau} = -\frac{\lambda_1\eta_1}{\xi_1\varphi(1+\lambda_1+\lambda_2)} + \frac{\mu_1\beta_1(1+\lambda_2)}{\xi_1\varphi(1+\lambda_1+\lambda_2)} - \frac{\lambda_2\eta_1}{\xi_1\varphi(1+\lambda_1+\lambda_2)} + \frac{\mu_2\beta_2(1+\lambda_1)}{\xi_1\varphi\omega(1+\lambda_1+\lambda_2)}$$
$$+ \frac{\mu_1\beta_1}{\xi_1\varphi}(1-\mathrm{P}(B_a)) + \frac{\mu_2\beta_2}{\xi_1\varphi\omega}(1-\mathrm{P}(R_a)) - \rho_8\eta_1 + \frac{\rho_8\eta_3}{\xi_1} + \frac{\rho_9\eta_2\xi_2}{\xi_1}(1-\mathrm{f}_{1\mathrm{L}})(1-\mathrm{f}_{2\mathrm{L}})$$
$$+ \frac{\rho_7\eta_4\xi_2}{\xi_1}(1-\mathrm{f}_{1\mathrm{L}})(\mathrm{f}_{2\mathrm{L}})$$

26

$$\frac{\mathrm{d}L_{ia}}{\mathrm{d}t} = \frac{\mathrm{n}}{\mathrm{N}_{\mathrm{av}}\mathrm{Vol}_{\mathrm{e}}}[-\mathrm{k}_{\mathrm{f5}} R_{ia} L_{ia} + \mathrm{k}_{\mathrm{r5}} C_{ia} - \mathrm{k}_{\mathrm{f6}} B_{ia} L_{ia} + \mathrm{k}_{\mathrm{r6}} X_{ia}] - \mathrm{k}_{\mathrm{deg}} L_{ia}(\mathrm{f}_{1\mathrm{L}}) - \mathrm{k}_{\mathrm{rec}} L_{ia}(1-\mathrm{f}_{1\mathrm{L}})(1-\mathrm{f}_{2\mathrm{L}})$$
$$- \mathrm{k}_{\mathrm{trans}} L_{ia}(1-\mathrm{f}_{1\mathrm{L}})(\mathrm{f}_{2\mathrm{L}})$$

$$\frac{\mathrm{d}\eta_2}{\mathrm{d}\tau} = -\frac{\lambda_5\eta_2}{\xi_2\varphi} + \frac{\mu_5\varepsilon_1}{\xi_2\varphi} - \frac{\lambda_6\eta_2}{\xi_2\varphi} + \frac{\mu_6\varepsilon_2}{\xi_2\varphi\omega} - \rho_{10}\eta_2(\mathrm{f}_{1\mathrm{L}}) - \rho_9\eta_2(1-\mathrm{f}_{1\mathrm{L}})(1-\mathrm{f}_{2\mathrm{L}}) - \rho_7\eta_2(1-\mathrm{f}_{1\mathrm{L}})(\mathrm{f}_{2\mathrm{L}})$$

27

$$\frac{\mathrm{d}L_b}{\mathrm{d}t} = \frac{\mathrm{n}}{\mathrm{N_{av}Vol_b}}[-\mathrm{k_{f9}}R_bL_b + \mathrm{k_{r9}}C_b - \mathrm{k_{f10}}B_bL_b + \mathrm{k_{r10}}X_b + \mathrm{k_{off9}}C_b(1-\mathrm{P}(B_b)) + \mathrm{k_{off10}}X_b(1-\mathrm{P}(R_b))]$$
$$-\mathrm{k_{para}}L_b + \mathrm{k_{para}}L_a + \mathrm{k_{rec}}L_{ib}(1-\mathrm{f_{1L}})(1-\mathrm{f_{2L}}) + \mathrm{k_{trans}}L_{ia}(1-\mathrm{f_{1L}})(\mathrm{f_{2L}})$$

$$\frac{\mathrm{d}\eta_3}{\mathrm{d}\tau} = -\frac{\lambda_9\eta_3}{\varphi(1+\lambda_9+\lambda_{10})} + \frac{\mu_9\beta_{10}(1+\lambda_{10})}{\varphi(1+\lambda_9+\lambda_{10})} - \frac{\lambda_{10}\eta_3}{\varphi(1+\lambda_9+\lambda_{10})} + \frac{\mu_9\beta_3(1+\lambda_9)}{\varphi\omega(1+\lambda_9+\lambda_{10})}$$
$$+\frac{\mu_9\beta_3}{\varphi}(1-\mathrm{P}(B_b)) + \frac{\mu_{10}\beta_4}{\varphi\omega}(1-\mathrm{P}(R_b)) - \rho_8\eta_3 + \rho_8\eta_1\xi_1 + \rho_9\eta_4\xi_2(1-\mathrm{f_{1L}})(1-\mathrm{f_{2L}})$$
$$+\rho_7\eta_2\xi_2(1-\mathrm{f_{1L}})(\mathrm{f_{2L}})$$

28

$$\frac{\mathrm{d}L_{ib}}{\mathrm{d}t} = \frac{\mathrm{n}}{\mathrm{N_{av}Vol_e}}[-\mathrm{k_{f5}}R_{ib}L_{ib} + \mathrm{k_{r5}}C_{ib} - \mathrm{k_{f6}}B_{ib}L_{ib} + \mathrm{k_{r6}}X_{ib}] - \mathrm{k_{deg}}L_{ib}(\mathrm{f_{1L}}) - \mathrm{k_{rec}}L_{ib}(1-\mathrm{f_{1L}})(1-\mathrm{f_{2L}})$$
$$-\mathrm{k_{trans}}L_{ib}(1-\mathrm{f_{1L}})(\mathrm{f_{2L}})$$

$$\frac{\mathrm{d}\eta_4}{\mathrm{d}\tau} = -\frac{\lambda_{13}\eta_4}{\xi_2\varphi} + \frac{\mu_5\varepsilon_3}{\xi_2\varphi} - \frac{\lambda_{14}\eta_4}{\xi_2\varphi} + \frac{\mu_6\varepsilon_4}{\xi_2\varphi\omega} - \rho_{10}\eta_4(\mathrm{f_{1L}}) - \rho_9\eta_4(1-\mathrm{f_{1L}})(1-\mathrm{f_{2L}}) - \rho_7\eta_4(1-\mathrm{f_{1L}})(\mathrm{f_{2L}})$$

29

$$\frac{\mathrm{d}I_{1a}}{\mathrm{d}t} = \frac{\mathrm{n}}{\mathrm{N_{av}Vol_a}}[-\mathrm{k_{f3}}R_aI_{1a} + \mathrm{k_{r3}}Z_a] - \mathrm{k_{para}}I_{1a} + \mathrm{k_{para}}I_{1b}$$
$$+\mathrm{k_{rec}}I_{i1a}(1-\mathrm{f_{1I1}})(1-\mathrm{f_{2I1}}) + \mathrm{k_{trans}}I_{i1b}(1-\mathrm{f_{1I1}})(\mathrm{f_{2I1}})$$

$$\frac{\mathrm{d}\theta_1}{\mathrm{d}\tau} = -\frac{\lambda_3\theta_1}{\xi_1\varphi(1+\lambda_3)} + \frac{\mu_3\gamma_1}{\xi_1\varphi(1+\lambda_3)} - \rho_8\theta_1 + \frac{\rho_8\theta_3}{\xi_1}$$
$$+\frac{\rho_9\theta_2\xi_2}{\xi_1}(1-\mathrm{f_{1I1}})(1-\mathrm{f_{2I1}}) + \frac{\rho_7\theta_4\xi_2}{\xi_1}(1-\mathrm{f_{1I1}})(\mathrm{f_{2I1}})$$

30

$$\frac{\mathrm{d}I_{i1a}}{\mathrm{d}t} = \frac{\mathrm{n}}{\mathrm{N_{av}Vol_e}}[-\mathrm{k_{f7}}R_{ia}I_{i1a} + \mathrm{k_{r7}}Z_{ia}] - \mathrm{k_{deg}}I_{i1a}(\mathrm{f_{1I1}}) - \mathrm{k_{rec}}I_{i1a}(1-\mathrm{f_{1I1}})(1-\mathrm{f_{2I1}})$$
$$-\mathrm{k_{trans}}I_{i1a}(1-\mathrm{f_{1I1}})(\mathrm{f_{2I1}})$$

$$\frac{\mathrm{d}\theta_2}{\mathrm{d}\tau} = -\frac{\lambda_7\theta_2}{\xi_2\varphi} + \frac{\mu_7\varsigma_1}{\xi_2\varphi} - \rho_{10}\theta_2(\mathrm{f_{1I1}}) - \rho_9\theta_2(1-\mathrm{f_{1I1}})(1-\mathrm{f_{2I1}}) - \rho_7\theta_2(1-\mathrm{f_{1I1}})(\mathrm{f_{2I1}})$$

31

$$\frac{\mathrm{d}I_{1b}}{\mathrm{d}t} = \frac{\mathrm{n}}{\mathrm{N_{av}Vol_b}}[-\mathrm{k_{f11}}R_b I_{1b} + \mathrm{k_{r11}}Z_b] - \mathrm{k_{para}}I_{1b} + \mathrm{k_{para}}I_{1a}$$
$$+\mathrm{k_{rec}}I_{i1b}(1-\mathrm{f_{1I1}})(1-\mathrm{f_{2I1}}) + \mathrm{k_{trans}}I_{i1b}(1-\mathrm{f_{1I1}})(\mathrm{f_{2I1}})$$

$$\frac{\mathrm{d}\theta_3}{\mathrm{d}\tau} = -\frac{\lambda_{11}\theta_3}{\varphi(1+\lambda_{11})} + \frac{\mu_{11}\gamma_3}{\varphi(1+\lambda_{11})} - \rho_8\theta_3 + \rho_8\theta_1\xi_1$$
$$+\rho_9\theta_4\xi_2(1-\mathrm{f_{1I1}})(1-\mathrm{f_{2I1}}) + \rho_7\theta_2\xi_2(1-\mathrm{f_{1I1}})(\mathrm{f_{2I1}})$$

32

$$\frac{\mathrm{d}I_{i1b}}{\mathrm{d}t} = \frac{\mathrm{n}}{\mathrm{N_{av}Vol_e}}[-\mathrm{k_{f15}}R_{ib}I_{i1b} + \mathrm{k_{r15}}Z_{ib}] - \mathrm{k_{deg}}I_{i1b}(\mathrm{f_{1I1}}) - \mathrm{k_{rec}}I_{i1b}(1-\mathrm{f_{1I1}})(1-\mathrm{f_{2I1}})$$
$$-\mathrm{k_{trans}}I_{i1b}(1-\mathrm{f_{1I1}})(\mathrm{f_{2I1}})$$

$$\frac{\mathrm{d}\theta_4}{\mathrm{d}\tau} = -\frac{\lambda_{15}\theta_4}{\xi_2\varphi} + \frac{\mu_7\varsigma_3}{\xi_2\varphi} - \rho_{10}\theta_4(\mathrm{f_{1I1}}) - \rho_9\theta_4(1-\mathrm{f_{1I1}})(1-\mathrm{f_{2I1}}) - \rho_7\theta_4(1-\mathrm{f_{1I1}})(\mathrm{f_{2I1}})$$

33

$$\frac{\mathrm{d}I_{2a}}{\mathrm{d}t} = \frac{\mathrm{n}}{\mathrm{N_{av}Vol_a}}[-\mathrm{k_{f4}}B_a I_{2a} + \mathrm{k_{r4}}Y_a] - \mathrm{k_{para}}I_{2a} + \mathrm{k_{para}}I_{2b}$$
$$+\mathrm{k_{rec}}I_{i2a}(1-\mathrm{f_{1I2}})(1-\mathrm{f_{2I2}}) + \mathrm{k_{trans}}I_{i2b}(1-\mathrm{f_{1I2}})(\mathrm{f_{2I2}})$$

$$\frac{\mathrm{d}\sigma_1}{\mathrm{d}\tau} = -\frac{\lambda_4\sigma_1}{\xi_1\varphi(1+\lambda_4)} + \frac{\mu_4\gamma_2}{\xi_1\varphi(1+\lambda_4)} - \rho_8\sigma_1 + \frac{\rho_8\sigma_3}{\xi_1}$$
$$+\frac{\rho_9\sigma_2\xi_2}{\xi_1}(1-\mathrm{f_{1I2}})(1-\mathrm{f_{2I2}}) + \frac{\rho_7\sigma_4\xi_2}{\xi_1}(1-\mathrm{f_{1I2}})(\mathrm{f_{2I2}})$$

34

$$\frac{\mathrm{d}I_{i2a}}{\mathrm{d}t} = \frac{\mathrm{n}}{\mathrm{N_{av}Vol_e}}[-\mathrm{k_{f8}}B_{ia}I_{i2a} + \mathrm{k_{r8}}Y_{ia}] - \mathrm{k_{deg}}I_{i2a}(\mathrm{f_{1I2}}) - \mathrm{k_{rec}}I_{i2a}(1-\mathrm{f_{1I2}})(1-\mathrm{f_{2I2}})$$
$$-\mathrm{k_{trans}}I_{i2a}(1-\mathrm{f_{1I2}})(\mathrm{f_{2I2}})$$

$$\frac{\mathrm{d}\sigma_2}{\mathrm{d}\tau} = -\frac{\lambda_8\sigma_2}{\xi_2\varphi} + \frac{\mu_8\varsigma_2}{\xi_2\varphi} - \rho_{10}\sigma_2(\mathrm{f_{1I2}}) - \rho_9\sigma_2(1-\mathrm{f_{1I2}})(1-\mathrm{f_{2I2}}) - \rho_7\sigma_2(1-\mathrm{f_{1I2}})(\mathrm{f_{2I2}})$$

35

$$\frac{dI_{2b}}{dt} = \frac{n}{N_{av}Vol_b}[-k_{f12}B_bI_{2b} + k_{r12}Y_b] - k_{para}I_{2b} + k_{para}I_{2a}$$
$$+ k_{rec}I_{i2b}(1-f_{1I2})(1-f_{2I2}) + k_{trans}I_{i2b}(1-f_{1I2})(f_{2I2})$$

$$\frac{d\sigma_3}{d\tau} = -\frac{\lambda_{12}\sigma_3}{\varphi(1+\lambda_{12})} + \frac{\mu_{12}\gamma_4}{\varphi(1+\lambda_{12})} - \rho_8\sigma_3 + \rho_8\sigma_1\xi_1$$
$$+ \rho_9\sigma_4\xi_2(1-f_{1I2})(1-f_{2I2}) + \rho_7\sigma_2\xi_2(1-f_{1I2})(f_{2I2})$$

36

$$\frac{dI_{i2b}}{dt} = \frac{n}{N_{av}Vol_e}[-k_{f16}B_{ib}I_{i2b} + k_{r16}Y_{ib}] - k_{deg}I_{i2b}(f_{1I2}) - k_{rec}I_{i2b}(1-f_{1I2})(1-f_{2I2})$$
$$- k_{trans}I_{i2b}(1-f_{1I2})(f_{2I2})$$

$$\frac{d\sigma_4}{d\tau} = -\frac{\lambda_{16}\sigma_4}{\xi_2\varphi} + \frac{\mu_8\varsigma_4}{\xi_2\varphi} - \rho_{10}\sigma_4(f_{1I2}) - \rho_9\sigma_4(1-f_{1I2})(1-f_{2I2}) - \rho_7\sigma_4(1-f_{1I2})(f_{2I2})$$

37

$$\frac{dR_{deg}}{dt} = k_{deg}R_{ia}(f_{1R}) + k_{deg}R_{ib}(f_{1R})$$

38

$$\frac{dB_{deg}}{dt} = k_{deg}B_{ia}(f_{1B}) + k_{deg}B_{ib}(f_{1B})$$

39

$$\frac{dL_{deg}}{dt} = k_{deg}L_{ia}(f_{1L}) + k_{deg}L_{ib}(f_{1L})$$

40

$$\frac{dC_{deg}}{dt} = k_{deg}C_{ia}(f_{1C}) + k_{deg}C_{ib}(f_{1C})$$

41

$$\frac{\mathrm{d}X_{\mathrm{deg}}}{\mathrm{d}t} = \mathrm{k}_{\mathrm{deg}} X_{ia}(\mathrm{f}_{1\mathrm{X}}) + \mathrm{k}_{\mathrm{deg}} X_{ib}(\mathrm{f}_{1\mathrm{X}})$$

42

$$\frac{\mathrm{d}I_{1\mathrm{deg}}}{\mathrm{d}t} = \mathrm{k}_{\mathrm{deg}} I_{i1a}(\mathrm{f}_{1\mathrm{I1}}) + \mathrm{k}_{\mathrm{deg}} I_{i1b}(\mathrm{f}_{1\mathrm{I1}})$$

43

$$\frac{\mathrm{d}\mathrm{Z}_{\mathrm{deg}}}{\mathrm{d}t} = \mathrm{k}_{\mathrm{deg}} Z_{ia}(\mathrm{f}_{1\mathrm{Z}}) + \mathrm{k}_{\mathrm{deg}} Z_{ib}(\mathrm{f}_{1\mathrm{Z}})$$

44

$$\frac{\mathrm{d}I_{2\mathrm{deg}}}{\mathrm{d}t} = \mathrm{k}_{\mathrm{deg}} I_{i2a}(\mathrm{f}_{1\mathrm{I2}}) + \mathrm{k}_{\mathrm{deg}} I_{i2b}(\mathrm{f}_{1\mathrm{I2}})$$

45

$$\frac{\mathrm{d}Y_{\mathrm{deg}}}{\mathrm{d}t} = \mathrm{k}_{\mathrm{deg}} Y_{ia}(\mathrm{f}_{1\mathrm{Y}}) + \mathrm{k}_{\mathrm{deg}} Y_{ib}(\mathrm{f}_{1\mathrm{Y}})$$

Appendix B: MATLAB code

B.1 Main program

```
clear
global kon mu omega Rto Bto kplus rho f1 f2 phi xi
%%%%%%%%%%%%%%%%%%%%%%%%%%%%%%%%%%%%%%%%%%
%
I1a=0
I2a=0
I1b=0;
I2b=0;
kon(1)=4.7e5*60;                % pH 7.4     < M-1 min-1>
koff(1)=0.001128*60;      % pH 7.4     < min-1 >
kon(2)=3.67e5*60;         % pH 7.4     < M-1 min-1>
koff(2)=0.052848;         % pH 7.4     < min-1 >
kon(9)=kon(1);                  % pH 7.4
koff(9)=koff(1);                % pH 7.4
kon(10)=kon(2);                 % pH 7.4
koff(10)=koff(2);               % pH 7.4

kon(5)=kon(1);                  % pH 5.8     < M-1 min-1>
koff(5)=3*koff(1);        % pH 5.8

kon(6)=6.67e5*60;         % pH 5.8     < M-1 min-1>
koff(6)=koff(2)*2.5;      % pH 5.8

%UNCOMMENT THE FOLLOWING 4 LINES TO INCLUDE COMPETING COLD
IGF-I
%I1a=2.7e-7; %          < M >
%I2a=2.7e-7; %          < M >
```

```
%I1b=2.7e-7; %            < M >
%I2b=2.7e-7; %            < M >

kon(3)=kon(1);                    % pH 7.4       < M-1 min-1>
koff(3)=koff(1);            % pH 7.4
kon(11)=kon(3);                   % pH 7.4
koff(11)=koff(3);                 % pH 7.4
kon(4)=kon(2);                    % pH 7.4       < M-1 min-1>
koff(4)=koff(2);                  % pH 7.4
kon(12)=kon(4);                   % pH 7.4
koff(12)=koff(4);                 % pH 7.4

kon(7)=kon(5);                    % pH 5.8       < M-1 min-1>
koff(7)=koff(5);                  % pH 5.8
kon(8)=kon(6);                    % pH 5.8       < M-1 min-1>
koff(8)=koff(6);                  % pH 5.8

%%%%%%%%%%%%%%%%%%%%%%%%%%%%%%%%%%%%%%%%%%%%%%%%%%%%
%
%UNCOMMENT THIS SECTION TO INCLUDE COMPETING COLD INSULIN
%I1a=1.7e-6;                      % < M >
%I1b=1.7e-6;                      % < M >

%kon(3)=kon(1);             % pH 7.4       < M-1 min-1>
%koff(3)=100*koff(1);       % pH 7.4
%kon(11)=kon(3);            % pH 7.4
%koff(11)=koff(3);          % pH 7.4

%kon(7)=kon(3);             % pH 5.8
%koff(7)=3*koff(3);         % pH 5.8
```

```
%%%%%%%%%%%%%%%%%%%%%%%%%%%%%%%%%%%%%%%%%%
%
%%%%%%%%%%%%%%%%%%%%%%%%%%%%%%%%%%%%%%%%%%
%
%UNCOMMENT THIS SECTION TO INCLUDE COMPETING COLD Y60L

%I2a=2.7e-7;                  %< M >
%I2b=2.7e-7;                  %< M >

%kon(4)=kon(2);               % pH 7.4      < M-1 min-1>
%koff(4)=koff(2);         % pH 7.4
%kon(12)=kon(4);              % pH 7.4
%koff(12)=koff(4);            % pH 7.4

%kon(8)=kon(6);               % pH 5.8
%koff(8)=koff(6);         % pH 5.8
%%%%%%%%%%%%%%%%%%%%%%%%%%%%%%%%%%%%%%%%%%
%
porosity=.25;
radius=5E-4;              %<cm cell-1 >
diff=2.1E-6;              % < cm2 s-1 >
sD=radius*diff*60/1000;   % < L min-1 >         radius*diff
N=6.02e23;                % < # cell-1 >        avogadro's number
cell=351356;                  % < # >               from DNA counts
Vole=10e-14;                  % < L cell-1 >
Vole=Vole*cell;           % < L >               endosome volume
Vola=0.5e-3;                  % < L >               apical volume
Volb=1.5e-3;                  % < L >               baso volume

% APICAL SURFACE
% initial conditions
```

```
Ra=35000;               % < # cell-1 >   from equilibrium binding experiment
%Ra=1e-100;                  % Uncomment to simulate no apical receptors
Ba=80000;               % < # cell-1 >   from equilibrium binding experiment
%Ba=1e-100                   % Uncomment to simulate no apical IGFBPS
La=0.53e-9;             % < M >
%La=0                        % Uncomment to simulate steady state (no ligand)

%BASO SURFACE
% initial conditions
Rb=1e-10;               %< # cell-1 >   from equilibrium binding experiment
Bb=51000;               % < # cell-1 >   from equilibrium binding experiment
%Bb=1e-100                   % Uncomment to simulate no baso IGFBPS
%Lb=0.53e-9;                 % Uncomment to simulate baso addition of IGF-I
Lb=0;
%%%%%%%%%%%%%%%%%%%%%%%%%%%%%%%%%%%%%%%%%%%%%%%%%%%%%%%%%%%%%%%%%%%%%%%%%%%%
%
Rto=Ra+Rb;
Bto=Ba+Bb;
kplus=4*pi*sD*N;
ke=0.007;
omega=Rto/Bto;
xi(1)=Vola/Volb;
xi(2)=Vole/Volb;
phi=N*Volb*ke/(cell*kplus);

%mu
mu(1)=koff(1)/ke;
mu(2)=koff(2)/ke;
mu(3)=koff(3)/ke;
mu(4)=koff(4)/ke;
mu(5)=koff(5)/ke;
```

```
mu(6)=koff(6)/ke;
mu(7)=koff(7)/ke;
mu(8)=koff(8)/ke;
mu(9)=koff(9)/ke;
mu(10)=koff(10)/ke;
mu(11)=koff(11)/ke;
mu(12)=koff(12)/ke;

%rho=(ker;keb;kec;kex;kez;key;ktrans;kpara;krec;kdeg)
%          1  2    3    4    5   6      7       8      9      10
rho(1)=0.007/ke;                % < min-1 >
rho(2)=0.0000000000001/ke;          % < min-1 >
rho(3)=0.076/ke;                % < min-1 >      measured by internalization experiments
rho(4)=0.0000000000001/ke;          % < min-1 >
rho(5)=0.076/ke;                % < min-1 >
rho(6)=0.0000000000001/ke;          % < min-1 >
rho(7)=.11/ke;                      % < min-1 >
rho(8)=porosity*kplus/(N*Volb*ke/(cell*phi));
rho(9)=.11/ke;                      % < min-1 >
rho(10)=0.035;                  % < min-1 >

% Uncomment this section to look just at surface events (4C)
%rho(1)=0;
%rho(2)=0;
%rho(3)=0;
%rho(4)=0;
%rho(5)=0;
%rho(6)=0;
%rho(7)=0;
%rho(8)=0
%rho(9)=0;
```

```
%rho(10)=0;
%%%%%%%%%%%%%%%%%%%%%%%%%%%%%%%%%%%%%%%%%%%%%%%%%%%
%
% f1: fraction of internalized entities entering degradation pathway
% f1=[R;B;L;C;X;I1;Z;I2;Y]
%       1 2  3  4  5  6  7  8   9
f1(1)=.25;
f1(2)=.25;
f1(3)=0.75;
f1(4)=0.25;
f1(5)=0.25;
f1(6)=0.75;
f1(7)=0.25;
f1(8)=0.75;
f1(9)=0.25

% f2: fraction of non degraded entities entering transport (not recycling) pathway
% f2=[R;B;L;C;X;I1;Z;I2;Y]
%       1  2 3  4  5  6  7  8  9
f2(1)=.25;
f2(2)=.25;
f2(3)=.25;
f2(4)=.75;
f2(5)=.25;
f2(6)=.25;
f2(7)=.75;
f2(8)=.25;
f2(9)=.25

%    y=(alpha1 alpha2 alpha3 alpha4 beta1 beta2 beta3 beta4
%          1        2         3         4        5       6       7       8
```

```
%          Ra     Ba     Rb     Bb     Ca    Xa   Cb   Xb
%
%     gamma1 gamma2 gamma3 gamma4 delta1 delta2 delta3 delta4
%       9        10       11       12      13      14      15    16
%       Za       Ya       Zb       Yb      Ria     Bia     Rib   Bib
%
%     epsilon1 epsilon2 epsilon3 epsilon4 zeta1 zeta2 zeta3 zeta4
%       17       18       19       20      21    22   23    24
%       Cia      Xia      Cib      Xib     Zia   Yia  Zib   Yib
%
%     eta1 eta2 eta3 eta4 theta1 theta2 theta3 theta4 sigma1 sigma2 sigma3 sigma4
%      25   26   27   28    29     30     31     32     33     34     35     36
%      La   Lia  Lb   Lib   I1a    Ii1a   I1b    Ii1b   I2a    Ii2a   I2b    Ii2b

parameters=[porosity; radius; diff; cell; Vole; Vola; Volb; kplus; ke; kon(1); kon(2);
kon(3); kon(4); kon(5); kon(6); kon(7); kon(8); kon(9); kon(10); kon(11); kon(12);
koff(1); koff(2); koff(3); koff(4); koff(5); koff(6); koff(7); koff(8); koff(9); koff(10);
koff(11); koff(12); rho(1); rho(2); rho(3); rho(4); rho(5); rho(6); rho(7); rho(8); rho(9);
rho(10); f1(1); f1(2); f1(3); f1(4); f1(5); f1(6); f1(7); f1(8); f1(9); f2(1); f2(2); f2(3);
f2(4); f2(5); f2(6); f2(7); f2(8); f2(9); I1a; I1b; I2a; I2b; Ra; Ba; La; Rb; Bb; Lb]

Rao=Ra/Rto;
Rbo=Rb/Rto;
Bao=Ba/Bto;
Bbo=Bb/Bto;
Lao=La*kplus/(Rto*ke);
Lbo=Lb*kplus/(Rto*ke);
I1ao=I1a*kplus/(Rto*ke);
I1bo=I1b*kplus/(Rto*ke);
I2ao=I2a*kplus/(Bto*ke);
I2bo=I2b*kplus/(Bto*ke);
```

```
y0=[Rao,Bao,Rbo,Bbo, 0, 0, 0, 0, 0, 0, 0, 0, 0, 0, 0, 0, 0, 0, 0, 0, 0, 0, 0, 0,Lao, 0,Lbo,
0,I1ao, 0,I1bo, 0 ,I2ao, 0,I2bo, 0, 0, 0, 0, 0, 0, 0, 0, 0, 0, 0]

time=720;                    %min
tau=time*ke;
options=odeset('BDF','on')
[t,y]=ode15s('Dimensionless',[0 tau], y0,options);


normaltime=t/ke
normal(:,1)=y(:,1)*Rto;
normal(:,2)=y(:,2)*Bto;
normal(:,3)=y(:,3)*Rto;
normal(:,4)=y(:,4)*Bto;
normal(:,5)=y(:,5)*Rto;
normal(:,6)=y(:,6)*Bto;
normal(:,7)=y(:,7)*Rto;
normal(:,8)=y(:,8)*Bto;
normal(:,9)=y(:,9)*Rto;
normal(:,10)=y(:,10)*Bto;
normal(:,11)=y(:,11)*Rto;
normal(:,12)=y(:,12)*Bto;
normal(:,13)=y(:,13)*Rto;
normal(:,14)=y(:,14)*Bto;
normal(:,15)=y(:,15)*Rto;
normal(:,16)=y(:,16)*Bto;
normal(:,17)=y(:,17)*Rto;
normal(:,18)=y(:,18)*Bto;
normal(:,19)=y(:,19)*Rto;
normal(:,20)=y(:,20)*Bto;
```

```
normal(:,21)=y(:,21)*Rto;
normal(:,22)=y(:,22)*Bto;
normal(:,23)=y(:,23)*Rto;
normal(:,24)=y(:,24)*Bto;
normal(:,25)=y(:,25)*Rto*ke/kplus;
normal(:,26)=y(:,26)*Rto*ke/kplus;
normal(:,27)=y(:,27)*Rto*ke/kplus;
normal(:,28)=y(:,28)*Rto*ke/kplus;
normal(:,29)=y(:,29)*Rto*ke/kplus;
normal(:,30)=y(:,30)*Rto*ke/kplus;
normal(:,31)=y(:,31)*Rto*ke/kplus;
normal(:,32)=y(:,32)*Rto*ke/kplus;
normal(:,33)=y(:,33)*Bto*ke/kplus;
normal(:,34)=y(:,34)*Bto*ke/kplus;
normal(:,35)=y(:,35)*Bto*ke/kplus;
normal(:,36)=y(:,36)*Bto*ke/kplus;
normal(:,37)=y(:,37)*Rto;
normal(:,38)=y(:,38)*Bto;
normal(:,39)=y(:,39)*Rto*ke/kplus;
normal(:,40)=y(:,40)*Rto;
normal(:,41)=y(:,41)*Bto;
normal(:,42)=y(:,42)*Rto*ke/kplus;
normal(:,43)=y(:,43)*Rto;
normal(:,44)=y(:,44)*Bto*ke/kplus;
normal(:,45)=y(:,45)*Bto;

totalmatrix=[normaltime normal];

save <insert the name of your file> totalmatrix /ascii;
save <insert the name of your file>_parameters parameters /ascii;
```

```
% UNCOMMENT THE FOLLOWING TO RUN A PULSE CHASE EXPERIMENT
% THE PORTION ABOVE IS THE PULSE PORTION
% THE PORTION BELOW IS THE CHASE PORTION
%size(y);
%y1=size(y)
%y0=y(y1(1),:)
%y0(25)=0%

%time=<insert the chase duration>; %min
%tau=time*ke;
%options=odeset('BDF','on')
%[t,y]=ode15s('Dimensionless',[0 tau], y0,options);


%normaltime2=t/ke
%normal2(:,1)=y(:,1)*Rto;
%normal2(:,2)=y(:,2)*Bto;
%normal2(:,3)=y(:,3)*Rto;
%normal2(:,4)=y(:,4)*Bto;
%normal2(:,5)=y(:,5)*Rto;
%normal2(:,6)=y(:,6)*Bto;
%normal2(:,7)=y(:,7)*Rto;
%normal2(:,8)=y(:,8)*Bto;
%normal2(:,9)=y(:,9)*Rto;
%normal2(:,10)=y(:,10)*Bto;
%normal2(:,11)=y(:,11)*Rto;
%normal2(:,12)=y(:,12)*Bto;
%normal2(:,13)=y(:,13)*Rto;
%normal2(:,14)=y(:,14)*Bto;
%normal2(:,15)=y(:,15)*Rto;
%normal2(:,16)=y(:,16)*Bto;
```

```
%normal2(:,17)=y(:,17)*Rto;
%normal2(:,18)=y(:,18)*Bto;
%normal2(:,19)=y(:,19)*Rto;
%normal2(:,20)=y(:,20)*Bto;
%normal2(:,21)=y(:,21)*Rto;
%normal2(:,22)=y(:,22)*Bto;
%normal2(:,23)=y(:,23)*Rto;
%normal2(:,24)=y(:,24)*Bto;
%normal2(:,25)=y(:,25)*Rto*ke/kplus;
%normal2(:,26)=y(:,26)*Rto*ke/kplus;
%normal2(:,27)=y(:,27)*Rto*ke/kplus;
%normal2(:,28)=y(:,28)*Rto*ke/kplus;
%normal2(:,29)=y(:,29)*Rto*ke/kplus;
%normal2(:,30)=y(:,30)*Rto*ke/kplus;
%normal2(:,31)=y(:,31)*Rto*ke/kplus;
%normal2(:,32)=y(:,32)*Rto*ke/kplus;
%normal2(:,33)=y(:,33)*Bto*ke/kplus;
%normal2(:,34)=y(:,34)*Bto*ke/kplus;
%normal2(:,35)=y(:,35)*Bto*ke/kplus;
%normal2(:,36)=y(:,36)*Bto*ke/kplus;
%normal2(:,37)=y(:,37)*Rto;
%normal2(:,38)=y(:,38)*Bto;
%normal2(:,39)=y(:,39)*Rto*ke/kplus;
%normal2(:,40)=y(:,40)*Rto;
%normal2(:,41)=y(:,41)*Bto;
%normal2(:,42)=y(:,42)*Rto*ke/kplus;
%normal2(:,43)=y(:,43)*Rto;
%normal2(:,44)=y(:,44)*Bto*ke/kplus;
%normal2(:,45)=y(:,45)*Bto;
%totalmatrix2=[normaltime2 normal2];
%save <insert file name here>_chase totalmatrix2 /ascii;
```

B.2 Differential Equations

```
function yp=Dimensionless(t,y)
global kon mu omega Rto Bto kplus rho f1 f2 phi xi

fra =-3.73+0.743*log10(y(1)*Rto);
if fra <= 0;
   fra=0;
elseif fra > 1;
   fra = 1;
else
   fra =-3.73+0.743*log10(y(1)*Rto);
end

fba =-3.73+0.743*log10(y(2)*Bto);
if fba <= 0;
   fba=0;
elseif fba > 1;
   fba = 1;
else
   fba =-3.73+0.743*log10(y(2)*Bto);
end
%%%%%%%%%%%%%%%%%%%%%%%%%%%%%%%%%%%%%%%%%%%%%%%%%%%%%%
%
frb =-3.73+0.743*log10(y(3)*Rto);
if frb <= 0;
   frb=0;
elseif frb > 1;
   frb = 1;
```

```
else
   frb =-3.73+0.743*log10(y(3)*Rto);
end

fbb =-3.73+0.743*log10(y(4)*Bto);
if fbb <= 0;
   fbb=0;
elseif fbb > 1;
   fbb = 1;
else
   fbb =-3.73+0.743*log10(y(4)*Bto );
end

% lambda
lambda(1)=kon(1)*y(1)*Rto/kplus;   % kon1*Ra/4 pi sD
lambda(2)=kon(2)*y(2)*Bto/kplus;   % kon2*Ba/4 pi sD
lambda(3)=kon(3)*y(1)*Rto/kplus;   % kon3*Ra/4 pi sD
lambda(4)=kon(4)*y(2)*Bto/kplus;   % kon4*Ba/4 pi sD
lambda(5)=kon(5)*y(13)*Rto/kplus;  % kon5*Ria/4 pi sD
lambda(6)=kon(6)*y(14)*Bto/kplus;  % kon6*Bia/4 pi sD
lambda(7)=kon(7)*y(13)*Rto/kplus;  % kon7*Ria/4 pi sD
lambda(8)=kon(8)*y(14)*Bto/kplus;  % kon8*Bia/4 pi sD
lambda(9)=kon(9)*y(3)*Rto/kplus;   % kon9*Rb/4 pi sD
lambda(10)=kon(10)*y(4)*Bto/kplus; % kon10*Bb/4 pi sD
lambda(11)=kon(11)*y(3)*Rto/kplus; % kon11*Rb/4 pi sD
lambda(12)=kon(12)*y(4)*Bto/kplus; % kon12*Bb/4 pi sD
lambda(13)=kon(5)*y(15)*Rto/kplus; % kon5*Rib/4 pi sD
lambda(14)=kon(6)*y(16)*Bto/kplus; % kon6*Bib/4 pi sD
lambda(15)=kon(7)*y(15)*Rto/kplus; % kon7*Rib/4 pi sD
lambda(16)=kon(8)*y(16)*Bto/kplus; % kon8*Bib/4 pi sD
```

```
upsilon(1)=rho(1)*y(1)-(rho(9)*y(13)*(1-f1(1))*(1-f2(1)))-(rho(7)*y(15)*(1-
f1(1))*f2(1));
upsilon(2)=rho(2)*y(2)-(rho(9)*y(14)*(1-f1(2))*(1-f2(2)))-(rho(7)*y(16)*(1-
f1(2))*f2(2));
upsilon(3)=(rho(1)*y(3))-(rho(9)*y(15)*(1-f1(1))*(1-f2(1)))-(rho(7)*y(13)*(1-
f1(1))*f2(1));
upsilon(4)=(rho(2)*y(4))-(rho(9)*y(16)*(1-f1(2))*(1-f2(2)))-(rho(7)*y(14)*(1-
f1(2))*f2(2));

%Ra
yp(1)=-(lambda(1)*y(25)/(1+lambda(1)+lambda(2)))...
   +(mu(1)*y(5)*(1+lambda(2))/(1+lambda(1)+lambda(2)))...
   -(lambda(3)*y(29)/(1+lambda(3)))...
   +(mu(3)*y(9)/(1+lambda(3)))...
   -(mu(2)*y(6)*fra/omega)...
   +(upsilon(1))...
   -(rho(1)*y(1))...
   +(rho(9)*y(13)*(1-f1(1))*(1-f2(1)))...
   +(rho(7)*y(15)*(1-f1(1))*f2(1));

%Ba
yp(2)=-(lambda(2)*y(25)*omega/(1+lambda(2)+lambda(1)))...
   +(mu(2)*y(6)*(1+lambda(1))/(1+lambda(1)+lambda(2)))...
   -(lambda(4)*y(33)/(1+lambda(4)))...
   +(mu(4)*y(10)/(1+lambda(4)))...
   -(mu(1)*y(5)*omega*fba)...
   +(upsilon(2))...
   -(rho(2)*y(2))...
   +(rho(9)*y(14)*(1-f1(2))*(1-f2(2)))...
   +(rho(7)*y(16)*(1-f1(2))*f2(2));
```

```
%Rb
yp(3)=-(lambda(9)*y(27)/(1+lambda(9)+lambda(10)))...
   +(mu(9)*y(7)*(1+lambda(10))/(1+lambda(10)+lambda(9)))...
   -(lambda(11)*y(31)/(1+lambda(11)))...
   +(mu(11)*y(11)/(1+lambda(11)))...
   -(mu(10)*y(8)*frb/omega)...
   +(upsilon(3))...
   -(rho(1)*y(3))...
   +(rho(9)*y(15)*(1-f1(1))*(1-f2(1)))...
   +(rho(7)*y(13)*(1-f1(1))*f2(1));

%Bb
yp(4)=-(lambda(10)*y(27)*omega/(1+lambda(10)+lambda(9)))...
   +(mu(10)*y(8)*(1+lambda(9))/(1+lambda(9)+lambda(10)))...
   -(lambda(12)*y(35)/(1+lambda(12)))...
   +(mu(12)*y(12)/(1+lambda(12)))...
   -(mu(9)*y(7)*omega*fbb)...
   +(upsilon(4))...
   -(rho(2)*y(4))...
   +(rho(9)*y(16)*(1-f1(2))*(1-f2(2)))...
   +(rho(7)*y(14)*(1-f1(2))*f2(2));

%Ca
yp(5)=(lambda(1)*y(25)/(1+lambda(1)+lambda(2)))...
   -(mu(1)*y(5)*(1+lambda(2))/(1+lambda(1)+lambda(2)))...
   +(mu(2)*y(6)*fra/omega)...
   -(rho(3)*y(5))...
   +(rho(9)*y(17)*(1-f1(4))*(1-f2(4)))...
   +(rho(7)*y(19)*(1-f1(4))*f2(4));

%Xa
```

```
yp(6)=(lambda(2)*y(25)*omega/(1+lambda(2)+lambda(1)))...
   -(mu(2)*y(6)*(1+lambda(1))/(1+lambda(1)+lambda(2)))...
   +(mu(1)*y(5)*omega*fba)...
   -(rho(4)*y(6))...
   +(rho(9)*y(18)*(1-f1(5))*(1-f2(5)))...
   +(rho(7)*y(20)*(1-f1(5))*f2(5));

%Cb
yp(7)=(lambda(9)*y(27)/(1+lambda(9)+lambda(10)))...
   -(mu(9)*y(7)*(1+lambda(10))/(1+lambda(10)+lambda(9)))...
   +(mu(10)*y(8)*frb/omega)...
   -(rho(3)*y(7))...
   +(rho(9)*y(19)*(1-f1(4))*(1-f2(4)))...
   +(rho(7)*y(17)*(1-f1(4))*f2(4));

%Xb
yp(8)=(lambda(10)*y(27)*omega/(1+lambda(10)+lambda(9)))...
   -(mu(10)*y(8)*(1+lambda(9))/(1+lambda(10)+lambda(9)))...
   +(mu(9)*y(7)*omega*fbb)...
   -(rho(4)*y(8))...
   +(rho(9)*y(20)*(1-f1(5))*(1-f2(5)))...
   +(rho(7)*y(18)*(1-f1(5))*f2(5));

%Za
yp(9)=(lambda(3)*y(29)/(1+lambda(3)))...
   -(mu(3)*y(9)/(1+lambda(3)))...
   -(rho(5)*y(9))...
   +(rho(9)*y(21)*(1-f1(7))*(1-f2(7)))...
   +(rho(7)*y(23)*(1-f1(7))*f2(7));

%Ya
```

```
yp(10)=(lambda(4)*y(33)/(1+lambda(4)))...
   -(mu(4)*y(10)/(1+lambda(4)))...
   -(rho(6)*y(10))...
   +(rho(9)*y(22)*(1-f1(9))*(1-f2(9)))...
   +(rho(7)*y(24)*(1-f1(9)*f2(9)));

%Zb
yp(11)=(lambda(11)*y(31)/(1+lambda(11)))...
   -(mu(11)*y(11)/(1+lambda(11)))...
   -(rho(5)*y(11))...
   +(rho(9)*y(23)*(1-f1(7))*(1-f2(7)))...
   +(rho(7)*y(21)*(1-f1(7))*f2(7));

%Yb
yp(12)=(lambda(12)*y(35)/(1+lambda(12)))...
   -(mu(12)*y(12)/(1+lambda(12)))...
   -(rho(6)*y(12))...
   +(rho(9)*y(24)*(1-f1(9))*(1-f2(9)))...
   +(rho(7)*y(22)*(1-f1(9)*f2(9)));

%Ria
yp(13)=-(lambda(5)*y(26))...
   +(mu(5)*y(17))...
   -(lambda(7)*y(30))...
   +(mu(7)*y(21))...
   +(rho(1)*y(1))...
   -(rho(10)*y(13)*f1(1))...
   -(rho(9)*y(13)*(1-f1(1))*(1-f2(1)))...
   -(rho(7)*y(13)*(1-f1(1))*f2(1));

%Bia
```

```
yp(14)=-(lambda(6)*y(26)*omega)...
   +(mu(6)*y(18))...
   -(lambda(8)*y(34))...
   +(mu(8)*y(22))...
   +(rho(2)*y(2))...
   -(rho(10)*y(14)*f1(2))...
   -(rho(9)*y(14)*(1-f1(2))*(1-f2(2)))...
   -(rho(7)*y(14)*(1-f1(2))*f2(2));

%Rib
yp(15)=-(lambda(13)*y(28))...
   +(mu(5)*y(19))...
   -(lambda(15)*y(32))...
   +(mu(7)*y(23))...
   +(rho(1)*y(3))...
   -(rho(10)*y(15)*f1(1))...
   -(rho(9)*y(15)*(1-f1(1))*(1-f2(1)))...
   -(rho(7)*y(15)*(1-f1(1))*f1(1));

%Bib
yp(16)=-(lambda(14)*y(28)*omega)...
   +(mu(6)*y(20))...
   -(lambda(16)*y(36))...
   +(mu(8)*y(24))...
   +(rho(2)*y(4))...
   -(rho(10)*y(16)*f1(2))...
   -(rho(9)*y(16)*(1-f1(2))*(1-f2(2)))...
   -(rho(7)*y(16)*(1-f1(2))*f2(2));

%Cia
yp(17)=(lambda(5)*y(26))...
```

```
    -(mu(5)*y(17))...
    +(rho(3)*y(5))...
    -(rho(10)*y(17)*f1(4))...
    -(rho(9)*y(17)*(1-f1(4))*(1-f2(4)))...
    -(rho(7)*y(17)*(1-f1(4))*f2(4));

%Xia
yp(18)=(lambda(6)*y(26)*omega)...
    -(mu(6)*y(18))...
    +(rho(4)*y(6))...
    -(rho(10)*y(18)*f1(5))...
    -(rho(9)*y(18)*(1-f1(5))*(1-f2(5)))...
    -(rho(7)*y(18)*(1-f1(5))*f2(5));

%Cib
yp(19)=(lambda(13)*y(28))...
    -(mu(5)*y(19))...
    +(rho(3)*y(7))...
    -(rho(10)*y(19)*f1(4))...
    -(rho(9)*y(19)*(1-f1(4))*(1-f2(4)))...
    -(rho(7)*y(19)*(1-f1(4))*f2(4));

%Xib
yp(20)=(lambda(14)*y(28)*omega)...
    -(mu(6)*y(20))...
    +(rho(4)*y(8))...
    -(rho(10)*y(20)*f1(5))...
    -(rho(9)*y(20)*(1-f1(5))*(1-f2(5)))...
    -(rho(7)*y(20)*(1-f1(5))*f2(5));

%Zia
```

```
yp(21)=(lambda(7)*y(30))...
   -(mu(7)*y(21))...
   +(rho(5)*y(9))...
   -(rho(10)*y(21)*f1(7))...
   -(rho(9)*y(21)*(1-f1(7))*(1-f2(7)))...
   -(rho(7)*y(21)*(1-f1(7))*f2(7));

%Yia
yp(22)=(lambda(8)*y(34))...
   -(mu(8)*y(22))...
   +(rho(6)*y(10))...
   -(rho(10)*y(22)*f1(9))...
   -(rho(9)*y(22)*(1-f1(9))*(1-f2(9)))...
   -(rho(7)*y(22)*(1-f1(9))*f2(9));

%Zib
yp(23)=(lambda(15)*y(32))...
   -(mu(7)*y(23))...
   +(rho(5)*y(11))...
   -(rho(10)*y(23)*f1(7))...
   -(rho(9)*y(23)*(1-f1(7))*(1-f2(7)))...
   -(rho(7)*y(23)*(1-f1(7))*f2(7));

%Yib
yp(24)=(lambda(16)*y(36))...
   -(mu(8)*y(24))...
   +(rho(6)*y(12))...
   -(rho(10)*y(24)*f1(9))...
   -(rho(9)*y(24)*(1-f1(9))*(1-f2(9)))...
   -(rho(7)*y(24)*(1-f1(9))*f2(9));
```

```
%L -> ligand -> IGF-I
yp(25)=-(lambda(1)*y(25)/(phi*xi(1)*(1+lambda(1)+lambda(2))))...
   +(mu(1)*y(5)*(1-fba)*(1+lambda(2))/(phi*xi(1)*(1+lambda(1)+lambda(2))))...
   -(lambda(2)*y(25)/(phi*xi(1)*(1+lambda(1)+lambda(2))))...
   +(mu(2)*y(6)*(1-
fra)*(1+lambda(1))/(phi*xi(1)*omega*(1+lambda(1)+lambda(2))))...
   -(rho(8)*y(25))...
   +(rho(8)*y(27)/xi(1))...
   +(rho(9)*y(26)*xi(2)*(1-f1(3))*(1-f2(3))/xi(1))...
   +(rho(7)*y(28)*xi(2)*(1-f1(3))*f2(3)/xi(1));
yp(26)=-(lambda(5)*y(26)/(phi*xi(2)))...
   +(mu(5)*y(17)/(phi*xi(2)))...
   -(lambda(6)*y(26)/(phi*xi(2)))...
   +(mu(6)*y(18)/(phi*xi(2)*omega))...
   -(rho(10)*y(26)*f1(3))...
   -(rho(9)*y(26)*(1-f1(3))*(1-f2(3)))...
   -(rho(7)*y(26)*(1-f1(3))*f2(3));
yp(27)=-(lambda(9)*y(27)/(phi*(1+lambda(9)+lambda(10))))...
   +(mu(9)*y(7)*(1-fbb)*(1+lambda(10))/(phi*(1+lambda(9)+lambda(10))))...
   -(lambda(10)*y(27)/(phi*(1+lambda(9)+lambda(10))))...
   +(mu(10)*y(8)*(1-frb)*(1+lambda(9))/(omega*phi*(1+lambda(9)+lambda(10))))...
   -(rho(8)*y(27))...
   +(rho(8)*y(25)*xi(1))...
   +(rho(9)*y(28)*xi(2)*(1-f1(3))*(1-f2(3)))...
   +(rho(7)*y(26)*xi(2)*(1-f1(3))*f2(3));
yp(28)=-(lambda(13)*y(28)/(phi*xi(2)))...
   +(mu(5)*y(19)/(phi*xi(2)))...
   -(lambda(14)*y(28)/(phi*xi(2)))...
   +(mu(6)*y(20)/(omega*phi*xi(2)))...
   -(rho(10)*y(28)*f1(3))...
   -(rho(9)*y(28)*(1-f1(3))*(1-f2(3)))...
```

```
   -(rho(7)*y(28)*(1-f1(3))*f2(3));

%I1 -> Insulin
yp(29)=-(lambda(3)*y(29)/(phi*xi(1)*(1+lambda(3))))...
   +(mu(3)*y(9)/(phi*xi(1)*(1+lambda(3))))...
   -(rho(8)*y(29))...
   +(rho(8)*y(31)/xi(1))...
   +(rho(9)*y(30)*xi(2)*(1-f1(6))*(1-f2(6))/xi(1))...
   +(rho(7)*y(32)*xi(2)*(1-f1(6))*f2(6)/xi(1));
yp(30)=-(lambda(7)*y(30)/(phi*xi(2)))...
   +(mu(7)*y(21)/(phi*xi(2)))...
   -(rho(10)*y(30)*f1(6))...
   -(rho(9)*y(30)*(1-f1(6))*(1-f2(6)))...
   -(rho(7)*y(30)*(1-f1(6))*f2(6));
yp(31)=-(lambda(11)*y(31)/(phi*(1+lambda(11))))...
   +(mu(11)*y(11)/(phi*(1+lambda(11))))...
   -(rho(8)*y(31))...
   +(rho(8)*y(29)*xi(1))...
   +(rho(9)*y(32)*xi(2)*(1-f1(6))*(1-f2(6)))...
   +(rho(7)*y(30)*xi(2)*(1-f1(6))*f2(6));
yp(32)=-(lambda(15)*y(32)/(phi*xi(2)))...
   +(mu(7)*y(23)/(phi*xi(2)))...
   -(rho(10)*y(32)*f1(6))...
   -(rho(9)*y(32)*(1-f1(6))*(1-f2(6)))...
   -(rho(7)*y(32)*(1-f1(6))*f2(6));

%I2 -> Y60L
yp(33)=-(lambda(4)*y(33)/(phi*xi(1)*(1+lambda(4))))...
   +(mu(4)*y(10)/(phi*xi(1)*(1+lambda(4))))...
   -(rho(8)*y(33))...
   +(rho(8)*y(35)/xi(1))...
```

```
   +(rho(9)*y(34)*xi(2)*(1-f1(8))*(1-f2(8))/xi(1))...
   +(rho(7)*y(36)*xi(2)*(1-f1(8))*f2(8)/xi(1));
yp(34)=-(lambda(8)*y(34)/(phi*xi(2)))...
   +(mu(8)*y(22)/(phi*xi(2)))...
   -(rho(10)*y(34)*f1(8))...
   -(rho(9)*y(34)*(1-f1(8))*(1-f2(8)))...
   -(rho(7)*y(34)*(1-f1(8))*f2(8));
yp(35)=-(lambda(12)*y(35)/(phi*(1+lambda(12))))...
   +(mu(12)*y(12)/(phi*(1+lambda(12))))...
   -(rho(8)*y(35))...
   +(rho(8)*y(33)*xi(1))...
   +(rho(9)*y(36)*xi(2)*(1-f1(8))*(1-f2(8)))...
   +(rho(7)*y(34)*xi(2)*(1-f1(8))*f2(8));
yp(36)=-(lambda(16)*y(36)/(phi*xi(2)))...
   +(mu(8)*y(24)/(phi*xi(2)))...
   -(rho(10)*y(36)*f1(8))...
   -(rho(9)*y(36)*(1-f1(8))*(1-f2(8)))...
   -(rho(7)*y(36)*(1-f1(8))*f2(8));

yp(37)=(rho(10)*y(13)*f1(1))+(rho(10)*y(15)*f1(1));
yp(38)=(rho(10)*y(14)*f1(2))+(rho(10)*y(16)*f1(2));
yp(39)=(rho(10)*y(26)*xi(2)*f1(3))+(rho(10)*y(28)*xi(2)*f1(3));
yp(40)=(rho(10)*y(17)*f1(4))+(rho(10)*y(19)*f1(4));
yp(41)=(rho(10)*y(18)*f1(5))+(rho(10)*y(20)*f1(5));
yp(42)=(rho(10)*y(30)*xi(2)*f1(6))+(rho(10)*y(32)*xi(2)*f1(6));
yp(43)=(rho(10)*y(21)*f1(7))+(rho(10)*y(23)*f1(7));
yp(44)=(rho(10)*y(34)*xi(2)*f1(8))+(rho(10)*y(36)*xi(2)*f1(8));
yp(45)=(rho(10)*y(22)*f1(9))+(rho(10)*y(24)*f1(9));

yp=yp';
t
```

Appendix C: Baseline Model Validation

C.1 Methods

Tests of the mathematical model described in Chapter 5 were conducted to demonstrate that the equations were entered correctly and that the mathematical solver was functioning properly. The model, which is composed of a system of 45 ordinary differential equations (Appendix A), was solved using MATLAB (version 6 release 12, The Mathworks) and the stiff ordinary differential equation solver, ode15s, with all default options except that the backward differentiation formulas option was used. Relevant parameter values are listed in Table 5.2 and discussed in further detail in Chapter 5.

C.2 Results

To validate that the mathematical model functioned properly at steady state, the model was run in the absence of any ligand and binding site levels were recorded. As expected, both IGF-IR levels and IGFBP levels remained at their steady state values (Figure C1).

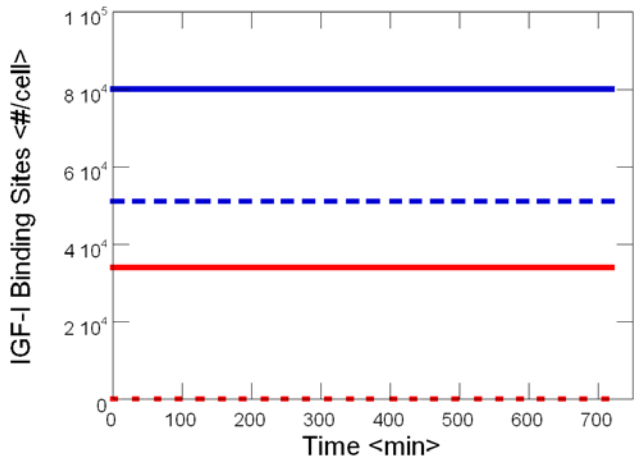

Figure C. 1: Steady state levels of IGF-IR and IGFBPs.

Levels of IGF-IRs and IGFBPs on both the apical (— and —, respectively) and basolateral (– – and – –, respectively) cell membranes

Once it was established that the model accurately described the cell system in the absence of ligand, simulations of binding studies were conducted. To simulate the reduced temperature utilized in binding experiments, the parameters that define membrane internalization were reduced to zero. When IGF-I is added, in the absence of competitors, to the apical side of the cell monolayer, IGF-I binds with both cell surface IGFBPs and IGF-IRs (Figure C2A). As expected, when all binding sites are blocked by excess IGF-I, there is a decrease in the number of IGF-I complexes (Figure C2B). Similarly, inclusion of Y60L-IGF-I prevents binding to IGFBPs (Figure C2C) and

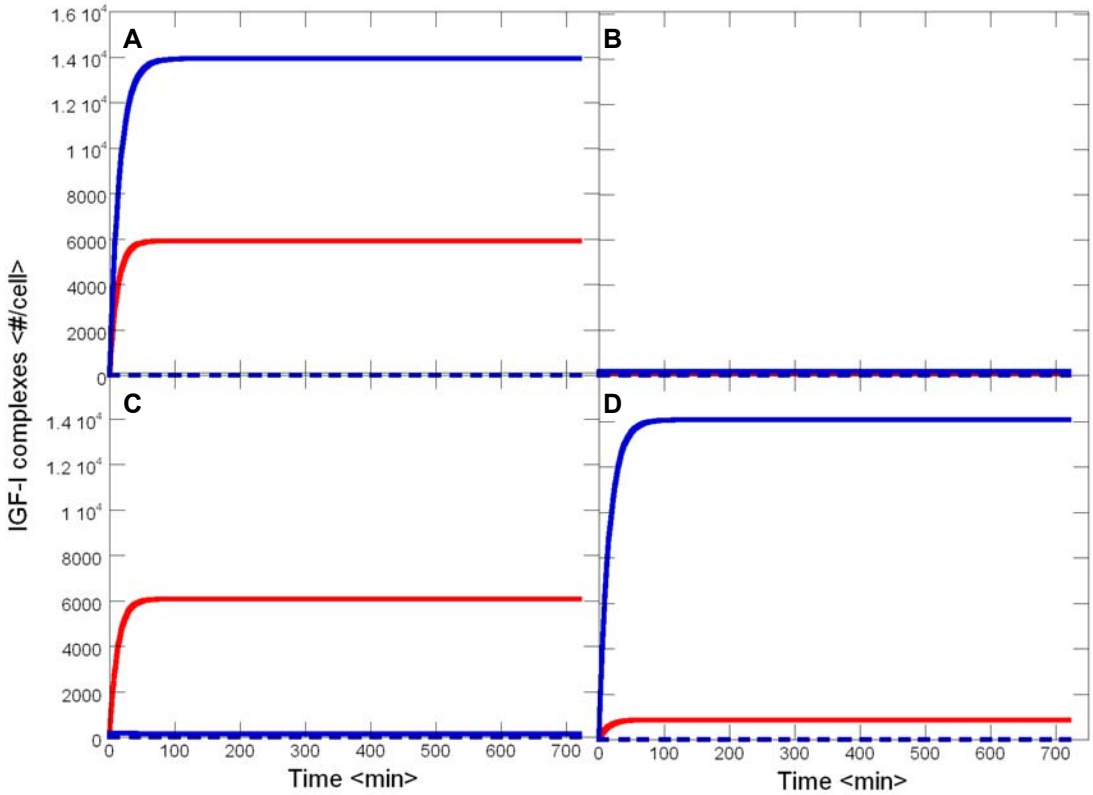

Figure C. 2: Apical binding of IGF-I to model endothelial cells.

Internalization was inhibited and IGF-I was added to the apical side of the cell surface to form apical (—) or basolateral (– –) IGF-I / IGF-IR complexes or apical (—) or basolateral (– –) IGF-I / IGFBP complexes. Simulations were conducting in the absence (A) or presence of binding competitors (IGF-I (B), Y60L-IGF-I (C), or insulin (D)).

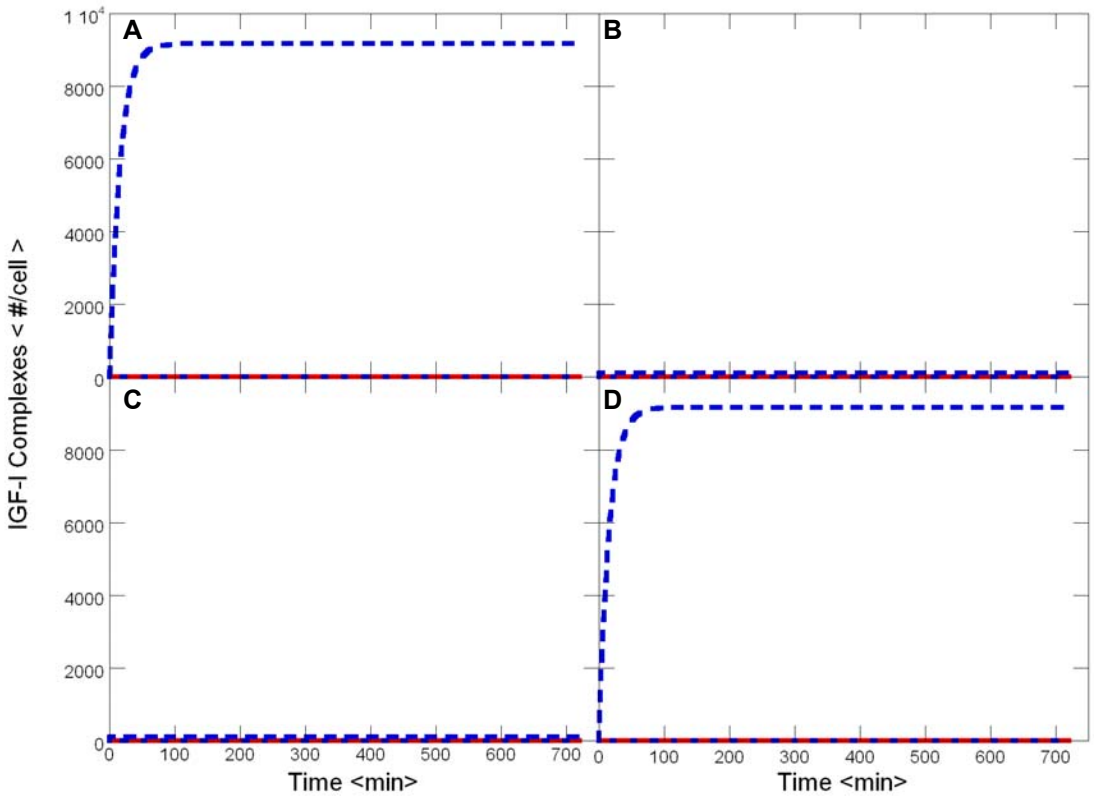

Figure C. 3: Basolateral binding of IGF-I to model endothelial cells.

Internalization was inhibited and IGF-I was added to the basolateral side of the cell surface to form apical (—) or basolateral (– –) IGF-I / IGF-IR complexes or apical (—) or basolateral (– –) IGF-I / IGFBP complexes. Simulations were conducting in the absence (A) or presence of binding competitors (IGF-I (B), Y60L-IGF-I (C), or insulin (D)).

inclusion insulin prevents binding to IGF-IRs (Figure C2D). Since the affinity between insulin and IGF-IR is substantially less than that between IGF-I and IGF-IR, inclusion of insulin does not completely prevent IGF-I/IGF-IR complex formation, even when added in excess (Figure C2D). Similar results are seen when IGF-I is added to the basolateral side of the cell monolayer (Figure C3), except there are no IGF-IRs on the basolateral surface, so there is no formation of IGF-I/IGF-IR complexes. Further, since IGF-I was not allowed to enter the cell, there was no formation of internal complexes and all levels remained at their steady state values.

Appendix D: Phenol Red Transport Across Transfect Variants of MAC-T Cells

D.1 Introduction

Since differences in cell-cell connectivity were detected between parental (MAC-T) cells and transfected MAC-T (SV40-IGF-I and TK-IGF-I) cells, further studies were pursued to demonstrate that these differences were the result of the production of IGF-I, not the transfection process.

D.2 Materials and Methods

Phenol red transport was measured as described in section 2.3.3. In addition to the parental (MAC-T) and constitute IGF-I-secreting (SV40-IGF-I) cells, an inducible IGF-I secreting (MD-IGF-I) cell line and 9 clones of a control cell line (SV40-Mock) were generously provided by Dr. R. Michael Akers in the Department of Dairy Science at Virginia Tech. Two clones of the parental cells that were transfected to constitutively secrete IGFBP-3 (BP3 and BP3CL2) and a control cell line that contained the promoter but not the IGFBP-3 cDNA (BP3-Mock) were also tested. These cells were generously provided by Dr. Wendie Cohick in the Department of Animal Sciences at Rutgers University. As described in section 2.3.1, hygromycin B was included in growth media for SV40-Mock, BP3, BP3CL2, and BP3-Mock cells.

D.3 Results

As reported in section 2.4.1, after eight days of growth, IGF-I secreting cells failed to form a transport barrier against phenol red, while parental cells formed a nearly exclusive barrier. Long term culture of SV40-IGF-I cells for up to 16 days did not improve their barrier properties (Figure D.1). The barrier properties of the MAC-T cells slightly increased following 14 days of growth, but this was likely due to increased cell death since the cells were over confluent. Phenol red transport was also

measured across MAC-T cells transfected to induce IGF-I production in the presence of dexamethasone (MD-IGF-I). MD-IGF-I cells in the absence of dexamethasone formed transport barriers that were substantially more restrictive than IGF-I secreting cell lines. However, these barriers were also substantially more permeable than those formed by MAC-T cells, possibly due to very low production of IGF-I.

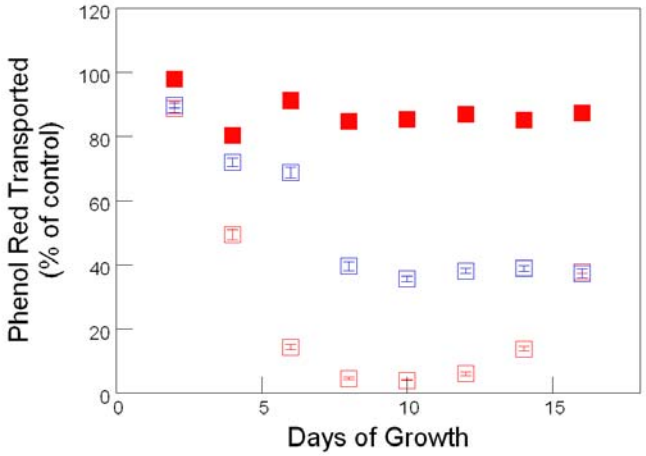

Figure D. 1: Long term measurement of phenol red transport

Phenol red transported across MAC-T (□), MD-IGF-I (□), and SV40-IGF-I (■) cells plated on tissue culture inserts at an initial density of 5 x 10^4 cells/cm^2. Measurements (mean ± S.E., n=4) are representative of 2 independent experiments.

Additional cells lines that contained the promoter but no IGF-I cDNA (SV40-Mock) were generated in the lab of Dr. Akers. Phenol red transport across SV40-Mock clones was varied, but all clones formed significantly ($p < 0.05$) better barriers than SV40-IGF-I cells after 12 days of growth and one clone formed a significantly better barrier than MAC-T cells (Figure D.2).

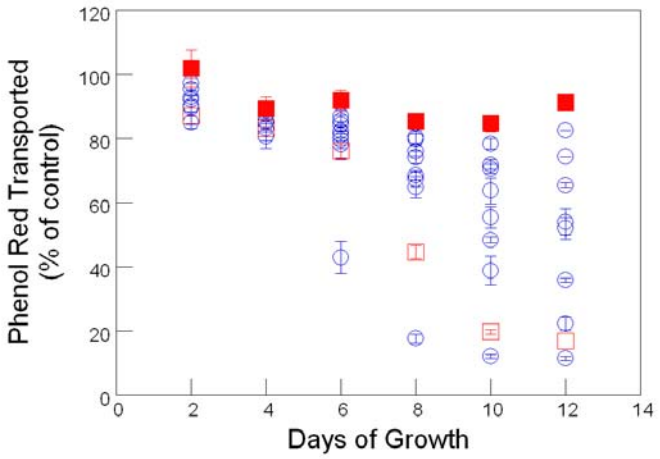

Figure D. 2: Phenol red transport across SV40-Mock cells

Phenol red transport across MAC-T (□), SV40-IGF-I (■), and SV40-Mock (○) cells plated on tissue culture inserts at an initial density of 5 x 10^4 cells/cm^2. Measurements (mean ± S.E., n=2) are representative of 2 independent experiments.

Since IGF-I secreting cells also secreted increased levels of IGFBP-3 (Figure 2.5A), the transport properties of several IGFBP-3 secreting cell lines (BP3 and BP3CL2) were also tested. Phenol red transport across BP3 and BP3CL2 cells was significantly less

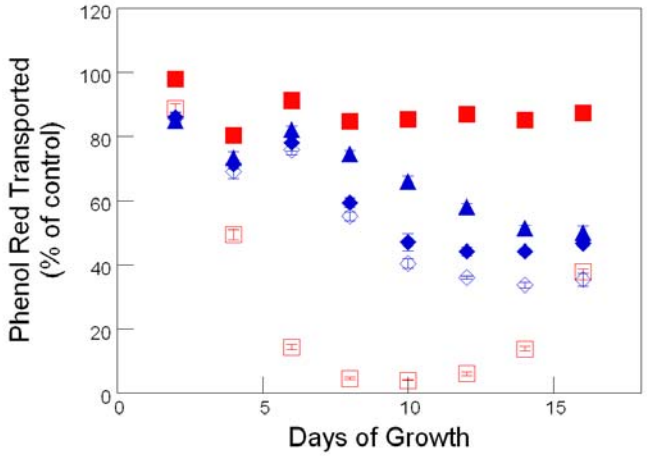

Figure D. 3: Phenol red transported across IGFBP-3 autocrine cells

Phenol red transported across MAC-T (□), SV40-IGF-I (■), BP3 (♦), BP3CL2 (▲), and BP3-Mock (◊) cells plated on tissue culture inserts at an initial density of 5 x 10^4 cells/cm^2. Measurements (mean ± S.E., n=2) are representative of 2 independent experiments.

than SV40-IGF-I cells but significantly more than the parental (MAC-T) cells. However, the transport barriers of these cell lines were similar to those of their control cell line (BP3-Mock).

Appendix E: Western Immunoblots for Occludin and Akt

E.1 Introduction

Addition western immunoblots were conducted as described in Section 2.3.7 to detect occludin and Akt levels following 10 min stimulation with IGF-I (100 ng/ml). Following treatment with IGF-I, samples were collected in Laemmli buffer, loaded into 7% tris-glycine gels, separated at constant voltage and transferred to PVDF membranes. Membranes were then probed with rabbit anti-occludin (1:16,000) (Zymed, South San Francisco CA) and anti-rabbit (1:20,000) (Zymed), rabbit anti-Akt (1:15,000) (Cell Signaling Technology, Beverly MA) and anti-rabbit (1:15,000) (Zymed), or rabbit anti-phospho-Akt (1:15,000) (Cell Signaling Technology) and anti-rabbit (1:15,000) (Zymed).

E.2 Results

Similar to results for the junction components E-cadherin and β-catenin (Figure 2.7), MAC-T cells had higher levels of the tight junction component, occludin, than either IGF-I secreting cell line (Figure E.1 A). As expected, this expression was not affected by addition of IGF-I since protein synthesis requires more than 10 minutes, which was the duration of stimulation.

In their unstimulated state, there was no endogenous activation of the PI3K signaling component Akt in the parental MAC-T cell line (Figure E.1B and C). However, MAC-T cells do retain their ability to signal through phosphor-Akt upon stimulation by IGF-I (Figure E.1B), even though their cell surface receptors have been partially down regulated (Figure 2.8). Interestingly, activation of Akt occurs in SV40-IGF-I cells even in the absence of exogenous IGF-I, likely due to autocrine stimulation by IGF-I. Activation of Akt in SV40-IGF-I and TK-IGF-I cell is enhanced upon addition of exogenous IGF-I (Figure E.1B and C).

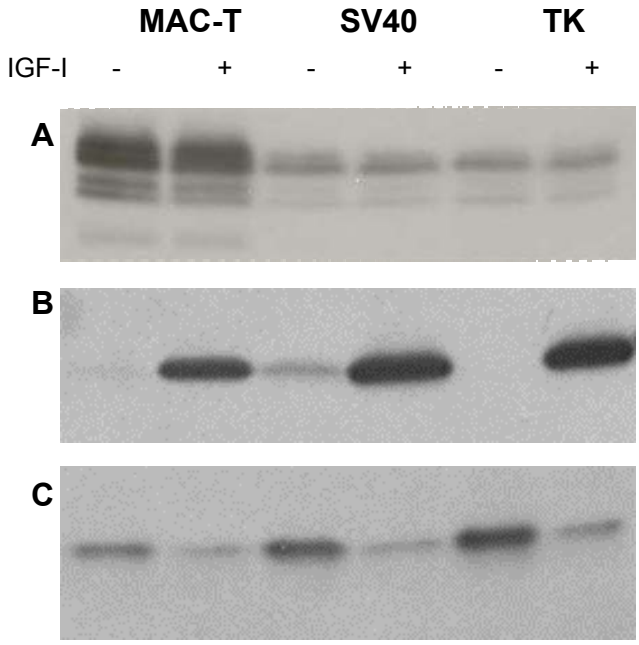

Figure E. 1: Western immunoblots for occludin and Akt

Western immunoblots of MAC-T, SV40-IGF-I, and TK-IGF-I cell lysates, unstimulated or stimulated with IGF-I (100 ng/ml) for 10 min Cells were plated on tissue culture inserts at 5 x 104 cells/cm2, lysed after 8 days of culture, and probed for occludin (A), phospho-Akt (B), and total Akt (C).

Appendix F: Mixed Cultures of Parental and IGF-I Secreting Cells (Experiment #147)

F.1 Purpose

To further investigate the mechanisms involved in the loss of barrier formation in IGF-I secreting cells, experiments were conducted with mixed cultures of these cells.

F.2 Results

Phenol red transport was measured across mixed cultures of MAC-T and SV40-IGF-I cells. After 8 days of growth, even inserts initially plated with 80% SV40-IGF-I cells and 20% MAC-T cells formed substantial barriers to the transport of phenol red and inserts plated initially with either 20% or 50% SV40-IGF-L cells formed almost totally exclusive barriers (Figure F.1).

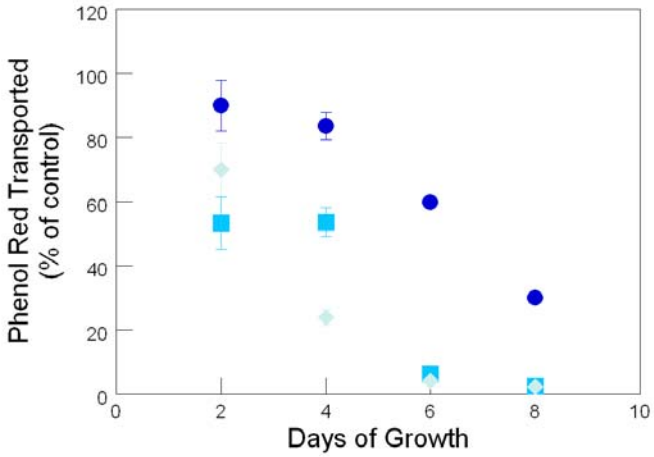

Figure F. 1: Phenol red transported across mixed cell cultures

Phenol red transported across mixed cultures of MAC-T and SV40-IGF-I cells. 20% MAC-T and 80% SV40-IGF-I (●); 50% MAC-T and 50% SV40-IGF-I (■); and 80% MAC-T and 20% SV40-IGF-I (◆) cells plated on tissue culture inserts at an initial density of 5 x 10^4 cells/cm^2. Measurements (mean ± S.E., n=4) are representative of 1 independent experiments.

To determine if the formation of these barriers was due to loss of SV40-IGF-I cells and the increased presence of MAC-T cells, SV40-IGF-I cells were fluorescently labeled with DiI and plated in mixed culture with MAC-T cells. The percentage of the culture that fluoresced, indicating presence of SV40-IGF-I cells, was recorded over a period of 9 days (Figure F.2). Although these results are very preliminary and the protocol needs to be further optimized and repeated, after 9 days of growth, there was a significant number of SV40-IGF-I cells in culture, indicating that the insert is not dominated by MAC-T cells. This suggests that mixed culture with MAC-T cells, perhaps through enhanced junction formation due to higher levels of occludin and E-cadherin on MAC-T cells, promotes better barrier formation in SV40-IGF-I cells. Further studies are needed to test this hypothesis.

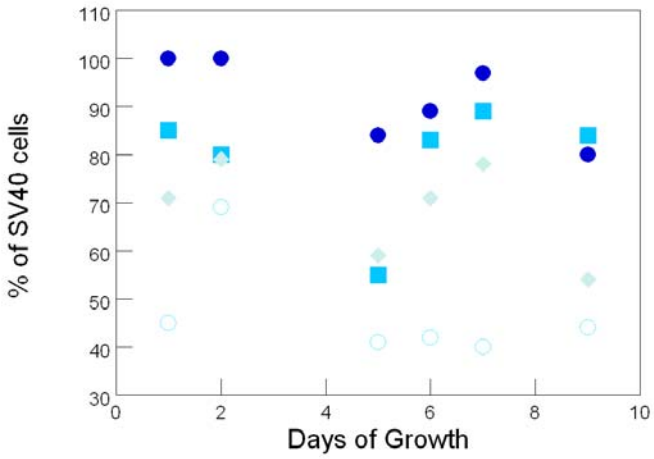

Figure F. 2: Fluorescent quantification of cells in mixed culture

Fluorescent detection of SV40-IGF-I cells present in mixed cultures of MAC-T and SV40-IGF-I cells initially plated at: 100% SV40-IGF-I (●); 25% MAC-T and 75% SV40-IGF-I (■); 50% MAC-T and 50% SV40-IGF-I cells (♦); and 75% MAC-T and 25% SV40-IGF-I (○). Measurements are representative of 1 independent experiments.

F.3 Acknowledgements

The fluorescent staining and imaging protocol was developed by Denise Goad during the summer of 2002. The fluorescent data reported in Figure F.2 was collected by Ms Goad.

Appendix G: Supplemental Results for Chapter 4

G.1 Introduction

This appendix reports additional results in support of Chapter 4

G.2 Results

G.2.1 Western ligand blot

As reported in Section 4.4.2, the IGFBPs detected in conditioned media from the apical side of bovine aortic endothelia cells have molecular weights consistent with IGFBPs 2, 3, and 4 (Figure F.1), with the predominant species being IGFBP-4. Further, no IGFBPs were detected in conditioned media collected from the basolateral side of the monolayers.

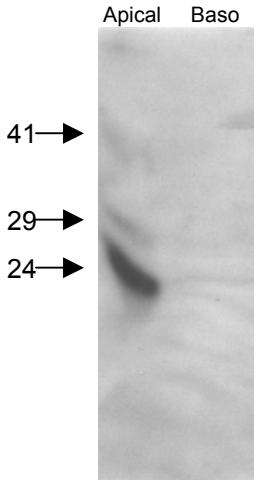

Figure G. 1: Ligand blot of conditioned media from BAEC

Western ligand blot of BAEC conditioned media. Conditioned media was collected from the apical (0.5 ml) and basolateral (1.5 ml) compartments and treated as described in the Section 4.3.8. Blot is representative of 3 independent experiments.

G.2.2 Satin analysis

As described in Section 4.3.10 and reported in Section 4.4.3, internalization of IGF-I by IGF-IRs and IGFBPs was analyzed using Satin plots. Satin analysis resulted in a good fit (R^2= 0.97) of data collected from IGF-IR mediated internalization (Figure F.2A) but poor fit (R^2=0.62) of data collected from IGFBP mediated internalization (Figure F.2B). Although the results reported here are from 1 experiment, they are representative of 3 independent experiments. This suggested that IGF-IRs internalize IGF-I, but the IGFBPs present in this system do not.

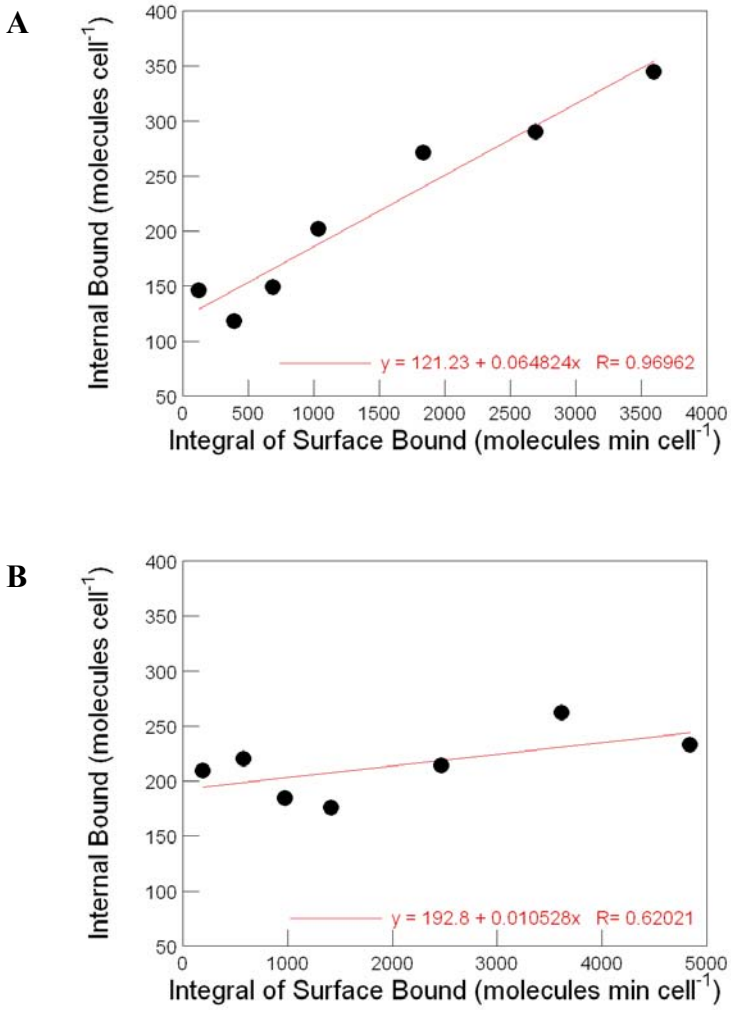

Figure G. 2: Satin analysis

Satin analysis of data collected from (A) IGF-IR mediated internalization and (B) IGFBP mediated internalization of IGF-I. Measurements are representative of 3 independent experiments.

G.2.3 Basolateral to Apical Transport of IGF-I

In addition to the apical to basolateral transport experiment presented in Chapter 4, basolateral to apical transport of IGF-I was also measured. Cells were plated and treated as described in Section 4.3.4. Following incubation at 37°C with treatments (IGF-I (2 μg/ml), Y60L-IGF-I (2 μg/ml), or insulin (10 μg/ml)), ^{125}I-IGF-I (4 ng/ml) was added to basolateral chambers. Samples were collected every 3 hours from the apical chamber and replenished with binding buffer and the appropriate treatment and analyzed as described in Section 4.4.4. There was no significant ($p < 0.05$) different in the transport of IGF-I in the absence (none) or presence of competitors (IGF-I, Y60L-IGF-I, or insulin) (Figure F.3). This is not surprising since, as reported in Chapter 4, basolateral binding experiments showed that there were no detectable IGF-IRs on the basolateral surface and half as many IGFBPs as were present on the apical surface.

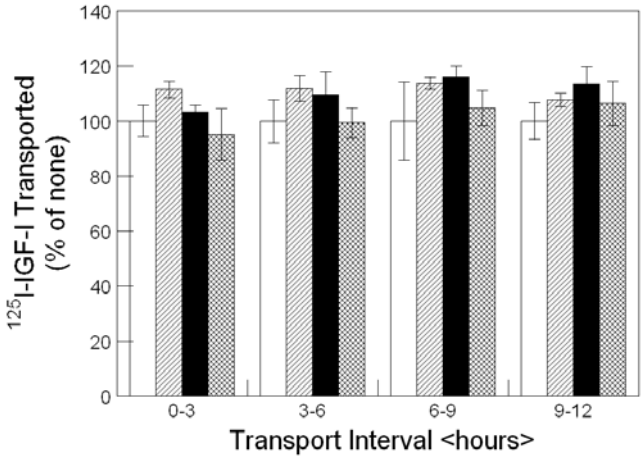

Figure G. 3: Basolateral to apical transport of IGF-I

^{125}I-IGF-I transported over 12 hrs from the basolateral to apical side of bovine aortic endothelial cells (BAECs) in the absence (none) (○) or presence of binding competitors (IGF-I (2 μg/ml) (∅), Y60L-IGF-I (2 μg/ml) (●), or insulin (10 μg/ml) (⊗)) at 37°C. BAECs were plated and cultured as described in Section (4.3.4). Results indicate the mean ± SEM (n = 3) and are representative of three independent experiments.

Vita

Julie Melissa Davis Paye received a Bachelor of Science in Chemical Engineering in 1998 from Florida Institute of Technology in Melbourne, Florida. During this time she completed a coop with Airbus Industries in Toulouse, France. She then began work on her doctoral dissertation in the Fall of 1998, and in addition obtained a Masters of Engineering in Chemical Engineering in 2001 from Virginia Polytechnic Institute & State University in Blacksburg, Virginia.